Alma Mater Studiorum – Università di Bologna

DOTTORATO DI RICERCA IN

CHIMICA INDUSTRIALE

Ciclo XXIV

Settore Concorsuale di afferenza: **03/C2**

Settore Scientifico disciplinare: **CHIM/04**

A chemical loop approach for methanol reforming

Presentata da

Stefano Cocchi

Coordinatore Dottorato

Prof. CAVANI Fabrizio

Relatore

Prof. CAVANI Fabrizio

Esame finale anno 2012

Steam iron process

Thermochemical reforming

Methanol reforming

Ferrite mixed oxide

Mössbauer spectroscopy

Hydrogen production

Abstract

Over the past few years, the switch towards renewable sources for energy production is considered as necessary for the future sustainability of the world environment. Hydrogen is one of the most promising energy vectors for the stocking of low density renewable sources such as wind, biomasses and sun. The production of hydrogen by the steam-iron process could be one of the most versatile approaches useful for the employment of different reducing bio-based fuels.

The steam iron process is a two-step chemical looping reaction based (i) on the reduction of an iron-based oxide with an organic compound followed by (ii) a reoxidation of the reduced solid material by water, which lead to the production of hydrogen. The overall reaction is the water oxidation of the organic fuel (gasification or reforming processes) but the inherent separation of the two semireactions allows the production of carbon-free hydrogen.

In this thesis, steam-iron cycle with methanol is proposed and three different oxides with the generic formula AFe_2O_4 (A=Co,Ni,Fe) are compared in order to understand how the chemical properties and the structural differences can affect the productivity of the overall process. The modifications occurred in used samples are deeply investigated by the analysis of used materials. A specific study on $CoFe_2O_4$-based process using both classical and in-situ/ex-situ analysis is reported employing many characterization techniques such as FTIR spectroscopy, TEM, XRD, XPS, BET, TPR and Mössbauer spectroscopy.

Summary

SUMMARY 1

1 INTRODUCTION 5

1.1 RENEWABLE ENERGIES: A SHORT OVERVIEW 7

1.1.1 The need to store energy 8

1.1.2 Specific problems about biomasses 10

1.2 HYDROGEN INDUSTRY 11

1.2.1 Hydrogen-based economy: the future perspectives 11

1.2.2 Hydrogen-based economy: technological state-of-the-art 13

1.2.2.1 Hydrogen storage 13

1.2.2.2 Fuel-cells 15

1.2.3 The hydrogen industry today 18

1.2.3.1 Hydrogen production 18

1.2.3.2 Hydrogen industrial use 22

1.3 LOW-IMPACT HYDROGEN PRODUCTION 23

1.3.1 Water Electrolysis 23

1.3.1.1 Alkaline electrolysis 24

1.3.1.2 PEM electrolyser 25

1.3.1.3 SOFC electrolyzers 25

1.3.2 Hydrogen from biomasses: non-thermal processes 25

1.3.3 Hydrogen from biomasses: thermal processes 26

1.3.3.1 Dry-Biomass gasification 29

1.3.3.2 Hydrogen from methanol 30

1.3.4 Photocatalytic water splitting 32

1.3.5 Thermochemical water splitting 32

1.3.5.1 The sulfur cycles 34

1.3.5.2 Low temperature cycles – the chloride and bromide family ... 35
1.3.5.3 Metal/Metal oxide thermochemical cycles ... 36
1.3.5.4 Mixed Ferrite cycles ... 38
1.4 THE STEAM IRON PROCESS: A CHEMICAL LOOP APPROACH TO HYDROGEN PRODUCTION ... 42
1.4.1.1 Chemical Looping Combustion (CLC) ... 42
1.4.1.2 Thermochemical Reforming ... 43
1.4.2 Steam-iron process: different reducing fuels ... 46
1.4.2.1 Hydrogen ... 46
1.4.2.2 Methane and gas from light hydrocarbons reforming ... 47
1.4.2.3 Syngas from coal gasification ... 49
1.4.2.4 Pyrolysis oil ... 49
1.4.2.5 Biomass gasification gas ... 50
1.4.3 Steam-iron process: modified materials analysis ... 51
1.5 AIM OF THE THESIS ... 53
2 EXPERIMENTAL PART ... 55
2.1 SYNTHESIS OF THE MATERIALS ... 55
2.2 CHARACTERIZATION TECHNIQUES ... 56
2.2.1 XRD ... 56
2.2.2 BET analysis ... 56
2.2.3 Temperature programmed analysis (TPR/TPO) ... 58
2.2.4 Infrared analysis ... 59
2.2.5 X-ray photoelectron spectroscopy ... 59
2.2.6 Mössbauer spectroscopy ... 60
2.3 CATALYTIC TESTS ... 61
2.3.1 Catalytic tests equipment ... 61
2.3.2 Catalytic tests parameters and calculations ... 65

2.4 SAFETY ISSUES ABOUT USED MATERIALS 70
2.4.1 Catalysts synthesis 70
2.4.2 Reactants 72
3 RESULTS AND DISCUSSION 75
3.1 ON THE CHEMICAL-PHYSICAL PROPERTIES OF $CoFe_2O_4$ 75
3.1.1 The effect of thermal annealing on bulk characteristics 75
3.1.2 The anaerobic oxidation of methanol 82
3.1.3 The effect of thermal annealing on surface characteristics: the interaction with methanol 95
3.1.4 Bulk characteristics of used catalysts 97
3.1.5 TPR investigation 102
3.1.6 Conclusions on the chemical-physical properties of Cobalt ferrites 107
3.2 MEOH THERMOCHEMICAL REFORMING 109
3.2.1 Characterization of the synthesized materials 109
3.2.2 Catalytic tests: the complete reductions of ferrites 112
3.2.2.1 Cobalt ferrite 112
3.2.2.2 Nickel ferrite 116
3.2.2.3 Magnetite 122
3.2.3 Catalytic tests: the repeated cycles 126
3.2.3.1 Definition of the parameters for the repeated cycles 126
3.2.3.2 CF450 repeated cycles 128
3.2.3.3 NF450 repeated cycles 131
3.2.3.4 FF450 repeated cycles 133
3.2.3.5 Characterization of the used materials 135
3.2.3.6 Conclusions about the repeated cycles 138

3.2.4 A preliminary screening of possible improvements for thermochemical MeOH reforming 140

3.2.4.1 Reoxidation in air of used samples 140

3.2.4.2 High-temperature repeated cycles on CF450, to increase the H_2/coke ratio 146

3.2.5 Conclusions on the MeOH thermochemical reforming 150

3.3 INVESTIGATION ON $CoFe_2O_4$ MODIFICATIONS DURING THE REDOX PROCESS 153

3.3.1 Characterization of synthesized compounds 153

3.3.2 Characterization of reduced materials 160

3.3.2.1 Different reduction degrees 160

3.3.2.2 Low reduced compounds 167

3.3.2.3 Complete reduction of CF450 172

3.3.3 Samples after complete redox cycles 173

3.3.3.1 One redox cycle with complete reduction of the solid 173

3.3.3.2 One redox cycle with low reduction degree 178

3.3.3.3 Repeated cycles on CF450 179

3.3.4 Reoxidation in air of used CF450 181

3.3.5 Conclusions about transformations of CF450 occurring during the steam-iron process 182

4 CONCLUSIONS AND PERSPECTIVES 185

5 BIBLIOGRAPHY 189

1 Introduction

Over the past few years, environmental problems such as climate change and air pollution have became more and more important due to their effect on the human being and the future sustainability of the Earth resources. It is well known and scientifically demonstrated that the anthropic contribution to these problems is not negligible; this is mainly caused by the high consumption of energy that our life-style requires.

Actually the production of energy is one of the main problems for climate change because of the nearly exclusive utilization of fossil-fuels derived compounds, that implies both the emission of CO_2 (which is considered the main greenhouse gas responsible for the global warming) and the usage of these sources in old and low-efficiency systems (i.e., the internal combustion engines typically used for transportation, especially in automotive applications).

This element, together with the continue increase of energy request has led the human being to think about new approaches in order to satisfy the world energy demand. Many solutions have been proposed both from the scientific research focused on this topic and from the policy world, but the main problem for the application of these solutions still is the cost of new technologies. This explains why the most relevant changes and steps forward are typically the consequence of international laws and treaties that all the nations have to obey in order to avoid penalties.

Apart from this, the solutions proposed by the scientific community can be divided in different categories:

- Reduction of the energy consumption by means of improving energy conservation during production and usage (i.e., decrease the heat loss in buildings by incrementing the thermal insulation)

- Reduction of the greenhouse gases emissions decreasing the usage of carbon-containing fossil fuels
- Utilization of renewable energy sources and of new technologies dedicated to these new type of sources

The first, easier-to-achieve improvements have already been applied and are still going on, depending on the political contest of the different nations. One of the best examples for these “first aid” measures is Germany, in which several new high-efficiency micro-cogeneration plants has been installed during the last 10 years, especially in rural zones where the transportation of energy is more difficult. Secondly, the improvement of energy efficiency of buildings has been a very important step forward to satisfy the first target on energy conservation.

For a mid-term solution, one of the most important topic, especially in different political agendas, has been the implementation of new nuclear energy plants. The technology is well known but the time required for the building of new plants is 20-30 years. This big interest added to the huge problems deriving from the risks related to this kind of infrastructures (i.e. Fukushima 2011), has led many countries to take difficult decisions; nowadays the trend of most of Western world is to abandon this technology.

The only solution for the short-, mid- and long-term perspective is the utilization of renewable energy sources (or low-environmental-impact energy) and the development of new technologies for using these new resources. The scientific community accepts this hypothesis because the technology for some applications is already scaled-up and commercially available, giving the possibility to achieve short- and mid-term solutions. For the long-term range, the total amount of energy that is possible to obtain from renewable sources is unlimited (as the name suggests), so

finally offering the opportunity to abandon the production of energy from fossil fuels.

1.1 Renewable energies: a short overview

Five main categories can be envisaged, in regard to “renewable energy sources”:

- Solar energy
- Wind energy
- Hydropower
- Energy from biomasses
- Geothermal energy

It’s clear that the term “renewable” is sometimes used instead of “low-environmental-impact”, because the solar energy is not a truly renewable source, but we can anyway consider it as being both unlimited (we will always have this kind of sources until the end of the human life) and without any considerable impacting on environmental parameters. For wind and geothermal energies the same arguments are also valid.

Concerning biomass and hydropower, the use of the term “renewable” as a categorization is completely correct, because they are obtained exploiting a natural cycle such as the carbon and the water ones.

Actually, the utilization of these sources and the related technologies are well developed and this is the reason why big investments especially in solar and wind energy have already begun, for the production of electric energy. Hydropower technology is well developed too, but sometimes the economic and energy balance for the construction of the required large infrastructures is not so favorable.

Finally, biomass is a huge category including many different resources deriving from both vegetal and animal spheres. The state-of-the-art of using biomasses as energy sources is really patchy depending on the biomass type and the technology involved for energy production. This is why biomasses utilization is still a very interesting topic for the scientific community, research activity being focused on two different topics:

- Biomasses as energy sources (disciplines involved: engineering, biology, chemistry)
- Biomasses as building block sources (mainly chemistry)

It's better to point out that the latter has been the most studied target during the last ten years in the industrial chemistry but, from a worldwide point of view, the greenhouse gases emissions and the air pollution deriving from the production of chemicals is very low if compared to the problems originated from energy production.

1.1.1 The need to store energy

The problems of using the mentioned energy sources are not related to the technology scaling-up, but derive from some intrinsic characteristics, which are:

- *the energy density:*
  the energy required to drive a car, to heat up a building or to air-conditioning ambient building cannot be totally taken just in the moment they are required

- *the irregularity of the sources:*
  it's impossible to have wind or sun sources available at every time during a day or during a year.

The solution is the accumulation of energy, in order to have a storage that can be used in every moment.

The solutions proposed until today derive from different scientific fields and are:

1. *Electrical storage.*

   The use of huge amounts of batteries is forecasted; the development of a completely electrical world is needed and this is why many demonstrating prototypes for electrical devices and machines (i.e., electric cars or hybrid cars) have been implemented. The problem might be the dependence from new political assets because of the need of minerals required for the production of batteries (i.e., the Lithium used for some type of batteries is nearly totally concentrated in Bolivia mines).

2. *Chemical storage.*

   Use of chemical molecules that can be easily produced, and then development of high-efficiency technologies for the production of energy from this "energy vectors" (i.e., the hydrogen economy based on the implementation of fuel-cells for automotive application).

3. *Direct use of biofuels.*

   This is easy to imagine if we consider the use of biomasses. Nowadays we already use this kind of renewable energy (i.e., biodiesel in EU or ethanol added to gasoline from fermentation of sugar-cane in Brazil and USA), but only in a low percentage because of technological problems deriving from the exclusive use of these fuels.

1.1.2 Specific problems about biomasses

Concerning biomasses, there are some additional problems that have to be analyzed before considering the utilization of this sources; the main two are:

- *Ethical problems.*
  The utilization of dedicated biomasses such as maize for energy production instead of nutritional aims raises ethical concerns when considering the problem of malnutrition in the Third World and the cost of life in the other nations. But the real success of the biomass industry will be the utilization of wastes deriving from cultivations and farms or using lands where the cultivation of foodstuff is impossible.

- *Chemical variability.*
  The quantity and the composition of biomasses sometimes are strongly related to the period of the year and this is the reason why the development of new processes can be difficult, since a very strong and versatile technology is needed.

The solutions to these two problems have been already assessed; the introduction of a second-generation biomass that is based on the use of either byproducts/wastes from the food industry or from non-edible vegetals, such as wood and lignin, can solve ethical problems.
The point concerning the irregularity of the biomasses supply, indeed is a problem only in some cases, and this is why the processes based on the utilization of alcohols deriving from fermentation and other more strong and versatile processes, such as pyrolysis and gasification, are the most promising ones. The biggest problems associated to the irregularity of

resources are mostly related to biological (i.e., biogas from municipal wastes) and extraction aspects.

1.2 Hydrogen industry

1.2.1 Hydrogen-based economy: the future perspectives

As it can be understood from the previous paragraph, one of the main problem is the need for an energy vector; in this regard, chemistry can help to find new means and technologies for the storage of all renewable sources. Another help can derive from the improvement of the technologies for the transformation of the biomasses, aimed at the production of new biofuels, and from the best energy carrier chosen.

One of the well-known solutions for the storage of renewable energy is the use of hydrogen as an energy-vector fuel, because of different motivations. First of all, the availability of the H element for the production of molecular hydrogen is very high, considering all the water that can be used to generate it; secondly, devices for the utilization of H_2 as a fuel are already well-known and developed: the fuel cells.

It's obvious that the production of hydrogen as a "clean" vector must derive from the employment of both renewable energy and renewable raw materials; this is why producing it exclusively from water is a big challenge (see the next paragraph "Low-impact hydrogen production" for a closer examination). By now, production of hydrogen is nearly totally carried out using methane as the source: this cannot drive us to reset the environmental problems initially exposed, and other developments are required.

However, it's necessary to point out that using hydrogen as an energy-vector derived from methane, both as energy source and as raw material,

is already a step forward in regard to the problems of air pollution and greenhouse effect. As a matter of fact, air pollution derives from the use of fossil fuels in small engines, like in cars or in buildings; hence, concentrating the energy production in big plants could improve the efficiency of these conversions, decreasing the total energy demand. Another possibility is to implement a CO_2 capture technology, in order to decrease the greenhouse gases emissions (CCS technology). For this reason, many efforts are being devoted to switch the behavior of big energy companies, and in general of all the economical system, to start now the changing of the energy infrastructure toward an hydrogen-based economy.

Another important consideration concerns the technology: as described in the next part, dealing with an overview about the state-of-the-art in hydrogen use, the fuel-cells are considered the best devices in the aim of an efficient use of hydrogen, but their cost is still too high. This is one reason why the hydrogen economy could also be based on the use of old devices, such internal combustion engines; in this case, the target of the reduction of the total amount of energy required will not be reached, but that one of the reduction of the environmental impact will be approached anyway.

With all this preliminary analysis, many economical studies have predicted a sort of timeline for the hydrogen economy introduction in everybody daily life; reasonably, all the conclusions state that hydrogen economy will enlarge his market during the 2020 decade, and it will take about 20-30 years to make a nearly complete switch[1].

1.2.2 Hydrogen-based economy: technological state-of-the-art

The development of an energetic system based on hydrogen as the main fuel is strictly related to the technological requirements and the time needed to build up of the needed infrastructure. In fact, the hydrogen issue is one of the larger sectors where different kinds of stakeholders are involved in (i.e., economy, politics, risk analysis, civil mechanical electrical and automotive engineering, chemistry, physics and others).

Concerning about the issue of the capillary and diffusion of the hydrogen fuel , the decision that has to be taken will be the result of the best compromise between environmental, economical, political and safety issues that can be managed with the available technologies.

The scientific community has to solve the problems related to both the end-user technology, particularly the storage for daily applications (cars, houses, …), and to the devices needed for the use of this fuel (fuel-cells or combustion devices)

1.2.2.1 Hydrogen storage

Hydrogen storage is the second most important barrier (after the cost of production) to the widespread commercialization of hydrogen-based vehicles; the automotive industry is the market inside which this technological point is very important. It has to satisfy different characteristics like low-pressure exercise, high driving range, packaging requirements as space occupation, cost/safety issues and finally performance comparable to the current technologies. Secondly, it’s necessary to develop an infrastructure based on safe, cheap and versatile refueling stations.

The hydrogen storage can be more easily handled when it's not necessary to move this stocking, and the space problems are lesser; for instance, a hydrogen storage for house-care applications can be located very close to the building, but not necessarily inside it. Furthermore, incrementing the use of electric devices can nearly reset the problem of on-site energy production.

The cited characteristics of the automotive industry are also the driving force for the several research activities about storage currently carried out[2,3], all of them being derived from one of the most exhaustive study elaborated by the FreedomCAR partnership between DOE and UScar, in 2002. In the later reports, targets outlined in that report have been changed, because the results achieved did not comply with the minimum target values reported in the timeline schedule up to that moment; the reduced targets are now reported in the last report of September 2009[4].

The main requirements for the automotive application are shown in a diagram in which the gravimetric density and the volumetric density have to be higher than defined values, in order to be comparable to diesel and gasoline classic storage. Furthermore, features such as cost, volume of the tank and others as well are taken into consideration: all these values are reported in the table 2 of the last report[4].

There are different approaches adopted to reach these minimal features that can be categorized into two big classes: chemical and physical storage. Hereafter, the various approaches currently under investigation are compiled.

Chemical storage

Metal hydrides, carbohydrates, synthesized hydrocarbons, ammonia, amine borane complexes, formic acid, imidazolium ionic liquids, phosphonium borate, carbonite substances

Physical storage

Liquid hydrogen, cryo-compressed h_2, carbon nanotubes, metal-organic frameworks, clathrate hydrates, glass capillary arrays, glass microspheres

In 2010 Ahuwalia et al*,* from Argonne National Laboratory presented the updated results of the performances reached by the different approaches[5]: for the first time the CcH2 (cryo-compressed hydrogen technology) could satisfy the requirements of the 2015 target. The MOF-177 (Molecular Organic framework) could satisfy the target for 2010 prevision too, opening new perspectives for hydrogen-fueled vehicles applications.

1.2.2.2 Fuel-cells

The devices for the efficient use of hydrogen are the fuel cells. This kind of electrochemical cell was discovered around the half of the XIX century, but development is still going on. Obviously, only during the last years the financial sources for the R&D of this technology have become relevant, because the interest for its application has grown up very quickly. Nowadays, the state-of-the-art is advanced, and the fields of application are numerous: for instance, mobile phones (fueled with organic solvent and not with hydrogen directly), vehicles, buses, computers, forklifts, emergency power systems even for hospitals, and many more.

The general scheme of a fuel-cell is reported in Figure 1-1, and the overall reaction is only the oxidation of hydrogen to water.

$$H_2 + \frac{1}{2}O_2 \rightarrow H_2O + \Delta V$$

Equation 1. Overall reaction in the fuel cell

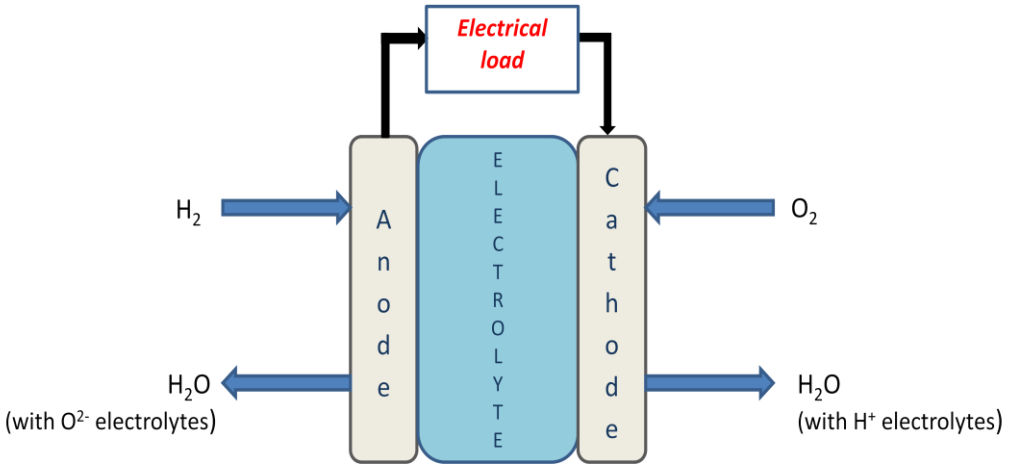

Figure 1-1. Fuel-cell general scheme

The main difference, if compared to the classical fuel combustion in which the energy is recovered as thermal energy, is that the energy deriving from this reaction is recovered using an electrical circuit, with a considerable improvement of the efficiency.

Fuel cells can be categorized on the basis of the electrolyte chosen, that allows the diffusion of different species; here, we summarize the different types of fuel-cells, outlining a short description of the main features for each one of them:

- *PEM - Polymer Electrolyte Membrane*
  The working temperature of this device is very low (80°C) and the use of a noble metal such as Pt at the anode for hydrogen splitting is required. This causes an increment of the cost of production and a very high sensitivity to CO poisoning, even when present in few ppm concentration.

- *Direct Methanol Fuel-Cell*
  Hydrogen is produced in a pre-reforming chamber through methanol reforming with water; the high concentration of

hydrogen atoms in methanol makes the latter suitable for this approach. One of the main advantages is that the need for hydrogen stocking is avoided.

- *Alkaline Fuel Cell*
  The electrolyte is typically a KOH solution, and in this case the ion crossing the membrane is the OH^-; the production of water occurs in the anode side. This was the first fuel cell used in the US space programs; the cost could be competitive only if the lifetime will be extended over 40000h.

- *Phosphoric acid Fuel Cell*
  This is considered as the first modern-age fuel-cell; the electrolyte is phosphoric acid that allows H^+ diffusion. Pt is requested in this cell too, and this is why the cost is still too high.

- *Molten carbonate Fuel-Cell*
  CO_3^{2-} is the charge-conducting species, to produce CO_2 and water in the cationic cell. High temperatures are required and no noble metals can be used as catalysts.

- *Solid oxide Fuel Cell*
  A ceramic electrolyte allows the conduction of O^{2-}, but a very high temperature is needed. This high temperature is still the main drawback to solve for automotive applications.

From this list, it's possible to understand that all the applications can find the more suitable type of fuel-cell to reach the target required; this high-versatile feature is already available but the problem remains the cost

with respect to conventional types of energy production devices (fuels or electricity).

For this reason, several studies dealing with the use of PEMFC for automotive application, are now focused on increasing the lifetime 2 or 3 times as much, by limiting the degradation of the materials in the fuel cell; so, the total cost will be considerably reduced[6].

The scientific community is still working on this; however, we have to take into account that the large-scale production of fuel cells will reduce the price of these devices. Therefore, political decisions could be the main driving force for the diffusion of this new technology in the next few years.

1.2.3 The hydrogen industry today

Nowadays the hydrogen industrially produced is totally employed in chemical processes. Its utilization as a new energy vector is just under investigation and only few demonstration plants have been installed (see, for instance, the HyCologne project[7]).

1.2.3.1 Hydrogen production

The total amount of H_2 yearly produced is more than 65 million tons (2007 data)[8] and nearly this entire amount derives from fossil fuels[9] (96% of the production); just a small part of it (4%) is derived from electrolysis of water, when a very high purity degree is required.

Sources used for hydrogen production can be divided in 4 main categories, as shown below (data referred to 2006):

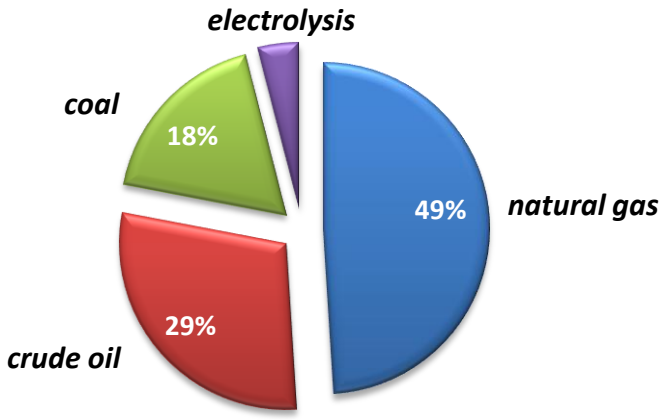

Figure 1-2. Sources for hydrogen production in 2006[9]

This graph demonstrates how difficult will be the switch toward a hydrogen production based on biomasses. Electrolysis is just the only production process with a low environmental impact that would be easy to scale up, because the technology is already well known. One further development with the aim of producing completely "green" hydrogen is the use of renewable energies for the generation of the electrical energy input required (for example, electricity from wind or solar energy, or using High Temperature Electrolysis implemented in nuclear energy plants).

Hydrogen production from fossil sources is obtained using the chemical process below described.

- **Steam methane reforming + Water Gas Shift reaction**

$$\text{SMR} \quad CH_4 + H_2O \rightarrow CO + 3H_2 \qquad \Delta H° = 206\ KJ/mol$$

This reaction is endothermal, and for this reason the process is performed at high temperature (700°C-800°C) with a metallic nickel-based catalyst. The industrial process uses a pressure of about 20-30atm for kinetic reasons, even if the thermodynamic analysis would

suggest to use low pressure. The main drawback at high temperatures is that the disproportion of CO (Boudouard reaction) takes place and the deposition of coke can compromise the catalyst activity; incrementing the Steam-to-Carbon ratio is possible, in order to try to limit this side reaction. Sintering phenomena is another problem and research about catalyst stability is still on-going.

Co-feeding of air to the steam-reformer is another approach already industrially used, with the aim of resetting the energy balance of the overall reaction, because of the exothermicity of methane combustion: the so-called “autothermal reforming” process.

WGSr $CO + H_2O \leftrightarrows CO_2 + H_2$ $\Delta H° = -41,1\ KJ/mol$

In a classic hydrogen production plant, the Water Gas Shift reactor is placed after the reforming unit. Due to the thermodynamic and kinetic constraints, the reaction is usually splitted into two parts, carried out into two in-series reactors; the first one operates at high temperature (350°C-400°C), with a Fe/Cr/Mg mixed oxide as the catalyst; using these operative parameters, the CO con be converted down to 2-3% of residual concentration. Downstream the first reactor, a reactor working at about 200°C with a Cu/Zn oxide as the catalyst converts residual CO down to 0,1-0,2% concentration.
In this way, the productivity is still high because the first reaction stage is faster due to the high temperature used; the reaction rate in the second stage is lower, but from a thermodynamic standpoint, it operates under conditions that are more favorable.
The purity of the H_2 required in PEM-FC, in order to avoid Pt poisoning, is still higher than that obtained with the SMR+WGS process; hence, three main solutions are proposed:

- membrane reactors, where hydrogen is concentrated using its better permeability through specific materials as compared to the other gases contained in the outlet stream.
- PSA (Pressure Swing Adsorption), where gases are selectively adsorbed on solid materials at high pressure.
- catalytic reaction called PrOx (Preferential oxidation), in which the remaining CO is oxidized to CO_2 with O_2,whereas the highly-concentrated hydrogen present in the stream is not oxidized. In this way, the concentration of residual CO can be decreased down to few ppm.

- **Thermal or Catalytic Partial Oxidation of fuels derived from crude oil**

Partial oxidation is a reaction performed with a sub-stoichiometric fuel-air mixture:

$$C_nH_m + {}^{n}/_{2}\ O_2 \rightarrow n\ CO + {}^{m}/_{2}\ H_2$$

The process could be either thermally conducted or catalyzed by Ni-based compounds. The ratio between C and H in the starting fuel is important for the final syngas composition, allowing the production of a hydrogen-rich syngas. The low cost of the raw material is often one of the main advantages of this process.

- **Gasification of coke**

$$C + H_2O \rightarrow CO + H_2$$

This reaction is endothermal, and so the temperature required is usually maintained by means of oxygen co-feeding; in this way, the exothermicity of C oxidation (partial oxidation is preferred rather than the complete one) gives the energy required. The reactors used can be either a fluidized-

bed one, or a fixed-bed or an entrained-bed; the main difference of these three technologies is the temperature of the process.
The drawback of this reaction is the presence of impurities in the feed and the consequent generation of by-products such as NO_x, SO_x and fly ashes; a deep stage of purification before the final stocking of the produced gas is required.
From the economical point of view, this technology is preferable only in locations where methane is very expensive while the price of the carbon is low (i.e., in China).

1.2.3.2 Hydrogen industrial use

Several processes require hydrogen as a reactant; however, nearly all of the produced hydrogen is used in three most important ones[9]:

- *The Haber-Bosch process* for the production of ammonia (>50%)
  the ammonia process is the base for the production of fertilizers
- *The hydro-treatment of oil* (>20-30%)
  the hydro-treatment of oil has became very important for fuel upgrading (the desulfurization is mandatory due to international laws that limit SO_x emissions).
- *The production of MeOH* (10-20%)
  MeOH is one of the most important chemical compound, due to its high chemical reactivity and physical properties; the use as a fuel is under development too.

These numbers demonstrate that hydrogen is important in a future perspective as a preferred energy vector, but nowadays is already one of the most important technical gas for the petrochemical industry.

1.3 Low-impact hydrogen production

The first paragraph underlines that the production of hydrogen from renewable sources (energies and materials) is necessary in order to develop a hydrogen-based economy. In this section, the most promising approaches are analyzed; however, it's necessary to point out that other technologies are currently under development, and that maybe the "best one" will be discovered in the future.

1.3.1 Water Electrolysis

Water Electrolysis is the only technology for the production of very high purity hydrogen that is already used industrially.

Electrolysis is the simple dissociation of water into hydrogen and oxygen, performed by means of an electric current that passes through water. The reaction involved is

$$H_2O + 1{,}23V \rightarrow H_2 + \tfrac{1}{2}\, O_2$$

The reaction is endothermal, and the voltage indicated is the minimal value to make this reaction thermodynamically favored at room temperature. The reduction of hydrogen from +1 to 0 formal oxidation state takes place at the cathode (negative electrode), so hydrogen is evolved in this part of the electrochemical cell. At the anode there is the oxidation of oxygen atom from -2 to 0 oxidation state, that causes the delivery of gaseous O_2 and the formation of a proton that allows the charge balance of the system.

Formally, the thermodynamic values involved in this process can be summarized as:

<u>*Anode*</u> $2\ H_2O_{(l)} \rightarrow O_{2(g)} + 4\ H^+_{(aq)} + 4e^-$ $E^o_{ox} = -1.23$ V

<u>*Cathode*</u> $2\ H^+_{(aq)} + 2e^- \rightarrow H_{2(g)}$ $E^o_{red} = 0.00$ V

The two semireactions show that the formation of H^+ ions at the anode and of OH^- at the cathode takes place, causing a concentration overpotential at both the electrodes that limits the conductivity of the pure water, which is already very low (0,055 μScm^{-1}). For this reason, the dissolution in water of an electrolyte is required in order to increase the conductibility of the solution. The common electrolytes satisfy features such as the low cost, the high solubility and the fact that are not competitors for H^+ and OH^- reduction and oxidation, respectively.

In order to improve the efficiency of the process, elements that can improve the kinetics of the process are deposited on the surface of the electrodes. For instance, Ni covered by Pt at the cathode and Ni or Cu at the anode accelerate the combination of hydrogen and oxygen atoms, respectively, and this step will not be the rate-determining one anymore.

Other improvements can help in the aim of optimizing the system, such as either increasing the working pressure and temperature, or design the cell with a more proper geometry.

Industrially, electrolysis is carried out by using three alternative technologies: alkaline electrolysis, planar SOFC high-temperature electrolysis, and PEM electrolysis.

1.3.1.1 <u>Alkaline electrolysis</u>

This is the most common type of electrolyser, already commercially available. The electrolyte is KOH, at about $30\%_w$ concentration, and the cathode is made of Pt-on-Ni; the working temperature is about 80°C. The main drawback is the corrosion by the very basic solution. Typical values are 80% efficiency, and 6÷10 kA/m^2 as current density.

1.3.1.2 PEM electrolyser

The technical background is derived from the fuel cell, for generating electric current by the reaction of H_2 with O_2; in this case, electricity is used to make the reverse reaction. For this reason, the geometry and the thickness are two strong advantages of this device.

Drawbacks derive from the high cost of the Nafion as electrolyte, the ultra-pure water needed for the feeding and the high cost of Pt as catalyst.

Despite this high-cost requirements, the PEM-Fuel Cell market is carrying away the diffusion of this new device.

1.3.1.3 SOFC electrolyzers

As for the PEM electrolyser, in this case also the technology is derived from that of SOFC-Fuel Cells; the advantage of this approach is that the theoretical highest efficiency is 95%, that derives from the high-temperature thermodynamics. For this reason, the nearly 1000°C required for the oxygen diffusion through the electrolyte (ceramic material) makes this kind of application useful in plants where this temperature is normally reached, as for instance in nuclear energy plants.

1.3.2 Hydrogen from biomasses: non-thermal processes

Hydrogen production is carried out in two stages: first, the fermentation of biomasses to a suitable feedstock; secondly, the products of fermentation can be used in further biological processes that produce bio-hydrogen.

Nowadays, researches dealing with both photofermentative and dark fermentation processes are focused on the genetic modification of

organisms, in the aim of maximizing the hydrogen production from microorganisms or enzymes all derived from algae group. For instance, a research about this topic is the HYVOLUTION project of EU, started in 2006[10]; the core issue of the process is the combination of a thermophilic fermentation with a photoheterotrophic fermentation.

Another approach is a non-natural enzymatic pathway that can improve the yields and the productivity of biological fermentative processes[11].

Finally, one more biochemical-type approach is the application of many aquatic plants for electrolysis in the so-called microbial fuel-cell[12].

1.3.3 Hydrogen from biomasses: thermal processes

Biomass is the renewable source most exploited all over the world. In 2010, about 10% of the world energy consumption derived from biomass upgrading[13] (more than half of the 16% of the total energy production from renewable sources). This is due to the easy technology required for the utilization (for instance, the combustion of biomass for the production of electricity and/or heating) and to the very large amount of the low-cost feedstock that is estimated to be 220 billion tons per year of residuals[14].

One of the important features for the biomass thermal treatments is the water content; this parameter allows the identification of two categories: dry biomass and wet biomass. The cost of transportation and the amount of the energy for the process maintenance are the most important parameters that have to be analyzed in order to evaluate the real energy balance. The former one is totally based on the weight of the material that in this case could be mostly water, while the latter has to take into account the evaporation of water that could be a very high energy-demanding step.

Even if the most employed thermochemical technology is the combustion (with only the 20-40% of efficiency), gasification and pyrolysis are considered the most promising developments, also because the oil price raising open new markets about the synthesis of chemical building blocks that can be derived from these two processes. Regarding the wet biomass, the hydrothermal gasification is still under study and the commercialization is forecasted in a mid- long-term period.

The other important thermal process for hydrogen production is the reforming of bio-based materials; this approach cannot be applied directly to the raw biomass, because of the wide variability of the composition and the high molecular weight of the compounds present in the untreated materials. For this reason, the reforming is under research only for five type of bio-based chemicals:

- Bio-Gas
- Bio-Glycerol
- Bio-Diesel
- Bio-Ethanol
- Bio-Methanol

The first case is only an upgrading of the normal reforming process for methane, considering the possible catalyst poisoning deriving from the presence of by-products obtained during the fermentative process.

Bio-Diesel is a bio-fuel that can be directly used for transportation and this is why the upgrading for hydrogen production is not still considered an important issue; in Europe, bio-diesel in automotive industry is already widely applied.

Glycerol is the co-product of the transesterification process of oils for the production of bio-diesel. This is why the total amount available for industrial application is huge; furthermore, raw glycerol is available at a

very low cost, due to the limited demand of this compound for chemical applications. For this reason the upgrading of glycerol either to a more valuable product or to hydrogen is one of the biggest challenge of the European research. The transformation of bio-glycerol to hydrogen, however, still is less important if compared to the conversion to C3 building blocks such as, for instance, acrolein, acrylic acid, glyceric acid and glycidol.

Finally, ethanol and methanol are the most studied bio-based starting compounds useful for hydrogen production.

First, it's better to point out that ethanol is already used as a bio-fuel (especially in Brazil and USA), together with gasoline. On the other hand, bio-methanol can be catalytically dehydrated to DME (Di Methyl Ether), that can be employed as a bio-fuel in diesel engine (cetane number 55, higher than that of oil-derived diesel fuel) or in mixture with LPG. Bio-methanol is produced from the syngas derived from biomass gasification; however, sometimes the direct production of hydrogen from the starting syngas via WGSr is energetically preferred. On the other hand, the stocking of syngas in the form of methanol is often preferred because the reforming of methanol co-produces CO_2, that allows using it directly in a fuel-cell (see examples of applications in the 1.2.2.2 paragraph). Despite all this, these two alcohols are considered to be good feedstock for hydrogen production due to their high hydrogen to carbon (H/C) atomic ratios, ease of handling and mass production[15,16].

As an interest of this thesis, only MeOH reforming will be more deeply discussed.

1.3.3.1 Dry-Biomass gasification

Biomass gasification can be performed with many different types of oxidative compounds such as oxygen, air, steam, carbon dioxide and mixture of these compounds. The product of this partial oxidative process is a gas mixture of hydrogen, carbon monoxide, methane and carbon dioxide depending on the reaction parameters[17].

The use of air as an oxidant has the drawback of nitrogen's high concentration, that gives a very low heat power to the produced gas; using pure oxygen is more profitable, but its generation could also increase the total cost of the process[18].

The feeding of steam is another good chance to obtain a high heating capacity of the final mixture but the overall process is endothermic; steam with co-feeding of air or oxygen is usually performed. This process is known as autothermal gasification of biomass.

Finally, CO_2 is used in the so-called *dry reforming*; this process is characterized by the very low intrinsic activity of this reactant and the development of the catalyst is still under investigation. Tar, char and methane *dry-reforming* using a Ni/Al catalyst are the most promising processes for the CO_2-based reforming.

The reactors-type developed for the gasification can be classified as follows: fixed-bed (or similarly moving-bed), fluidized bed and entrained bed reactors[19]. The first technology is already commercially used by at least 10 companies in Germany; the second one has different approaches (one or two-step reactor) and one example is in Gussing (Austria), and other plants are in the testing phase[18,20].

The applications of the resulting syngas are several[18], such as the conversion in methane or the production of Fischer-Tropsch fuel, but the only economically interesting approach for hydrogen production is either

via WGSr (that is considered the cheapest technology for hydrogen production from renewables[18]) or via methanol synthesis as bio-based starting compound for high-purity hydrogen production.

In pyrolysis processes the oxidant is not used during the thermal treatment of the biomass; the products obtained are strongly depending on both the heating rates and the maximum temperature reached (for agricultural wastes, typically 450°C-550°C temperature range is used). Usually bio-oils or gaseous mixtures are the main products, while char and tar are the undesired by-products. The process is endothermic and so, the heating power required is provided by firing the biomass involved in the process. Different studies are currently dealing with the use of farm or cultivation wastes, in order to avoid the cost for their disposal, as proposed by the National Non-Food Crops Centre and the FAO[21] (Food and Agriculture Organization of the United Nations).

1.3.3.2 Hydrogen from methanol

Bio-methanol steam reforming (MSR) for hydrogen production is still an active area of research[22,23,24,25]. When compared to other fuels, methanol presents both disadvantages and advantages; for instance, disadvantages are its toxicity and miscibility with water, and the lower reformed hydrogen content compared to the other fuels. Even though the hydrogen energy density of methanol is much lower than that of typical hydrocarbon fuels (being however roughly the same as that for hydrocarbon fuels when the stoichiometrically required water is considered), methanol has the advantage of producing low amount of CO during reforming, much less than with the other fuels. Moreover, the absence of a strong C–C bond facilitates the reforming at low temperatures (200–300°C), and limits coke formation (which instead is one main problem in reforming reactions of hydrocarbon which are

carried out at 400-500°C); this enables milder reaction platforms to extract hydrogen from alcohols. Finally, methanol is liquid, and biodegradable at atmospheric conditions. These peculiarities make methanol an interesting hydrogen-carrier fuel not only for portable and small power applications (e.g., for PEM fuel-cells), but also for larger ones. Catalysts for MSR can be divided in two main groups: copper-based and group 8–10 metal-based catalysts; the former systems are the most active ones, while the latter present better results in terms of both thermal and long-term stability.

On the other hand, other methods can be employed for the production of hydrogen from methanol, e.g., decomposition, partial oxidation and autothermal reforming[25]. Partial oxidation[26] has the advantage of being an exothermic reaction and a higher reaction rate is expected, which shortens the reaction time to reach the working temperature from the cold start-up conditions. In fact, there are several companies developing their processors based on alcohols oxidation. In general, two different approaches are possible for methanol catalytic partial oxidation, (a) direct and (b) indirect. In the former, methanol reacts with substoichiometric amounts of oxygen (catalytic partial oxidation, CPO), whereas in the latter total oxidation of methanol is combined with steam- and/or CO_2-reforming. Accordingly, CPO is a complex system; it has been proposed that both equilibrium conversion and non-equilibrium regimes establish, and hence several different paths for methanol conversion, such as oxidation, steam-reforming, and decomposition, may take place simultaneously[27,28,29,30,31,32,33]. Cu-ZnO and Pd are the most active catalysts for methanol CPO; various research groups have carried out detailed investigations on Cu-ZnO based catalysts -see, for instance[26] and refs therein reported-, a system where the activity and hydrogen selectivity are strongly correlated with Cu–Zn interactions. Finally, methanol decomposition can be performed on metals; again, Cu-ZnO

and group 10 and 11 metals are active for this reaction, among which Ni and Pd have been the most widely studied[34].

1.3.4 Photocatalytic water splitting

Water splitting into H_2 and O_2 can be obtained both thermically (T>2500°C) and electrolytically (V>1,23V at RT) but the cost of these processes is too high for a large-scale industrial application.

Photocatalysis target is to fulfill the energy gap required for the splitting reaction using the energy deriving from light or UV photons. A photoactive material is able to receive photons that can fulfill this energy gap, allowing the chemical reaction of water splitting.

Classical photoactive materials are TiO_2-based semiconductors, that can absorb photons and create a charge separation with enough energy to catalyze the reaction[35,36].

The research is focusing on new materials discovery and co-catalysts. Some materials used for this application are: Pt/TiO_2[35], $NaTaO_3$:La[37], $K_3Ta_3B_2O_{12}$[38], $(Ga_{.82}Zn_{.18})(N_{.82}O_{.18})$[39], Cobalt based systems[40], and GaN-Sb alloys[41,42].

1.3.5 Thermochemical water splitting

The thermal splitting of water into hydrogen and oxygen is thermodynamically allowed at temperatures higher than 2500°C, and this makes the industrial application forbidden.

The thermochemical approach is based on the exploitation of a chemical loop where the temperature of each step is lower than 2500°C, and the overall reaction is the water splitting reaction. Another feature necessary for the scale-up of these approaches is the intrinsic separation of H_2 and

O_2 in order to avoid the formation of explosive mixtures: usually these thermal cycles satisfy this requirement either spatially or temporally. A generic schematization could be written as

$$A + H_2O \rightarrow H_2 + A\text{-}O$$

$$A\text{-}O \rightarrow A + \tfrac{1}{2}O_2$$

where A can be a combination of either two steps or two different compounds or more.

These cycles have been studied since the 70's, during the oil crisis; later during the 90's, after the Kyoto Protocol subscription by many developed countries, the interest for this approach was renewed. The research community has proposed hundreds of possible cycles[43], but only few of them are considered feasible from an industrial point of view[44] (see *Table 1-1*).

	Steps	T max(°C)	Efficiency(%)
Sulphur cycles			
Hybrid sulphur (Westinghouse,ISPRA Mark 11)	2	900 *(1150 without cat.)*	43
S-I cycle (General Atomics,ISPRA Mark 16)	3	900 *(1150 without cat.)*	38
Hybrid copper-chloride	4	530	49
Zn/ZnO	2	1800	45
Iron oxide	2	2200	42
Cerium oxide	2	2000	68
Ferrites	2	1100-1800	43

Table 1-1. Most interesting thermochemical cycles under development

Data reported in the table demonstrate that cycles may include two or more chemical steps: for the evaluation of the feasibility of the corresponding technologies, five criteria were proposed[45]:

- Within the temperatures considered, the Gibbs free energy of the individual reactions must approach zero.
- The number of steps should be minimal.
- Each individual step must have both fast reaction rates and similar velocities to the other steps in the process.
- The reaction products cannot result in chemical-by-products, and any separation of the reaction products must be minimal in terms of cost and energy consumption.
- Intermediate products must be easy to handle.

1.3.5.1 The sulfur cycles

All the cycles reported have been classified in the same category because one of the reactions involved in these loops is always the same:

$$H_2SO_4 \rightarrow SO_2 + H_2O + O_2$$

that is thermodynamically spontaneous at temperatures above 850°C; for this reason, nuclear plants have always been considered the only possible integration for the scaling-up of these thermochemical cycles[46]. Regarding the two cycles reported in the table, the complete reactions are the following:

Westinghouse, ISPRA Mark 11

$H_2SO_4 \rightarrow SO_2 + H_2O + O_2$ *(T>850°C)*

$SO_2 + 2H_2O \rightarrow H_2SO_4 + H_2$ *(electrolysis reaction)*

General Atomics, ISPRA Mark 16

$H_2SO_4 \rightarrow SO_2 + H_2O + O_2$ *(T>850°C)*

$I_2 + SO_2 + 2H_2O \rightarrow H_2SO_4 + 2HI$ *(Bunsen reaction, 100°C)*

$2HI \rightarrow I_2 + H_2$ *(300°C<T<500°C)*

In the former case, the electrochemical reaction has a higher efficiency if compared with the classic water electrolysis, so the development of the process is still under investigation. In the latter case, pilot plants are already constructed with reactors made of either glass, or quartz or teflon; the stocking of SO_2 is avoided because the decomposition of the two acid species is simultaneous and the overall process is continuous: worth of note, in this case a spatial separation of the O_2 and H_2 produced is obtained.

Both the reported cycles and the other sulfur cycles as well (for instance, the SO_2 Cycle With HBr and the Advanced SO_2 Cycle, that is the only thermochemical cycle industrially implemented in a desulphurization plant in Italy) satisfy the five criteria. However, they are still not competitive with other hydrogen production technologies in terms of cost and efficiency. In addition, these processes require large inventories of highly hazardous corrosive materials. Furthermore, new high resistance materials are required because of the combination of high temperatures, high pressures and corrosive compounds. A better understanding of the relationship between capital costs, thermodynamic losses, and process thermal efficiency may lead to decreased hydrogen production costs[47].

1.3.5.2 Low temperature cycles – the chloride and bromide family

The aim of these cycles was to decrease the maximum temperature at 500°C for nuclear plant application[47].

The UT-3 cycle has been studied for 30 years and it was proposed by the Tokio University during the 70's. The reactions involved are:

$CaO + Br_2 \rightarrow CaBr_2 + ½O_2$	480 – 530°C
$CaBr_2 + H_2O \rightarrow CaO + 2HBr$	680 – 730°C
$Fe_3O_4 + 8HBr \rightarrow 3FeBr_2 + 4H_2O + Br_2$	230 – 280°C
$3FeBr_2 + 4H_2O \rightarrow Fe_3O_4 + 6HBr + H_2$	680 – 730°C

The temperatures involved are much lower than those used in the other approaches, but the main drawback is the material stability and the need of membranes for the separation of H_2. Another problem can derive from the sublimation of $CaBr_2$ and $FeBr_2$ (temperature of sublimation, 740°C and 690°C, respectively). The reported efficiency is as high as 45%, but recent papers estimate the real value to be close to 13%.

The other cycles belonging to this category are the "Hybrid copper chloride cycle" and the "Uranium europium cycle" that are still in a initial development stage[48,49]; the higher temperatures used in these cycles are 530°C and 300°C, respectively.

1.3.5.3 Metal/Metal oxide thermochemical cycles

This process has been developed for the employment of the solar concentration technology. The generic process scheme is:

$$MO_{(x+y)} \rightarrow MO_x + y/2\ O_2$$

$$MO_x + yH_2O \rightarrow MO_{(x+y)} + yH_2$$

This group of reactions shows higher efficiency, lower corrosive problems, generic lower cost depending on the metal used, less technological problems due to the only gas-solid phases and only two steps of reaction.

One of the main drawbacks is the high temperature often required for the thermal reduction of the metal oxide (1st step) and the consequent low productivity. For this reason, the reduction of the higher temperatures is the main target for further developments. The most important cycles of this class are hereafter reported[46].

- *Zn/ZnO*

  The thermal reduction takes place at 1900°C and the main problem concern the sublimation of Zn at such high temperatures. A modification of the cycle uses carbon to decrease the temperature of reduction down to 1100°C.

- *CeO_2/Ce_2O_3*

  The thermal reduction is carried out at 2000°C under vacuum, obtaining an efficiency as high as 68%. Many modifications has been reported[46] in the literature, showing lower temperatures, but the number of steps required is greater than two. Some additives proposed are, for instance, HCl (involving the production of H_2 and Cl_2), $Na_2P_2O_7$ (950°C with a $39\%_{eff}$), the water-soluble system $Ce_2(SO_3)_2SO_4 \cdot 4H_2O$ (involving 8 steps and an overall efficiency of 54%).

- *Fe_3O_4/FeO*

  This cycle is considered the most feasible one because of the chemical versatility and the low price of the material.

  The classical cycle was proposed by Nakamura[50] at the end of the 70's:

  $Fe_3O_4 \rightarrow 3FeO + ½O_2$ T>1600°C ($\Delta H° = 319,5$ KJ/mol)

  $3FeO + H_2O \rightarrow Fe_3O_4 + H_2$ T<500°C ($\Delta H° = -33,6$ KJ/mol)

  The use of a solar furnace can be implemented, with a concentration factor above 5000.

The possibility of a large-scale development of these oxides-based processes mainly concerns the iron cycle, because the possibility to prepare mixed iron oxides can remarkably affect the redox properties and consequently the thermal reduction temperature of the material.

1.3.5.4 Mixed Ferrite cycles

The redox properties of this spinel type mixed oxides are strictly related to both the chemical composition and some morphological properties.

Many mixed oxides were proposed in the literature, in the aim of decreasing the temperature of reduction, but on the other side, the reoxidation of the material with water will be thermodynamically possible only at higher temperatures than that used in the Fe_3O_4 cycle. Figure 1-3 shows that the free energy of the two reactions involved in the thermochemical cycles of Co_3O_4, Mn_3O_4 and Fe_3O_4 are strictly related.

It is possible to see that the material showing the lower temperature for thermal reduction (Co_3O_4) shows thermodynamic limitations in regard to the reoxidation of the reduced compound with water. On the other hand, the behavior of the Fe_3O_4 is the opposite: it's difficult to reduce only by means of thermal energy, but the reduced oxide is easily reoxidizable with water up to about 500°C.

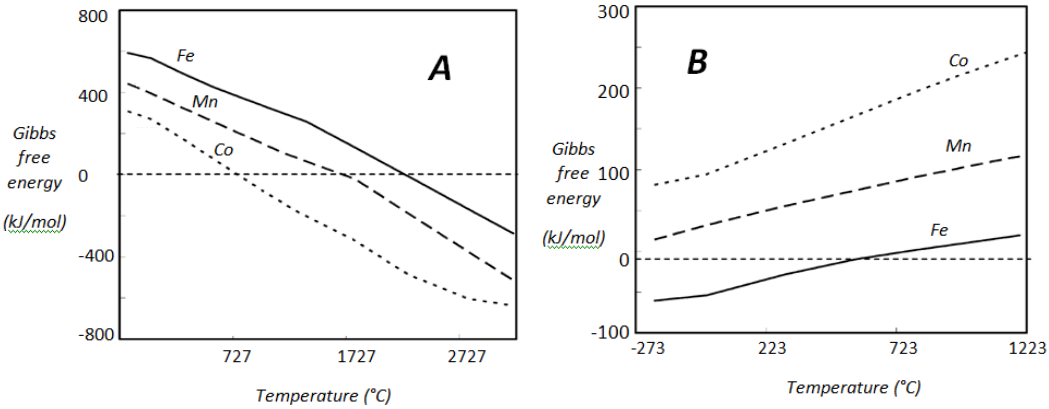

A: $Me_3O_4 \rightarrow MeO + O_2$ B: $MeO + H_2O \rightarrow Me_3O_4$

Figure 1-3. Gibbs free energy of the two reactions of the chemical loop for Co, Mn and Fe spinel-type oxides: (a) thermal reduction (b) water reoxidation.

Several papers in the literature describe the properties of iron-based spinels[51] (called ferrites) with the generic formula $A^{[2+]}Fe_2O_4$; hereafter we summarize some of the most important results.

$NiFe_2O_4$ shows a lower temperature for the thermal reduction step if compared to other ferrites[52,53]. Commercially available mixed oxides were compared by Fresno et al. by carrying out the reduction step at 1723°C, the nickel ferrite showed the greater reproducibility in oxygen delivery and, consequently, in hydrogen production during the second step.

Another paper from the same authors[54] compares ZrO_2-supported and un-supported samples which were annealed at different temperatures; the experimental results indicate an easier reduction of the supported samples (two-three times more of O_2 delivery per ferrite mass) probably due to a better distribution of the material and a consequent greater availability of the active species.

A study from Kodama et al.[55] deals with non-stochiometric nickel ferrite either supported or in bulk phase; also in this case, the oxygen and

consequential hydrogen production was the greater for the supported samples. A suitable reduction temperature for the oxide, after all the improvements made during these studies, is 1400°C, and a pilot plant simulation is under investigation[56].

$CoFe_2O_4$ is the second candidate amongst the most promising systems for the iron-based thermochemical cycle. The study of this material with a working temperature of 1400°C at different Co/Fe ratios was reported by Kodama et al.[57] and a deactivation effect was observed. The comparison with nickel ferrite is reported in a review paper from Kodama and Gokon[56]; it shows that during the first cycle the hydrogen production deriving from the use of $CoFe_2O_4/ZrO_2$ was higher than that obtained with $NiFe_2O_4/ZrO_2$. However, a further comparison study about these two materials was made in a paper[55] where Kodama finally concluded that nickel is more promising, when considering the average yields obtained at the same reducing temperature, but cobalt is the second candidate, especially if the deactivation phenomena can be avoided.

$ZnFe_2O_4$ was proposed by different groups[52,58,59] that use a reduction temperature of 1527°C (up to 1627°C), but at these temperatures the metallic Zn generated is volatile, that caused metal recovery problems.

The use of manganese ferrite was studied in a so-called “manganese ferrite plus activated sodium carbonate”; in this approach using the sodium carbonate in the chemical loop cycle allows to decrease the maximum temperature required down to 1000°C[60,61,62]. Furthermore, the classical route with Fe and other cations involved[63,64,65,53] was also taken into account, but the reduction temperature could not be decreased as it was in the $NiFe_2O_4$ cycle.

The same argument is valid for $CuFe_2O_4$ that shows a lower reduction degree at the same reduction temperature in comparison with $NiFe_2O_4$.

Mixed ferrites with Cu, Mn and Ni in different ratios were also tested, but the best material remains the Ni ferrite mixed oxide.

$Cu_{0,43}Al_{0,43}Fe_{2,14}O_4$ has been also studied by Kaneko et al[65]; they demonstrated that 1400°C is enough to have a little oxygen delivery and the consequent H_2 production in the second step; the problem is the yield obtained (0,37%), that is too low for a scale-up study.

1.4 The steam iron process: a chemical loop approach to hydrogen production

The aim of all the thermochemical cycles is to reduce the high temperature required for the thermal reduction: in order to reach this target, the employment of a carbon source in the first step has been proposed. The resulting process can be called in different ways such as Thermochemical Reforming, Two-step Reforming or sometimes Chemical Looping Reforming[i] in which the oxygen exchanged between the fuel and the water is mediated by a solid material, the so-called "Oxygen Vector" solid.

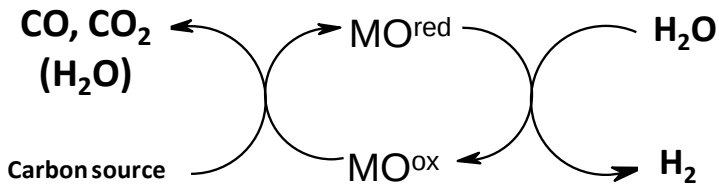

Figure 1-4 . Thermochemical reforming

1.4.1.1 Chemical Looping Combustion (CLC)

Another chemical cycling approach is the Chemical Looping Combustion in which air (or pure oxygen) is used as the oxidant for the recovery of the original oxidation state of the solid material. This process is now

[i] Chemical Looping reforming is often used for a different process in which during the first step water is co-fed with the fuel to obtain Syngas and the reduced metal too (usually Ni). Despite the presence of water the reduction to Ni^0 takes place and the following reoxidation step is performed using air like in the CLC.

briefly introduced because the experimental results on the oxygen-vector solid material are useful for better understanding the thermochemical reforming process (with water as the oxidant). The idea of CLC was introduced at the beginning of the 80's[66] justified by the better control of the process and a better reversibility of the two semi-reactions; the result is a lower temperature of the process and a high improvement of the efficiency. Another important feature is the recently growing interest on CCS technology (Carbon Capture and Storage); the CLC shows an "inherent carbon capture" because the unconverted oxygen is delivered only in the reoxidation step while the CO_2-rich gas is produced during the first step of the cycle[67,68,69,70]. The materials that are currently being investigated are transition-metal based oxides, such as Ni, Fe, Cu and Mn oxides, but the NiO/Ni redox pair seems to be the more performing one[71]. Research activity is mainly conducted by four groups in the world: Chalmers university in Sweden, Southeast University in China, CSIC (Instituto de Carboquimica) in Apian and Ohio State University in USA.

1.4.1.2 Thermochemical Reforming

Coming back to the Thermochemical Reforming (or two-step reforming) approach (Figure 1-4), the thermodynamics involved is clearly different from the classic thermochemical cycles, because the main feature required is only one: the possibility to reoxidize the reduced material with water. In the last paragraph, this feature was in contrast with that one concerning the need for a low reducing temperature[72] (see Paragraph 1.3.5.4).

As a matter of fact, the choice of the material can be extended to other elements and this is why Aoki et al. reported the thermodynamic study of suitable RedOx metal/oxide pairs for this application[73], followed by an experimental screening of the most interesting ones; Gupta et al.[74] also made a wide screening of materials that satisfy this thermodynamic

constraint. Furthermore, papers about single materials reduced with an organic compound are reported in the literature, for instance ZnO/Zn[75], WO_3/W[73], SnO_x/Sn[76], doped Cerium oxide[77], and perovskite-type oxide[78,79].

Due to the results obtained from these tests[73,74], the most studied redox cycle is still the iron-based one: the so-called ***"Steam-Iron Process"***. Since the beginning of the last century there are examples using this material because of its great availability, low cost, and the presence of already developed industrial applications of Fe that may provide an helpful know-how about the properties and reactivity of this element.

Actually, the first study about the employment of a reducing fuel on iron oxide, followed by hydrogen production with water, was carried out before the thermochemical process discovery. It was one of the first industrial technologies used for hydrogen production at the very beginning of the XX century by Howard Lane[80]. In this process, iron is oxidized by steam and then the reduced phase is restored by feeding on the "exhaust" material a low cost highly-calorific power gas, that probably is the gas deriving from coal gasification, the so called "city gas". This very old project was used for the first time in 1907 in St.Louis, to inflate hydrogen in the balloons for the Gordon-Bennet race. The "Lane method" is an evolution of a previous process, where the oxidized iron has to be replaced by a freshly reduced one (so only the reoxidation step was carried out). Many modifications to this first process were later applied, because the original one was not so durable due to the poisoning of the material and the maintenance costs, as reported in a review paper from S.Hurst[81] in 1939. From this latter work it comes out that this kind of approach was used until the Second World War all over the world, even if the methane reforming process had been already discovered in 1923 by

BASF. The industrial interest is demonstrated from the patents issued during that period[82,83].

After this first period, Phillips Petroleum Co[84] and Consolidation Coal Co[85] deposited some patents at the end of the 60's for the steam iron process, proposing some improvements from the material (barium doping or $ZnFe_2O_4$, claimed by Philips). Immediately after, the magnetite thermochemical process based on the thermal reduction[50] was proposed, probably because of the oil crisis period. The Institute of Gas Technology showed further attention about steam-iron process[86,87] in the same period (end of 70's).

After another period of low interest about this process, the cycle has recently assumed very high scientific relevance because of the very high purity hydrogen deriving from the water splitting step (if no coke is deposited during the first reducing step). This is a very important feature to consider, in the aim of possible integrated applications of this technology with fuel-cell systems. Even when considering the reduced iron as a hydrogen storage for vehicle applications, energy efficiency is also another very interesting parameter: depending on the heat recovered during hydrogen delivery and/or storage operation, a competitive value can be reached[88].

For the reasons reported in the first paragraph of the introduction, the carbon source used is the most important feature of every energy process: either bio-based or fossil fuels-derived. So, one of the possible classifications of these steam-iron process-like approaches concerns the reducing fuel adopted. A second type of articles focuses its attention on the chemical composition of the iron oxide-based material employed; this is an alternative way used in the aim of improving the material performance: using dopants, high-concentration co-elements or changing the stoichiometry of the mixed ferrite. Finally, an engineering approach is

another way to work on this process in the aim of improving the overall performance; in this case, the research is focused on the study of the reaction kinetics and the design of devices for the integration with fuel-cells. On this topic, see papers from the group of “Catalysis, Molecular Separations and Reactor Engineering” of the Aragón Institute of Engineering Research in Zaragoza[89,90].

Hereafter we will summarize the many results published about this topic; first, papers dealing with the study of different reducing fuels are discussed; then, works focused on the material synthesis are taken into consideration.

1.4.2 Steam-iron process: different reducing fuels

1.4.2.1 Hydrogen

Using hydrogen as the reducing fuel for iron oxides (Fe_3O_4 or Fe_2O_3 as well) is the approach used for hydrogen storage issue. In this case, the “fuel” that can be charged on a car is simply metallic iron plus a water tank which are able to produce pure hydrogen at low temperature (T<500°C).

$$3Fe + 4H_2O \rightarrow Fe_3O_4 + 4H_2$$

Many types of metal oxides were proposed for this approach, but the lower cost and better availability of iron are considered good features for this application. Furthermore, the reaction rate and the maximum amount of hydrogen that can be stored is considered to be high (4,8% per mass)[91], even though experimental tests demonstrate that only a lower value can be actually reached[92]. Further developments are about increasing the reaction rates by changing the chemical composition of

the oxide[93], the morphology of the material[88] or adding other elements[91], in order to improve the stability of the redox process.

Otsuka et al. proposed in 2011 another approach that uses hydrogen as the reducing fuel[94]; first, a complete dehydrogenation of methane into hydrogen and coke is carried out on a Ni/SiO_2 oxide and then the resulting gas stream made of unconverted methane and hydrogen is used for the reduction of the iron oxide. If the reduction step is carried out by hydrogen only (and not by methane), coke deposition is avoided, so that the reoxidation step will give pure hydrogen only; in this way we obtain high quality hydrogen and coke (the latter deposited on Ni), starting from methane.

This approach can also be considered as a hydrogen separation tool from a hydro-methane gas, and the interest is actually coming back because of the production of hydro-methane mixtures from biomass anaerobic fermentation, which gives a low environmental impact evaluation for the overall process.

1.4.2.2 Methane and gas from light hydrocarbons reforming

The reduction of the iron oxide using methane can be a real alternative to the classical SMR+WGS+PrOx process used for the production of high purity hydrogen, because *C-free hydrogen* can be produced in the oxidation step. ENI, Italian leader of energy production, has recently deposited a patent about a three-step cycle[95] with next extensions[96,97] using methane as the reducing agent, which demonstrates a high interest in industrial sectors for this technology. The three-step process consists in an overall autothermal reforming, because the third step is the oxidation of Fe_3O_4 to Fe_2O_3 with oxygen, which is an exothermic reaction that can provide the energy required for the first endothermic reduction step[98].

Modifications of the simple iron oxide are proposed; Takenaka et al.[99] used iron oxide doped with Cu^{2+} and Cr^{3+} in order to activate CH_4 decomposition and increase the structural stability avoiding sintering phenomena. The Ni/Cr pair was also tested[100], but deactivation of the material is reported because of the Ni segregation during redox cycles.

Galvita et al. proposed Pt-Fe_2O_3/Ce_0,$5Zr_{0,5}O_2$ as a suitable system to first produce syngas from methane on the Pt active sites and then achieve the reduction of iron oxide by H_2 and CO, producing CO_2 and H_2O. Ce and Zr are considered the best co-elements for the support composition, because they allow an increase of the reduction rate and of the structural stability of the system[101].

Others different mixed ferrites were also proposed such as $CuFe_2O_4$ supported on $CeZrO_x$[102,103,104] which seems to avoid coke deposition compared to Fe_3O_4.

$NiFe_2O_4$ has been studied by Kodama et al.[105] because of the higher oxidizing power observed in the thermochemical cycle[55,56]; the solar energy integration in the steam-iron approach is already considered in this paper.

As reported in the title of this classification, other publications use syngas as the reducing stream, derived from the reforming of light hydrocarbons; this approach is similar to that from methane because the real reducing agents are CO and H_2 obtained from methane decomposition (as previously discussed). Finally, CO_2 and H_2 are the desired products, so the overall process starting from CH_4 will be equivalent to the SMR+WGSr technology, while starting from $CO+H_2$ mixture it will be the equivalent of just the WGSr. Here we report about a few papers dealing with this kind of reaction.

Hacker[106] proposed in 2003 the use of light hydrocarbons reforming for the syngas production followed by the sponge iron reduction. The new idea is to recycle the out-coming gas from the reduction reactor (the 2nd one) in the reforming passage (the 1st reactor) because this gas is mainly composed by CO and H_2 that still have a reduction power for the reduction of iron oxide.

Li et al.[107] reported that the conversion of syngas is over 99%; for this reason, the recycling line is avoided. Heidebrecht and Sundmacher[108] have made a computational analysis of a fixed-bed reactor for the CWGSr (Cyclic water gas shift reaction), in which the study of the different oxidation states of the metal oxide is the basis for the reactor design.

1.4.2.3 Syngas from coal gasification

Actually, the original process developed at the beginning of the XX century (Lane hydrogen production) was based on the coal gasification gas, but it was not stable due to the material deactivation.

Currently, the interest of using coal-derived gas is low, and this is why the papers dealing with this topic are only a few[109,110]; a different approach is to use coal char as the reducing agent[111], in order to recover the energy lost because of this by-product generation during the gasification process.

1.4.2.4 Pyrolysis oil

This approach is exposed in two papers by Bleeker et al.[112,113] from University of Twente, using a pyrolysis oil deriving from pine wood. In these two papers, two different schemes of reaction were proposed, shown in Figure 1-5.

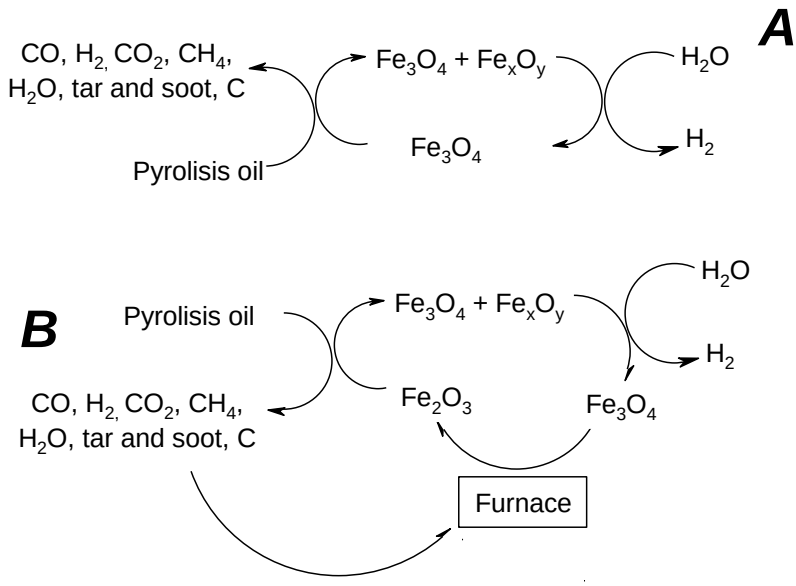

Figure 1-5. Two reaction schemes proposed by Bleeker et al.[112,113]

In the part B of the scheme, both iron oxide and lean gas from the reduction stage are oxidized in air for energy recovery, while in the first one only the produced gas can be used for this reason or for chemical upgrading too.

The main drawback is the coke deposition on the catalyst but the author suggests that C can also be used as a reducing material; so if we wait for the completion of this slow reaction, carbon deposition can be completely avoided, obtaining a high H_2 quality.

1.4.2.5 Biomass gasification gas

The use of biomass-derived gas is a very important topic if we think about a distributed production of hydrogen. The use of small-size plant is demonstrated to be economically competitive and with a sufficient hydrogen quality required for all Fuel-Cell applications[114].

Papers dealing with the utilization of this reducing fuel have been reported since 1998[115], in which the system used for the catalytic tests was fed with a gas similar to that one derived from biomass gasification. In the following years, integrated plants were proposed, both with a direct integration of the gasification part[116,117,118] and with the fuel-cell final utilization[114].

1.4.3 Steam-iron process: modified materials analysis

Another kind of works deal with the comparison of different materials, without focusing on the type of reducing fuel, that is considered like a "probe molecule". Anyway, in the last paragraph about the different reducing fuels employed, some articles with the focus on the solid material have been already discussed.

One of the best works in this direction was published by Otsuka et al. in 2003[119], where 26 elements were analyzed as promoters for iron oxide in small quantities (3% molar), and three different classes of materials where finally distinguished. According to Lorente et al.[120]:

- *Elements aimed at preventing deactivation*
  Al, Sc, Ti, V, Cr, Y, Zr, Mo and Ce

- *Elements with neutral/negative effect on stability*
  Mn, Co, Ni, Cu, Zn, Ga, Nb, W and Re

- *Elements aimed at Improving the reaction rate for oxidation:*
  Mg, Ca, Ru, Rh, Pd, Ag, Ir and Pt

After this classification, several researches have focused on the combination of at least two elements, in order to find the right synergy.

One of these studies was carried out by Lorente et al.[121], by means of changing the concentration of the dopant in the 1-to-10% range.

Three-elements systems have also been studied; for instance, Tatenaka et al. proposed the combination Mo and Rh[122], and of Cr and Ni with a variety of other elements[100,123]; Ryu et al.[124] proposed a 3% doping of iron oxide with two elements: they reported a classification of these elements perfectly in agreement with the Otsuka's one. Finally, a work from Lee et al.[125] report the doping with CeO_2 of a Fe/Zr/Rh (1/0,3/0,03) oxide material.

A different approach is the use of a mixed ferrite, like in the thermochemical cycling reported in the paragraph 1.3.5.4. dealing with Mixed Ferrite cycles. Examples of this approach were reported by Kodama et al.[105], Lorente et al.[93] and Kang et al.[102,103,104].

1.5 Aim of the thesis

My thesis work has been focused on the study of the Steam-Iron process using MeOH as the carbon-based reducing agent, as reported in Figure 1-6

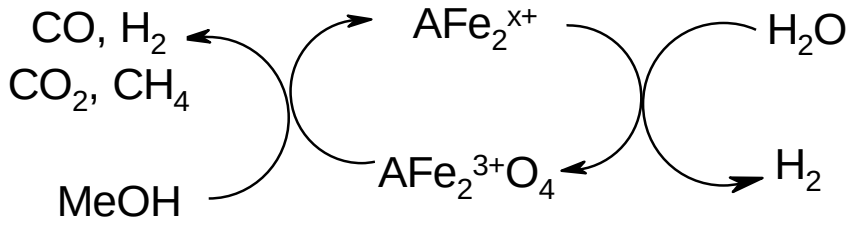

Figure 1-6. Steam-iron process with MeOH (A=Fe, Ni, Co)

The choice of MeOH is due to two main reasons:

1. as a probe molecule: the light compounds deriving from this reaction can be easily analyzed and used as “indicators” of the changes occurring in the material during the reduction step.
2. as a new approach to the bio-alcohols use in the steam-iron process

The use of various mixed ferrites will be useful to understand the differences between oxides in regard to the reaction products, morphological changes and cycles reproducibility.

Catalytic tests were performed mainly to understand the behavior of the materials during the complete reduction; then, shorter reduction steps followed by reoxidation with water were carried out, for hydrogen production during repeated cycle tests.

Characterizations of the fresh and used materials have been made in order to understand which modifications occur after use in complete redox cycles.

Finally, in-situ and ex-situ characterization of reduced materials has been carried out on $CoFe_2O_4$ in the aim of understanding the general behavior of the solid during the first reductive step. From these results, a different behavior in function of the chemical-physical properties of the Co ferrite was observed: for this reason, the first part of the Results and Discussion chapter is focused on these results, even though they are not strictly related to the final aim of my work.

The ultimate aim of this work is the identification of the advantages and drawbacks of each material used, and the consequent improvement and optimization of the redox cycle.

2 Experimental part

2.1 Synthesis of the materials

All the ferrites used have been prepared using the co-precipitation method described elsewhere[126].

Coprecipitation

An aqueous solution, 1M in $Fe(NO_3)_3*9H_2O$ and 0,5M in $Me(NO_3)_2*6H_2O$ (Me=Co,Ni), is slowly dropped into a solution of 2M NaOH of volume which is three times higher than that of the cations solution volume. For the synthesis of magnetite (Fe_3O_4), $Fe^{II}SO_4*7H_2O$ is used as precursor instead of the nitrate salt.

All along the dropping period, the pH is monitored and maintained over 13 with the addition of NaOH 6M, while the temperature of the NaOH solution is maintained between 50°C and 60°C. Finally the solution is digested for 1 hour.

The precipitate is recovered by vacuum filtration and washed with at least 1L of demineralized water per gram of final solid weight, in order to remove the Na^+ and NO_3^- ions.

Thermal treatments

In the case of Co-ferrite and Ni-ferrite, the filtered solid is dried in air at 120°C, while for magnetite the drying temperature is 80°C (in order to avoid the oxidation of Fe^{2+} to Fe^{3+}). These compounds are the precursors of the final mixed oxides, and therefore are labelled as CFp, NFp and FFp.

Finally, CFp and NFp are annealed in static air at 450°C (CF450 and NF450) or at 750°C in the case of CF750. FFp is calcined at 450°C too but in N_2 flow, in order to avoid the complete oxidation of iron into hematite. This compound is employed in catalytic tests within 2 months from the synthesis, again to prevent its oxidation.

2.2 Characterization techniques

2.2.1 XRD

XRD patterns are registered with a Philips PW 1050/81 controlled by a PW1710 unit (λ=0.15418nm, 40kV, 40mA). The range of analysis is 10°<2θ<80° with a scanning rate of 0,05°/s and Time-per-step=1s.

The interpretation of the patterns is made by using a software from PANalytical Company using the “ICSD Database FIZ Karlsruhe” library. The Debye-Scherrer equation is used for the calculation of crystallite dimensions, which is related to the FWHM (Full Width at Half Maximum) through the formula

$$\tau = \frac{K\lambda}{\beta \cos\theta}$$

K is the shape factor, λ is the x-ray wavelength, β is the line broadening at half of the maximum intensity (FWHM) in radians, θ is the Bragg angle and T is the mean size of the ordered (crystalline) domains.

2.2.2 BET analysis

The instrument used for specific surface area measurement is the Carlo Erba Sorpty 1700 based on the single point B.E.T. adsorption model

(Brunauer Emmet Teller). The method calculates the surface area of the sample from the volume of the gas corresponding to the monolayer adsorption. So, the variable that has to be measured from the analysis is the gas volume for the monolayer adsorption.

The single-point approximation is based only on one measurement of the pressure of adsorption and the corresponding gas volume adsorbed; the formula used is here reported:

$$\frac{P}{V(P_s - P)} = \frac{c-1}{V_m \cdot c} \cdot \frac{P}{P_s} + \frac{1}{V_m \cdot c}$$

where P is the pressure, P_s is the surface tension of the adsorbed gas (nitrogen in this case), V is the adsorbed gas volume, Vm is the monolayer gas volume and c is a constant related to the gas-surface interaction.

A second approximation made by the instrument software is that the constant *c* is very high compared to the other variables and so the final equation is

$$\frac{\mathrm{P}}{\mathrm{V}(\mathrm{P_s} - \mathrm{P})} = \frac{1}{\mathrm{V_m}} \cdot \frac{\mathrm{P}}{\mathrm{P_s}}$$

The percent error that derives from these approximations is about 5% on values over 3 m^2; below this limit, the surface area calculated cannot be considered reliable.

0.5g of the sample is placed inside the sample holder and the solid is heated at 150°C under vacuum (4 Pa) for the desorption of all the molecules adsorbed on it (for instance water and air). Secondly, the sample is put in liquid nitrogen and then the adsorption of the gaseous N_2 is carried out.

2.2.3 Temperature programmed analysis (TPR/TPO)

Temperature programmed analysis are very common analysis in catalysis for the study of the redox properties of the materials. The instrument used is the TPD/R/O 1100 *catalytic surface analyzer* of Thermo Quest Company.

TPR is a chemical reduction of the solid under analysis by a reducing gas with a progressive increasing of the temperature. In this case, a 5% H_2 in Ar is used as the reducing gas and the temperature program is

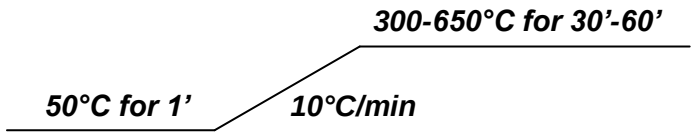

The incoming and the one passed though the sample are compared using a TCD detector; when the H_2 is consumed by the reduction, a signal is shown in the graph, demonstrating the presence of a redox species in the catalyst.

TPO analysis is commonly performed after the TPR one in order to recover the original oxidation state of the sample; the oxidizing gas used is 5%O_2 in He and the temperature ramp is always the same of the TPR one.

Usually, different TPR/O cycles are repeated in order to analyze the possible recovery of the original state after the first reduction; in this thesis, for instance, a three-cycle analysis is performed on CF450.

2.2.4 Infrared analysis

Infrared analysis has been collected at the “Dipartimento di Chimica IFM” of the Università degli Studi di Torino.

FTIR spectra in the mid-infrared region were obtained at 4 cm^{-1} resolution on a Bruker IFS113v spectrophotometer equipped with MCT cryodetector, and on a Bruker IFS88 spectrometer with DTGS detector, when it was necessary to reach lower wavenumbers. All samples were examined either in situ in the form of self-supporting pellets of the material as such (~20 mg cm^{-2}), or (in air) mixed with a proper amount of KBr powder (1:10 weight ratio). The spectra of probe molecules adsorbed on sample pellets were obtained with the solid sample contained in a home-made quartz cell, equipped with KBr windows, connected to a conventional high-vacuum line (UHV) that allows samples activation and spectra acquisition on the materials of interest in strictly in-situ conditions. Prior to spectroscopic analyses, sample pellets were preliminarily activated at 350°C (623 K), either in vacuum or in oxidizing conditions in the presence of O_2.

Far-infrared measurements were recorded at 2 cm^{-1} resolution on a Bruker Vertex 70 equipped with a Si beam splitter and a DTGS detector for far-IR region. Samples were examined in air in the form of self-supporting pellets mixed with a proper amount of paraffin wax. This material, unlike KBr powder, is transparent to IR radiation in the 400-100 cm^{-1} range.

2.2.5 X-ray photoelectron spectroscopy

XPS is a spectroscopy technique used for the quantitative analysis of the chemical composition of a solid surface.

Physically, the solid material under investigation adsorbs an X-ray photon, which allows the releasing of an electron from one of the surface atoms. XPS analyzes the kinetic energy distribution of the emitted photoelectrons to study the composition and electronic state of the surface region of a sample; the resulting peaks indicate the presence of a specific element in the sample. The quantification of the element on the surface is possible because of the linear relationship between the concentration of the atoms and the quantity of electrons emitted from each of them.

XPS was performed using an AXIS Ultra XPS spectrometer, operated at 13 kV and 10 mA with monochromator Al Kα radiation (1486.6 eV)., in collaboration with IRCE of French CNRs.

As it will be observed, C atoms are found even in the unused samples: this is caused by the reaction between the basic solid material with the atmospheric CO_2 that gives carbonate species on the catalyst surface. For this reason, the material is usually pretreated at 300°C in an inert gas before the catalytic reactions, but it was impossible to perform this treatment before XPS analyses.

2.2.6 Mössbauer spectroscopy

Mössbauer spectroscopy is a spectroscopy technique based on the Mössbauer effect, which consists in recoil-free, resonant adsorption and emission of γ-rays in solid materials. This technique probes very little changes in nuclear energy levels, which are depending on the electronic and chemical environment of the nucleus. The main nuclear interactions considered for the interpretation of the resonance spectra are three: isomer shift, quadrupole splitting and magnetic (or hyperfine) splitting.

One instrumental limitation is the need of a suitable γ-rays source for the element under investigation, which is usually generated by the employment of radioactive parent that decays to the desired isotope. It means that each atoms that can be analyzed by this spectroscopy needs the use of one particular radioactive source.

In this thesis, Mössbauer Spectroscopy has been used to analyze the characteristics of iron atoms in the fresh, used and reoxidized cobalt ferrites samples. A ^{57}Co/Rh γ-ray source and a conventional constant acceleration Mössbauer spectrometer were used for spectra collection. Isomer shifts are given with respect to α-Fe. All spectra were taken at room temperature and in ambient atmosphere; the Cobalt Ferrite samples were diluted in sucrose at about 50%$_w$ concentration to avoid auto adsorption and the spectra have been collected for about 24h each. The integrated areas under individual deconvoluted signals have been used to obtain the relative amounts of the different iron species, assuming an equal free recoil fraction for all these iron species.

2.3 Catalytic tests

2.3.1 Catalytic tests equipment

Catalytic investigations have been performed using a bench-scale plant that is schematized in Figure 2-1. The plant can be divided in three different zones: the feeding zone, the reactor and the analysis of outcoming gases. All the pipes used before and after the glass reactor are made by AISI 316L steel and have an external diameter of 1/8''.

Zone I

Nitrogen is used as inert gas during the reaction and its flow is controlled by a Brooks's mass flow meter with a 5-120sccm range (n°2 in the

figure). Then a pressure indicator and a flow meter controller are used to control both the overall pressure in the plant and the real flow of the inert gas, for safety reasons.

After, a Precidor Type 5003 (INFORS HT®) pump (n°5) is used to feed the liquid reactants (MeOH or water) within a range of 0,001ml/min-1ml/min if using a 5ml syringe (n°6). The liquid/gas mixture is heated at 140°C using a caulked resistance (n°7) in order to vaporize the reactant in the pipeline; and then the diluted vapors are fed into the reactor.

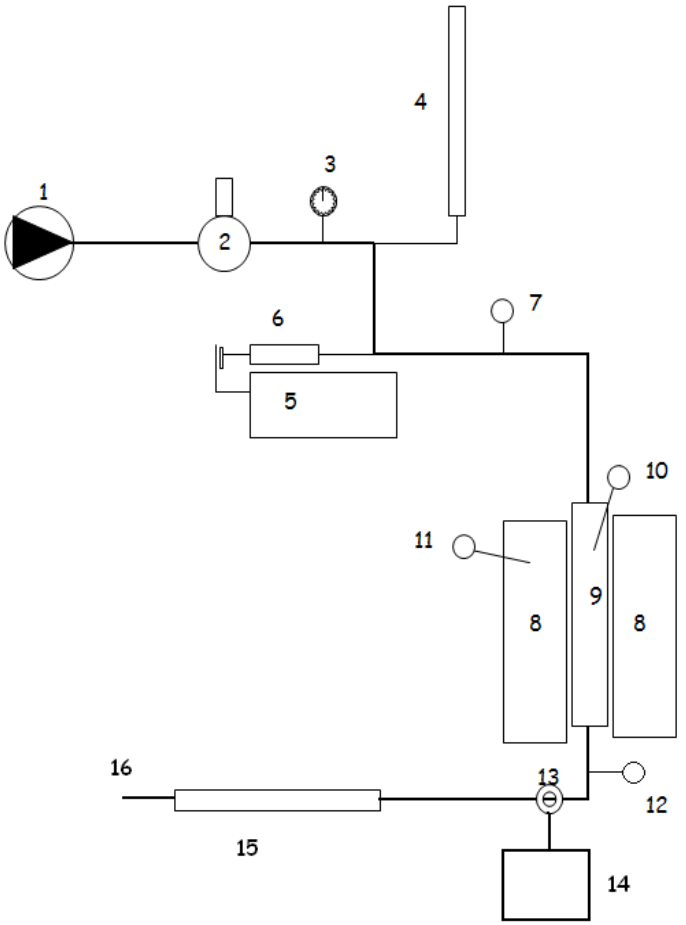

Figure 2-1. Scheme of the laboratory plant

1) Inert feed
2) Mass-flow meter
3) Pressure indicator
4) Flow verify with bubble flow meter
5) Infusion pump for liquid feed
6) Syringe for liquid solutions feeding
7) Temperature indicator
8) Oven
9) Glass reactor
10) Temperature indicator of catalyst bed
11) Oven temperature indicator
12) Temperature indicator
13) Vapor phase sampling
14) MicroGC
15) Flow verify with bubble flow meter
16) Vent system

Zone II

The reactor is made of glass and this is why the maximum temperature allowed for the tests is 480°C. The internal diameter of the reactor is 0,5cm and the length is 30cm. The catalyst bed is placed at the half height of the reactor, where the furnace (n°8) has an isothermal zone the temperature of which is very close to the set point.

The catalyst used is shaped in pellets of 30/60mesh (0,25-0,6mm) size, in order to limit friction losses. Usually 400mg of catalyst is charged for each catalytic test, that corresponds to a 0,3cc of catalyst volume.

The final part of the reactor, after the catalyst bed, is filled with an inert compound (usually corundum) to reduce the volume between the reaction zone and the analysis zone.

Zone III

The final part of the plant starts at the end of the reactor and it's made of a heated pipeline with temperature of at least 200°C. Then, there is a two-valve system used for the two steps of reaction. During the first step of reduction with methanol, the two valves are interconnected by a heated pipeline that is maintained at 140°C through a temperature controller; this is necessary to avoid the condensation of products such as water, unconverted methanol and intermediate compounds. For the

reoxidation step, during which water produced could reach a 30%$_v$ concentration, the two valves are linked by a RT pipeline within an adsorbing device filled with, drierite with a Co-based indicator of the saturation level. This drying procedure is required because the analysis instrument (MicroGC) cannot stand such a high water concentration, which can eventually block the pumping system inside it (usually a 5%$_v$ is considered as the upper concentration limit).

After the two-valves system, the inlet of the MicroGC is connected to the pipeline where the sample gas passes through; the GC will sample the gas by pumping in only a small fraction of the total gas flow. After this connection, the main pipeline is linked to a bubble flow control system followed by a crystal tube for the final venting of the gas.

The MicroGC is a Agilent MicroGC 3000A equipped with three modules; this system allows to perform chromatography analysis of light compounds (only C1, C2 and C3 and some of light C4 compounds can be eluted). The features of each column are now summarized:

- ***Column A***
  - Separation phase PlotQ
  - carrier He
  - separation of CH_4, CO_2, H_2O, MeOH
- ***Column B***
  - Separation phase OV1
  - Carrier He
  - Separation of CO_2, formaldehyde, H_2O, MeOH, methyl formate and formic acid
- ***Column C***
  - Separation phase Molecular sieve 5A
  - carrier Ar
  - Separation of H_2, O_2, N_2, CH_4, CO

- Backflush column PlotU (precolumn of CO_2 and H_2O purging)

2.3.2 Catalytic tests parameters and calculations

Reduction step

The first step of the chemical looping process is the anaerobic oxidation of MeOH by the iron-based oxide.

The temperature used for this step is comprised between 300°C and 420°C while the concentration of MeOH is fixed at 15,6%$_v$ in N_2. The resulting residence time deriving from the following equation

$$\tau(s) = \frac{V_{cat}\,(ml)}{\dot{V_{tot}}\,(ml/_s)}$$

is comprised between *0,20s* and *0,25s* for all the catalytic results shown. Only in few cases (see paragraph 3.1 and paragraph 3.3.2) a five-time higher residence time is used in order to reduce the reaction rates of the two steps.

Concerning the data interpretation, the results deriving from the MicroGC analysis are the %$_{vol}$ of all the compounds present in the outlet gaseous mixture. Because of this reason, the equations used for data elaboration are:

$$Y_{P,A} = \frac{\dot{n}^{P,out}}{\dot{n}^{A,in}} = \frac{\%_v^{P,out} * \dot{V}_{tot}^{out}}{\%_v^{Ain} * \dot{V}_{tot}^{in}} = \frac{\%_v^{P,out}}{\%_v^{A,in}} * F_{Vol}$$

$$X_A = \frac{\dot{n}^{A,in} - \dot{n}^{A,out}}{\dot{n}^{A,in}} = 1 - \frac{\%_v^{A,out}}{\%_v^{A,in} * F_{Vol}}$$

*A generic reaction A→ P is considered.

Stoichiometric coefficients have been considered for the calculations

As it's possible to notice, the Volume Factor (F_{vol}) is required to complete the calculations; this value is experimentally obtained by using N_2 as an internal standard.

$$F_{Vol} = \frac{\%_v^{N_2,out}}{\%_v^{N_2,in}}$$

Finally a normalization step is required in order to reset the very little variations deriving from the feeding system. In this study, normalization calculations are based on the yield sum of H-containing compounds which has to be 100%. The other elements fed (C and O) cannot be used as normalization elements because C shows a balance lower than 100% because of coke deposition, while the O balance is sometimes higher than 100%, because of the oxygen release by the oxide that is progressively reduced. As a consequence of this, the normalization of the concentration of all the compounds is obtained by dividing the experimental values by the yields sum of the H-containing products (which are mainly H_2 CH_4 and H_2O).

Due to the very high frequency of the analysis, a Visual Basic program has been written in order to perform all the calculations during the catalytic test.

This program also builds up many graphs that visualize parameters characteristic of the test; hereafter we report the description of these graphs:

1. Conversion and yields of the products as a function of time on stream (tos)

2. Conversion and yields of the intermediate products during tos

3. Oxygen balance and reduction degree of the material

The oxygen balance is a very important parameter in the aim of evaluating how much oxygen is delivered from the oxide during reduction. When finally this parameter stabilizes around the 100% value, the reduction is complete; furthermore, the integral value of the Oxygen Balance exceeding 100% gives the quantity of oxygen furnished by the oxide. This value can be compared to the total amount of oxygen present in the fresh catalyst, calculated from the stoichiometric formula of the oxide. The result gives the reduction degree of the catalyst during the first step as calculated from the product yields.

$$\%_{reduction}\ (t) = \frac{\int_0^t (Oxygen\ balance - 100) * \dot{n}_{MeOH}^{in}}{n_O^{solid}}$$

4. F_v and mass balance

   This graph shows the Volume Factor as a function of time-on-stream and the total mass balance, that is the sum of the H-containing compounds concentrations before the normalization process (an important parameter for monitoring the correct behavior of the feeding system).

5. Integral values

   This graph is a histogram plotting the conversion of MeOH and the average selectivities obtained from the integration over selected periods of time of the corresponding instantaneous values obtained from each single analysis.

Oxidation step

During this step, steam is made react with the reduced solid. As we described before, water is removed before the MicroGC sampling in order to avoid problems to the analytical instrumentation.

For this reason the first calculation done, with the aid of a Visual Basic program, is carried out to derive the real concentrations ($\%_{vol}$) before water removal.

$$Conc^{vol,i} = \%_{GC}^{vol,i} * \frac{\%_{in}^{vol,N2}}{\%_{GC}^{vol,N2}} \qquad (\text{where i} = H_2O, CO_2, CO, CH_4)$$

$$Conc^{vol,H2O} = 100 - Conc^{vol,H2} - \%_{in}^{vol,N2}$$

$$\%_{real}^{vol,j} = \frac{Conc^{vol,j}}{\sum Conc^{vol,j} + \%_{in}^{vol,N2}} \qquad (where\ j = H_2O, CO_2, CO, CH_4)$$

After, yields and selectivities are calculated and three main graphs are finally obtained:

1. %vol of the main compounds that are typically H_2, CO_2 and H_2O (without considering the inert gas) as a function of time on stream
2. Yields of H_2 and CO_2 as a function of time-on-stream
3. Yields of secondary products such as CO and CH_4

Product yields are calculated from the standard formula shown in the first part of this paragraph, dealing with the reduction step (see pag.65). Finally, integral values of the H_2 and CO_2 produced are made by integrating all the instantaneous values of yields of these two products, multiplied by the water incoming moles.

The last point to underline concerning this step is a visualization issue. Sometimes the most important moments of the reoxidation step are the very first minutes, because the initial water conversion is usually the highest. However, the water diffusion gives us an initial point where the yield of hydrogen is not the highest one; if the reactor were a perfect PFR, the first point of analysis would show the highest yield in hydrogen.

Repeated cycles

Repeated cycles are carried out in order to study if the oxide may withstand several redox changes, and therefore if the results obtained during the first cycle can be reproduced also during several cycles. Both catalytic tests and characterization of used materials are required to better understand the phenomena that take place in the oxides.

The data analysis for each reduction and oxidation step is made with the method explained in the previous paragraphs. However three main graphs which allow to infer a complete picture of cycles' results are drawn:

1. Reduction steps

   In this first graph, the integral values obtained for each reduction step are reported; furthermore, the final reduction degree of the catalyst is shown. This graph is useful to see how the conversion and yields of the products change from one reduction to the following one; in this way, deactivation phenomena can be immediately noticed; the loss/maintenance of the oxidizing power is well seen in this type of graph too, evaluating the reduction degree trend.

2. Correspondence between the hydrogen produced and the final reduction degree

   The hydrogen integral value, calculated from values obtained during the reoxidation step, is strictly related to the reduction degree of the catalyst obtained during the first step; in this graph we can easily see this relation for each cycle.

3. Ratio between the amount of hydrogen produced and of deposited carbon

   Hydrogen produced during the second step derives from the reoxidation of the material by water and from the gasification of coke too; for this reason, it's important to understand how much hydrogen derives from each reaction. Obviously higher values of this ratio are better than low ones because they demonstrate that hydrogen is produced from the desired reaction, where the material redox pair is involved, and not from the gasification of the carbon which had been deposited during the first step.

2.4 Safety issues about used materials

The main materials used during this research can be classified in three main categories: compounds used for catalyst synthesis, reactants, and products of reaction.

Actually, the products produced during the catalytic steps are in a very low amount because of the very low quantity involved in the reactions; secondly, all these products are immediately fed to the venting system. For these reasons, the analysis of the safety issues of these compounds is not reported in this thesis. The only thing to underline is that the most dangerous product formed is CO that is a highly toxic compound.

2.4.1 Catalysts synthesis

During catalysts synthesis these materials were used: nitrate salts as sources for the cations, NaOH and water. Except from water, all the other products show some dangerous issues, hereafter reported.

NaOH

May cause chemical burns, permanent injury or scarring if it contacts unprotected human; it may cause blindness if in contact with eyes. PPE is required such as such as rubber gloves, safety clothing and eye protection. The dissolution in water is a highly exothermic reaction and the resulting heat may cause heat burns or ignite flammables; avoid the use of NaOH solution with metal vessels.

Cobalt nitrate hexahydrate

It's a strong oxidizer: the contact with other material may cause fire. It is harmful if swallowed or inhaled and causes irritation to skin, eyes and respiratory tract. Chronic exposure may affect thyroid, lungs, heart, and kidneys.

Nickel nitrate hexahydrate

Like other nitrates, nickel nitrate is oxidizing, so that caution should be exercised when it contacts with reducing materials such as organic substances. It is also irritating to the eyes, skin and, upon inhalation of the dust, respiratory tract. It may cause skin allergy. Nickel nitrate is a carcinogen, along with most other nickel compounds. The nickel ion is also toxic to aquatic organisms.

Iron(III) nitrate nonahydrate

It may causes slight irritations if inhaled, ingested or in contact with skin. Under some circumstances methemoglobinemia occurs in individuals when the nitrate is converted by bacteria in the stomach to nitrite; chronic exposure may cause liver effects.

Iron sulphate heptahydrate

It is a non-combustible but excessive heat may decompose the material, liberating irritating and toxic sulphur dioxide gas. Contact with water in an emergency situation may generate an acidic solution that can pose a

threat to water courses. The material is mildly irritating to eyes and skin but is relatively non-toxic and poses little immediate hazard to emergency response personnel.

Iron oxides

Iron oxides synthesized are generally non-toxic compounds. The only dangerous issue is that Nickel Ferrite may cause cancer because of the presence of Ni^{2+} in the formula: careful handling and use of PPE is required.

2.4.2 Reactants

Methanol shows some dangerous issues that are hereafter reported.

Methanol

Methanol has a high toxicity in humans. If ingested as little as 10 mL of pure methanol can cause permanent blindness by destruction of the optic nerve, and 30 mL is potentially fatal, although the median lethal dose is typically 100 mL. Toxic effects take hours to start, and effective antidotes can often prevent permanent damage. Because of its similarities to ethanol (the alcohol in beverages), it is difficult to differentiate between the two (such is the case with denatured alcohol).

Methanol is toxic by two mechanisms. First, methanol (whether it enters the body by ingestion, inhalation, or absorption through the skin) can be fatal due to its CNS depressant properties in the same manner as ethanol poisoning. Second, in a process of toxication, it is metabolized to formic acid (which is present as the formate ion) via formaldehyde in a process initiated by the enzyme alcohol dehydrogenase in the liver.

The initial symptoms of methanol intoxication include central nervous system depression, headache, dizziness, nausea, lack of coordination,

confusion, and with sufficiently large doses, unconsciousness and death. The initial symptoms of methanol exposure are usually less severe than the symptoms resulting from the ingestion of a similar quantity of ethanol. Once the initial symptoms have passed, a second set of symptoms arises, 10 to as many as 30 hours after the initial exposure to methanol, including blurring or complete loss of vision and acidosis. These symptoms result from the accumulation of toxic levels of formate in the blood, and may progress to death by respiratory failure. Small amounts of methanol are produced by the metabolism of food and are generally harmless, being metabolized quickly and completely.

3 Results and discussion

3.1 On the chemical-physical properties of $CoFe_2O_4$

Co-ferrite has been annealed at different temperatures in order to obtain samples with different structural properties, with the aim of studying how the morphological features could influence the redox properties of these oxides.

3.1.1 The effect of thermal annealing on bulk characteristics

Table 1 compiles the main chemical-physical features of the $CoFe_2O_4$ samples after thermal treatment at two different temperatures, 450°C (CF450) and 750°C (CF750); these same samples were studied as catalysts for phenol gas-phase methylation with methanol in a previous work from this research group[126]. The table also reports the characteristics of some samples after redox cycles; these results will be discussed later on in this thesis.

The phase and variation in crystallite size was probed by powder XRD (Figure 3-1). The dried CF sample and the calcined CF450 and CF750 samples reveal a series of reflections consistent with the $CoFe_2O_4$ spinel structure. However, the temperature of calcinations has a profound effect on morphological features; Scherrer line broadening analysis on the (220), (311), (511) and (400) peaks reveal that the volume-averaged crystallite size increases from 12nm for CF450 to 36nm for CF750 (Table 3-1. Main characteristics of samples prepared). Particle sintering and

growth is accompanied by a significant decrease in surface area from $70 m^2 g^{-1}$ to $10 m^2 g^{-1}$.

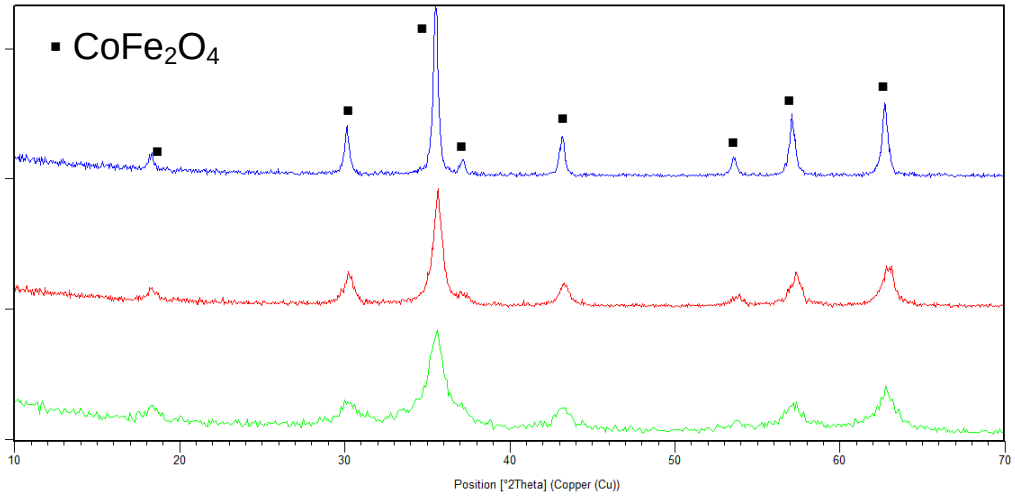

Figure 3-1. (from the bottom) XRD of CFp, CF450 and CF750

Sample	***Treatment of the sample***	***SSA (m^2/g)***	***Crystallite size (nm)***
CF450	Calcined (no reduction)	70	12
CF450	T 300°C, 30 min, τ 0.25 s	30	-
CF450	T 300°C, 300 min, τ 0.25 s	35*	-
CF450	T 420°C, 30 min, τ 0.25 s	9	-
CF450	T 420°C, 30 min, τ 1 s	23	32
CF450	T 420°C, 180 min, τ 1 s	11	64
CF750	Calcined (no reduction)	10	36
CF750	T 300°C, 30 min, τ 0.25 s	10	-
CF750	T 300°C, 300 min, τ 0.25 s	26*	-
CF750	T 420°C, 30 min, τ 0.25 s	10	-
CF750	T 420°C, 30 min, τ 1 s	10	35
CF750	T 420°C, 180 min, τ 1 s	7	57

Table 3-1. Main characteristics of samples prepared

Reoxidation was carried out in all cases at 420°C for 1 h, using a 29% steam in N_2 flow, with contact time of 0.25s or 1.0s
* high value due to contribution of coke deposited on the material

HR-TEM microscopy of annealed samples further confirms what has been deduced from XRD analysis. TEM images (reported in Figure 3-2. HR-TEM images of CF450 (left) and CF750 (right)) show crystalline particles with irregular shape with an average size of ~10 nm for CF450 and of ~25-30 nm for CF750 respectively; these values are similar to those calculated on the basis of XRD patterns. In both cases, particles contours are smooth and roundish.

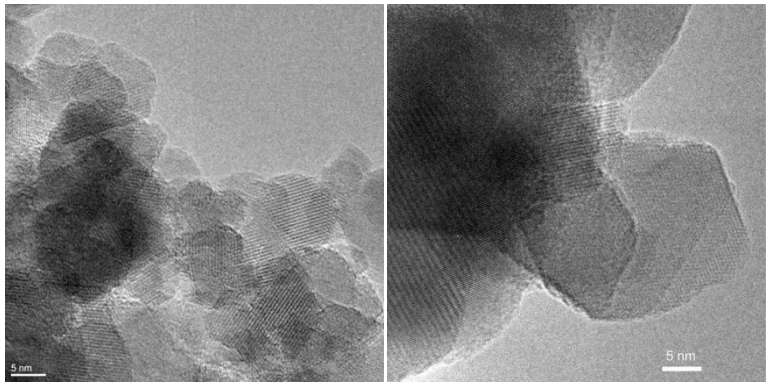

Figure 3-2. HR-TEM images of CF450 (left) and CF750 (right)

Infrared spectra of KBr pellets of the two fresh samples, recorded in the 900 - 400 cm^{-1} range, shows the presence of an intense and broad band centred at ~580 cm^{-1}, ascribable to one of the typical vibrational modes of cobalt ferrites[127,128] (Figure 3-3, top). In particular, this signal can be easily attributed to the Fe-O vibration in tetrahedral sites[129], whereas the octahedral site vibrations of Co-O and Fe-O cannot be observed, as they are expected to be located at wavenumbers lower than 400 cm^{-1} (which is the “cut-off” of KBr, present in both powder pellets and optics)[128].

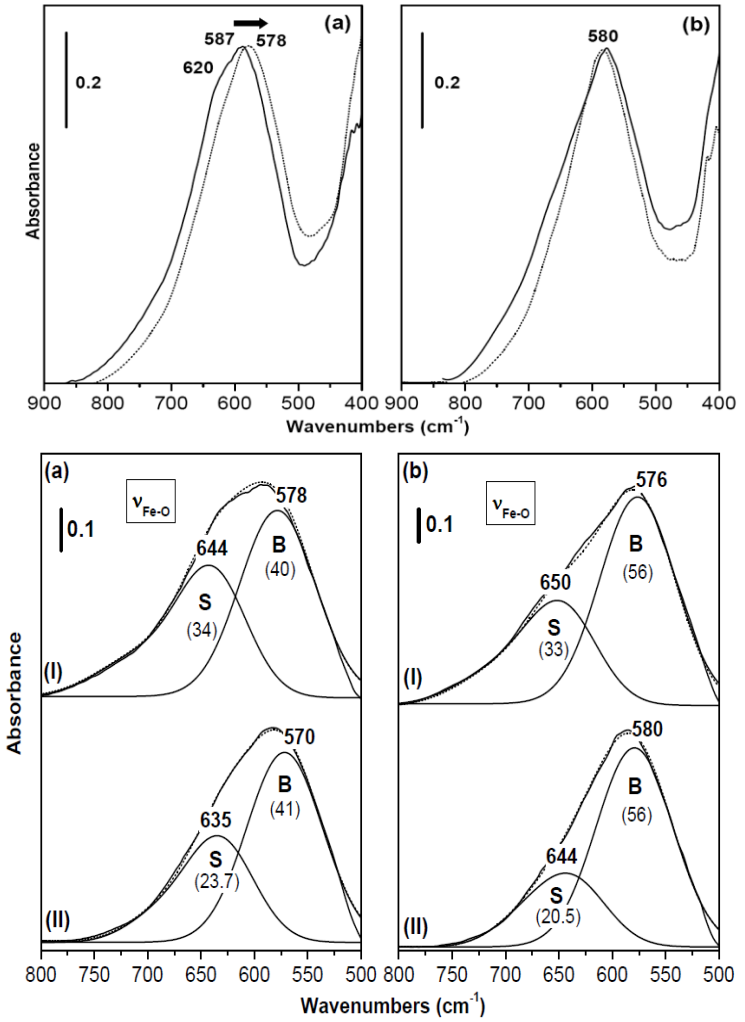

Figure 3-3. (*Top*): FTIR spectra in the 900-400 cm^{-1}range of KBr pellets of CF450 [section (a)] and CF750 [section (b)]. Full curves: calcined samples. Dotted curves: FTIR spectra of catalysts first completely reduced by contact with methanol at 420°C and then reoxidized with steam at 420°C. (*Bottom*): Band-resolved spectra in the 800-500 cm^{-1}range relative to CF450 [section (a)] and CF750 [section (b)]. Full-line complete spectra are the reconstructed ones, whereas broken-line traces are the experimental spectra. The numbers in brackets represent the integrated absorbance (cm^{-1}) of the individual spectral components. Section I: calcined samples. Section II: catalysts first completely reduced by contact with methanol at 420°C and then reoxidized with steam at 420°C.

For what concerns the fresh CF450 catalyst [section (a) of Figure 3-3, top] it is possible to distinguish two different and heavily overlapped signals, located at ~620 and ~587 cm^{-1}, respectively, both ascribable to Fe-O vibrations. In the case of the CF750 sample that possesses a much lower SSA with respect to the CF450 material, the 620cm^{-1} contribute is much lower (now we can observe only an asymmetric peak instead of a shoulder). This different contribution of this signal for the two samples can be probably attributed to the increased particles size, caused by sintering phenomena, in agreement with the literature[130,].

Band resolved spectra in the ν_{Fe-O} spectral range (800-500 cm^{-1}) of CF450 [section (a) of Figure 3-3, bottom] and CF750 [section (b)] point out the presence, in each band envelope, of two main components ascribable to the surface fraction of Fe-O modes (broad and asymmetric component at higher-ν, named S in the figure; this spectral component is made up of two symmetric sub-components of fairly different intensity, centred at 707 and 640 cm^{-1}, respectively) and to the bulk Fe-O vibrations (symmetric band at lower-ν, named B in the figure). It is possible to observe that the S/B integrated intensity ratio turns out to be appreciably different, depending on the calcination temperature; the S/B integrated intensity ratio was 0.85for CF450, whereas it was 0.59for CF750.

As mentioned above, the Me^{Oh}-O vibrations are expected to be located at wavenumbers lower than 400 cm^{-1} [127,128]. For this reason, spectra of CF450 and CF750 samples have been collected also in the far-IR region, as shown in Figure 3-4 (top). In both section (a) and (b), two distinct band envelopes are evident in the 600-200 cm^{-1} range, centred at ~580 cm^{-1} and ~360 cm^{-1}, respectively. The former envelope has been attributed above to Fe-O vibrations, whereas the latter one can be ascribed to Me^{Oh}-O vibrational modes (Co-O and Fe-O in octahedral sites)[128]. In the

case of the CF450 catalyst [section (a) of Figure 3-4, top] it is possible to distinguish two severely overlapped signals, approximately located at ~415 and ~360 cm^{-1}, respectively; as in the case of the Fe-O modes, the high-ν signal component can be ascribed to the surface fraction vibrations. In the case of the CF750 sample, a complex envelope of Me-O octahedral vibrations is evident in the spectrum at ~368 cm^{-1} [section (b)]. The shoulder at higher-ν (~415 cm^{-1}) is far less evident than in the case of the CF450 catalyst, confirming the main surface origin of this spectral component.

All the previous considerations can be confirmed by observing the band-resolved spectra reported in Figure 3-4 (bottom). In the case of octahedral vibrational modes, three different components can be observed. As anticipated above, the higher-ν component (termed S_1) can be ascribed to surface species, whereas the other two signals (termed B_1 and B_2 and located at ~370 cm^{-1} and ~310 cm^{-1}, respectively) are ascribable to Fe-O and Co-O bulk vibrations. In this case, it's impossible to calculate the S/B ratio of each species, because the S_2 component is probably overlapped to the B_1 vibration. So, we can only observe that in CF450 the S_1 component is higher, demonstrating again that the increase of the annealing temperature cause the decreasing of surface component in the spinel oxide.

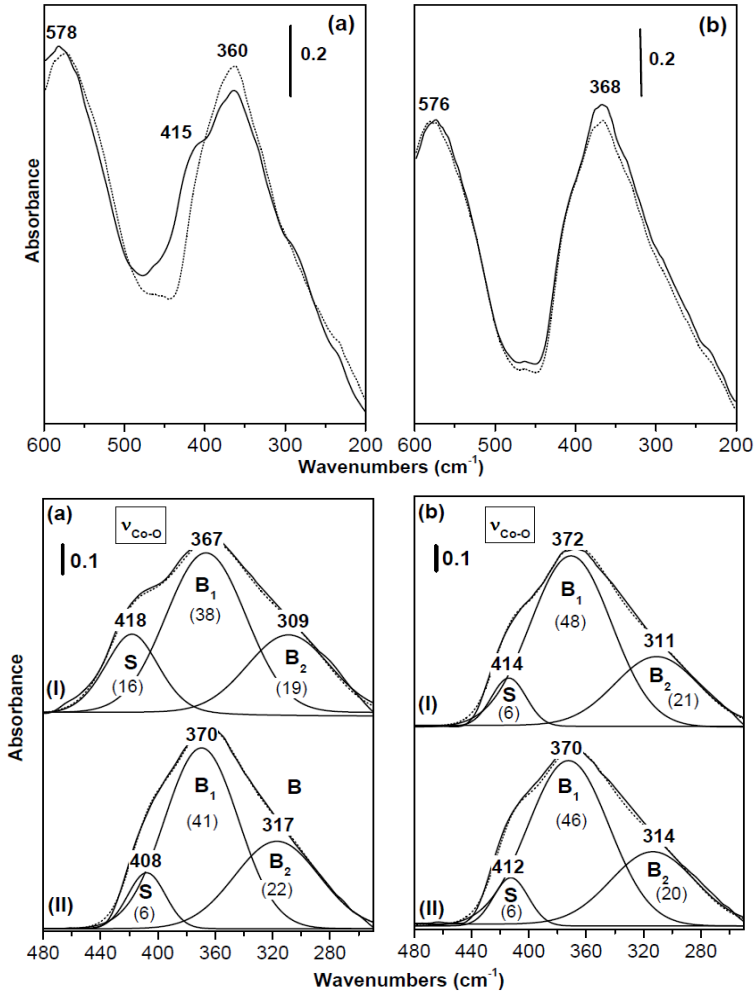

Figure 3-4. (*Top*): FTIR spectra in the 600-200 cm^{-1}range of paraffin wax pellets of CF450 [section (a)] and CF750 [section (b)]. Full curves: calcined samples. Dotted curves: FTIR spectra of catalysts first completely reduced by contact with methanol at 420°C and then reoxidized with steam at 420°C. (*Bottom*): Band-resolved spectra in the 480-250 cm^{-1}range relative to CF450 [section (a)] and CF750 [section (b)]. Full-line complete spectra are the reconstructed ones, whereas broken-line traces are the experimental spectra. The numbers in brackets represent the integrated absorbance (cm^{-1}) of the individual spectral components. Section I: calcined samples. Section II: catalysts first completely reduced by contact with methanol at 420°C and then reoxidized with steam at 420°C.

In $CoFe_2O_4$ inverse spinel, the (111) plane can be cut so that it exposes exclusively tetrahedral Fe^{3+} or octahedral Co^{2+}/Fe^{3+} sites; likewise the (100) face can expose a mixture of octahedral Co^{2+}/Fe^{3+} and tetrahedral Fe^{3+} sites or just octahedral Co^{2+}/Fe^{3+} sites. The equilibrium structure of small spinel clusters should expose more (111) and (110) faces whereas larger spinel clusters should be based on a (100) terminated structure. In a previous paper[126], we reported on how the surface composition of these oxide nanoparticles changed with their size (calcination temperature), with Fe content decreasing (the XPS Co/Fe ratio increased), indicative of a transition from (111) terminated to (110) or (100) terminated particles, with increasing crystallite size. The presence of highly reducible species in the smaller crystallites was attributed to the reduction of the Fe^{3+}-terminated (111) tetrahedral sites. Infrared spectra provide further information; the decrease of the S/B ratio is attributable to the lower contribution of surface sites, due to the increased crystallite size. As expected, CF750 shows a lower amount of both surface Co and Fe, due to its lower surface area.

3.1.2 The anaerobic oxidation of methanol

Figure 3-5 plots the conversion of methanol and the yield to the various products in function of the time-on-stream (tos), at the temperature of 300°C, for the CF450 sample; the bottom figure displays the detail of the firsts 50 minutes. Products were CO, CO_2 and H_2, with minor amounts of CH_4 and H_2O; the instantaneous amount of coke formed was determined by means of the C balance (see “Experimental part” chapter for details). Oxygenated products formed in very low amount (<1%), as detailed for each “Zone”(see below).

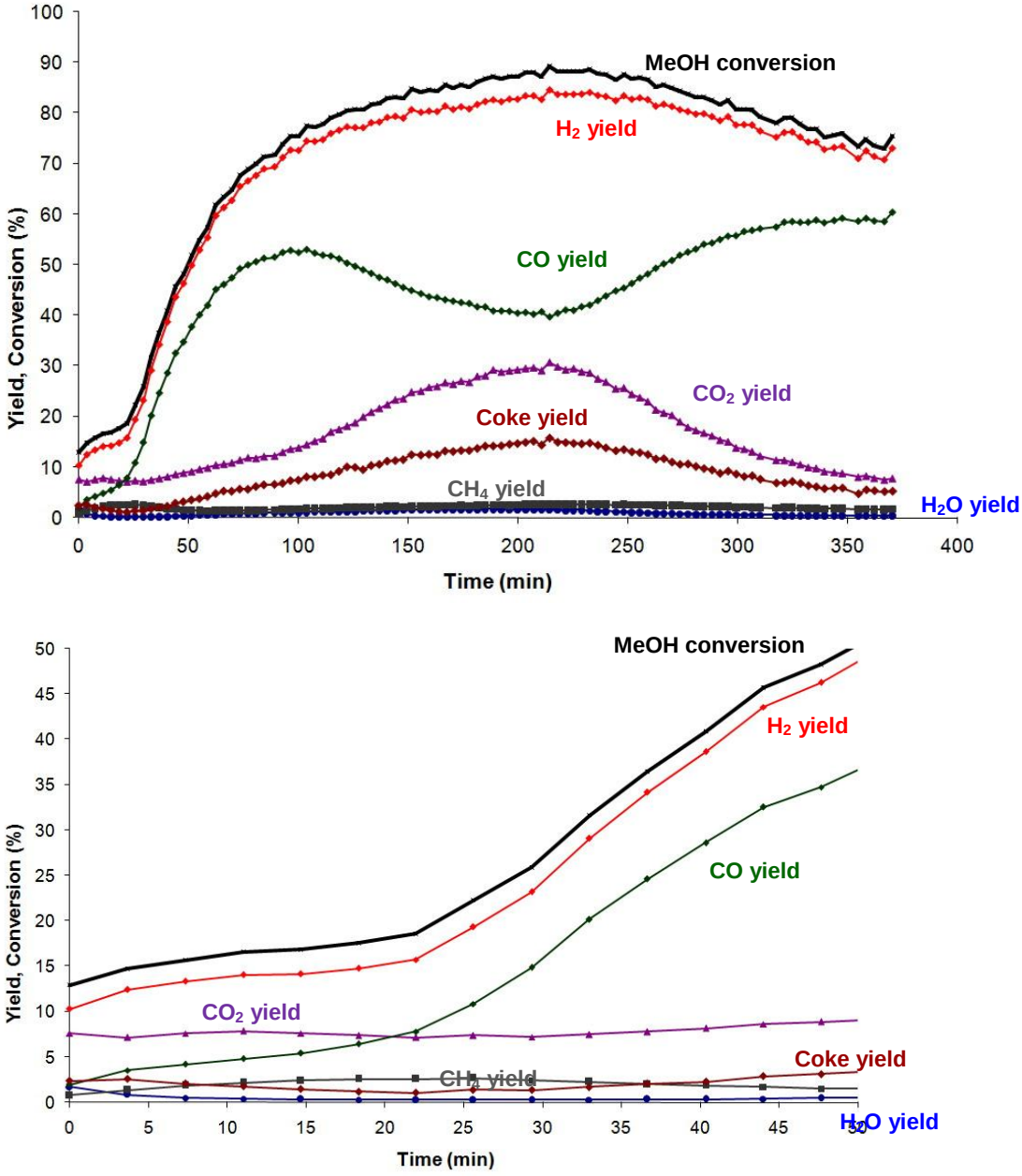

Figure 3-5. (*Top*) Methanol conversion and yields to products in function of the reaction time. Feed composition: 15.6mol% methanol, remainder N_2; overall contact time 0.2 s; temperature 300°C. (*Bottom*): detail of the first 50 min reaction time. Catalyst CF450.

Figure 3-6 plots the O balance in function of tos; a value of O balance higher than 100% indicates that the overall O content contained in products was higher than that fed to the reactor (i.e., contained in methanol), because of the O furnished by the solid. This allows calculating the degree of spinel reduction, which also is plotted in Figure 3-6, using the formula described in the experimental of this thesis.

The data registered highlight that the amount of each product was greatly affected by the degree of metal oxide reduction. Specifically, by combining results plotted in Figure 3-5 and Figure 3-6, we can distinguish different zones, during which the spinel underwent a progressive reduction by methanol:

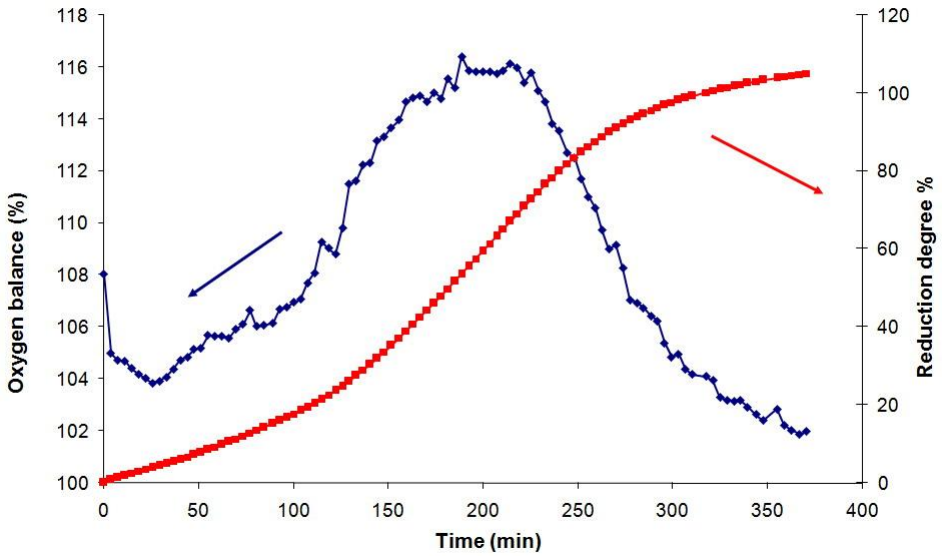

Figure 3-6. O balance and calculated degree of spinel reduction in function of reaction time. Conditions and catalyst as in Figure 3-5.

During the initial 22 min tos (Zone I), the conversion of methanol increased slowly from 13% to 19%; main products observed in Zone I were H_2 and CO_2, with low amount of coke also; at the very beginning,

these were the only products formed. However, the formation of CO and CH_4 (which was nil at the very beginning) increased during Zone I, and at the same time the formation of H_2 also increased and that of coke slightly diminished. Therefore, the reactions involved during Zone I were:

$$CH_3OH + Me^{n+}O \rightarrow CO_2 + 2\ H_2 + Me^{(n-2)+} \quad (1)$$

$$CH_3OH + Me^{(n-2)+} \rightarrow C + 2H_2 + Me^{n+}O \quad (2)$$

$$CH_3OH \rightarrow CO + 2H_2 \quad (3)$$

and

$$C + 2H_2 \rightarrow CH_4 \quad (4)$$

We can now exclude the hydrogenation of CO and CO_2 to account for methane formation, because both reactions would have led to the formation of H_2O, which instead did not form during Zone I, with the exception of the very first minutes reaction time, probably deriving from the total oxidation of the MeOH by the solid oxide.

$$CH_3OH + 2Me^{n+}O \rightarrow CO_2 + 2\ H_2O + 2Me^{(n-2)+} \quad (5)$$

Alternatively, the formation of coke might derive from Boudouard reaction:

$$2\ CO \rightarrow CO_2 + C \quad (6)$$

which however can be discarded (at least during Zone I), because small amount of coke formed from the very beginning, but CO did not.

During Zone I, we also observed the formation of oxygenated products, specifically: (i) methylformate (initial yield 0.11%, which became nil after 4 min tos); (ii) dimethoxymethane (initial yield 0.07%, nil after 4 min tos); (iii) formaldehyde (initial yield 0.01%, nil after 4 min tos); and (iv) formic acid (initial yield 0%, and then increasing up to 0.03% at the end of Zone I.

Figure 3-6 shows that during Zone I, the O released from the spinel because of reaction (1), reaction (5) and reactions leading to the formation of the light oxygenated compounds (first formaldehyde and then methylformate, etc) decreased. This is probably due to the decreased formation of these intermediate compounds and because of the slightly declining contribution of reactions (1) and (5).

During the period 22-100 minutes (Zone II), yields to CO and H_2 showed a similar rapid raise, and the same behavior was observed in regard to methanol conversion. This implies that reactions responsible for the decomposition of methanol into CO and H_2 occurred over sites the surface concentration of which increased during exposure to the reactants stream (for example, on the $Me^{(n-2)+}$sites generated by reaction 1); also the formation of CO_2 increased during Zone II. Therefore, during this Zone main reactions involved were:

$$CH_3OH \rightarrow CO + 2H_2 \qquad (3)$$

and

$$CH_3OH + Me^{n+}O \rightarrow CO_2 + 2\,H_2 + Me^{(n-2)+} \qquad (1)$$

Reaction (1) was the main responsible for the increasing degree of O uptake from the solid (Figure 3-6). Finally, also coke formation increased during Zone II, which means a raising contribution of either reaction (2):

$$CH_3OH + Me^{(n-2)+} \rightarrow C + 2H_2 + Me^{n+}O \qquad (2)$$

or reaction (6):

$$2\,CO \rightarrow CO_2 + C \qquad (6)$$

which might explain the parallel increase of CO_2 and C yield (however, reaction (6) cannot take account of the increasing O uptake from the oxide). A contribution to O uptake might also derive from the formation of

the oxygenated compounds: (i) formic acid, the yield of which increased from 0.03% (at 22 min tos) to 0.16% (after 100 min tos), and (ii) methylformate, a product showing a constant yield around 0.01%.

During the period 100-210 min tos (Zone III), methanol conversion increased and finally reached the maximum value of 88%. Yields to coke and CO_2 both increased (the latter more pronouncedly than the former, apparently because of the overlapping of two different contributions), and yield to CO decreased from the initial higher value of 53% down to 40% at 210 min tos. Yield to H_2 raised also, as also those to H_2O and CH_4 did (both remained however very low). Oxygen uptake from the solid showed a very rapid raise, which can be associated to the CO_2 yield increase. Therefore, main reactions occurring during Zone III were:

$$CH_3OH + Me^{n+}O \rightarrow CO_2 + 2H_2 + Me^{(n-2)+} \quad (1)$$

which explains the increase of CO_2 and H_2 yield, as well as the raise of O uptake from the solid, and

$$2\ CO \rightarrow CO_2 + C \quad (6)$$

which explains the raise of CO_2 and C and the concomitant decrease of CO yield, whereas the very low formation of H_2O may occur via total oxidation of MeOH (reaction 5).

Concerning the oxygenated compounds, during Zone III the yield to formic acid increased continuously, reaching the value of 0.40% after 210 min tos (the maximum however was obtained at 270 min tos, with 0.55% yield); methylformate yield increased from 0.01% to 0.03%.

During the period 210-380 min tos (Zone IV), methanol conversion decreased, and a continuous decrease of coke and CO_2 formation was observed too, with a concomitant raise of CO formation. Since the formation of H_2 did decrease at the same time, and the amount of O released from the solid decreased too, this implies that the phenomenon

observed was due to a lower contribution of reactions (1) and (5) (leading to both CO_2 and H_2 formation) and of reaction (6) (leading to both coke and CO_2 formation). The spinel reduction rate progressively decreased, approaching the limit value corresponding to the total spinel reduction. Finally, the only reaction contributing to methanol conversion was reaction (3):

$$CH_3OH \rightarrow CO + 2H_2 \qquad (3)$$

as also shown by the trend of the yields to CO and H_2, which finally approached similar values. In regard to oxygenated compounds, during Zone IV, methylformate yield decreased continuously from 0.03% to 0% at 330 min tos, whereas yield to formic acid first reached a maximum value (0.55% at 270 min tos), and then decreased down to 0.25% at 380 min tos.

When the reaction with methanol was carried out at 420°C (Figure 3-7), all the phenomena occurred much faster, and the various Zones were hardly distinguished; Zone I was missed, and maximum reduction of 82% was reached after 70 min only (see Figure 3-8). The yield to CO did not show the waved trend observed at 300°C, but instead a continuous increase with the maximum yield to CO_2 observed after 11 minutes only, which also coincided with the maximum yield to H_2O. However, one major difference with results obtained at 300°C concerned the trend regarding coke formation: yield to coke increased continuously in the range 0-70 min (yield 40%), and then remained constant for reaction times longer than 70 min.

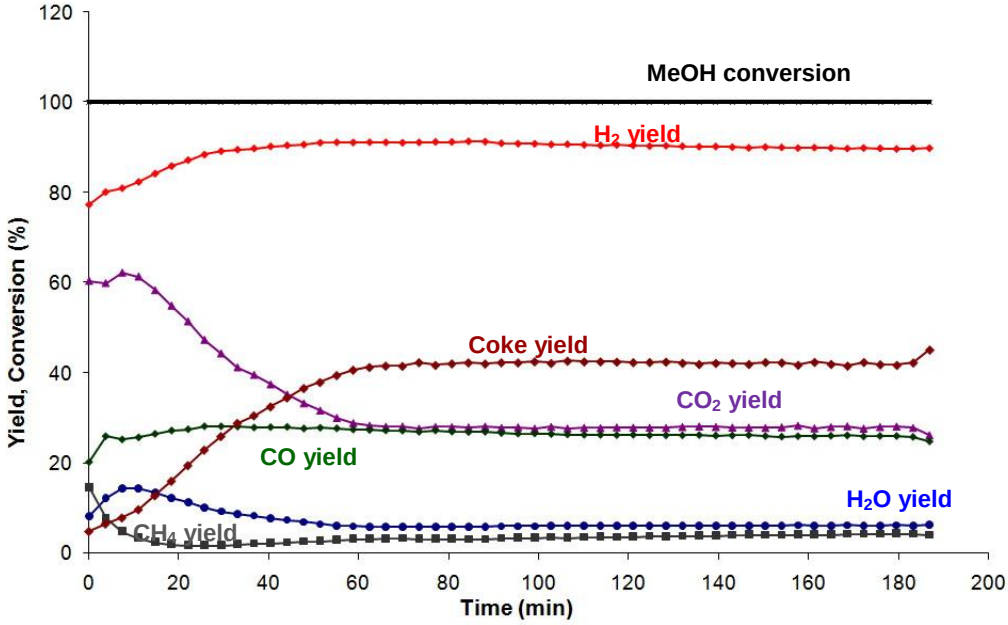

Figure 3-7. CF450 in contact with MeOH at 420°C

These trends demonstrate the presence of another reaction, compared to the 300°C test, which is the Reverse WGSr:

$$CO_2 + H_2 \rightarrow CO + H_2O \qquad (7)$$

This may explain a higher yield of coke than to CO_2 (the complete dehydrogenation of methanol to give coke cannot justify both the lower yield to H_2 and the higher one to water).

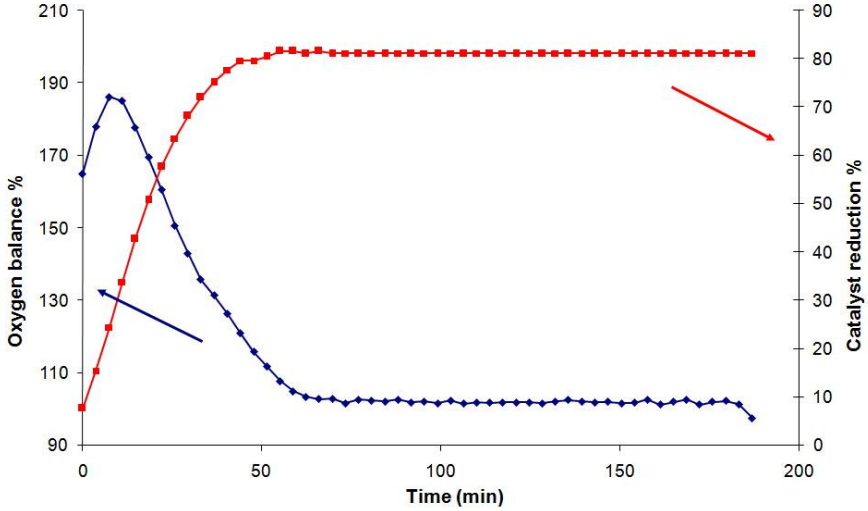

Figure 3-8. O balance and calculated degree of spinel reduction in function of reaction time. Conditions and catalyst as in Figure 3-7.

Figure 3-9 plots the experimental results obtained with CF750. In general, the catalytic behavior was very similar to that shown by CF450; however, some important differences are worth of being mentioned:

Zone I took much shorter time to occur; after 4 min, in fact, O uptake from the solid started to raise. In this case also, during Zone I the main products formed were CO_2 and H_2.

Zones II was completed within 90-100 min tos (that is, in a similar time range as compared to sample CF450), whereas Zone III end occurred after 140 min tos, in correspondence of which (i) the maximum degree of O uptake, (ii) the maximum methanol conversion, (iii) the higher yield to CO_2 and coke and (iv) the lower yield to CO were registered.

Zone IV led to a maximum value of CO yield (recorded at 260 min tos), after which a continuous decrease of methanol conversion, and yields to CO and H_2 as well, were observed. During this last Zone, coke formation was low.

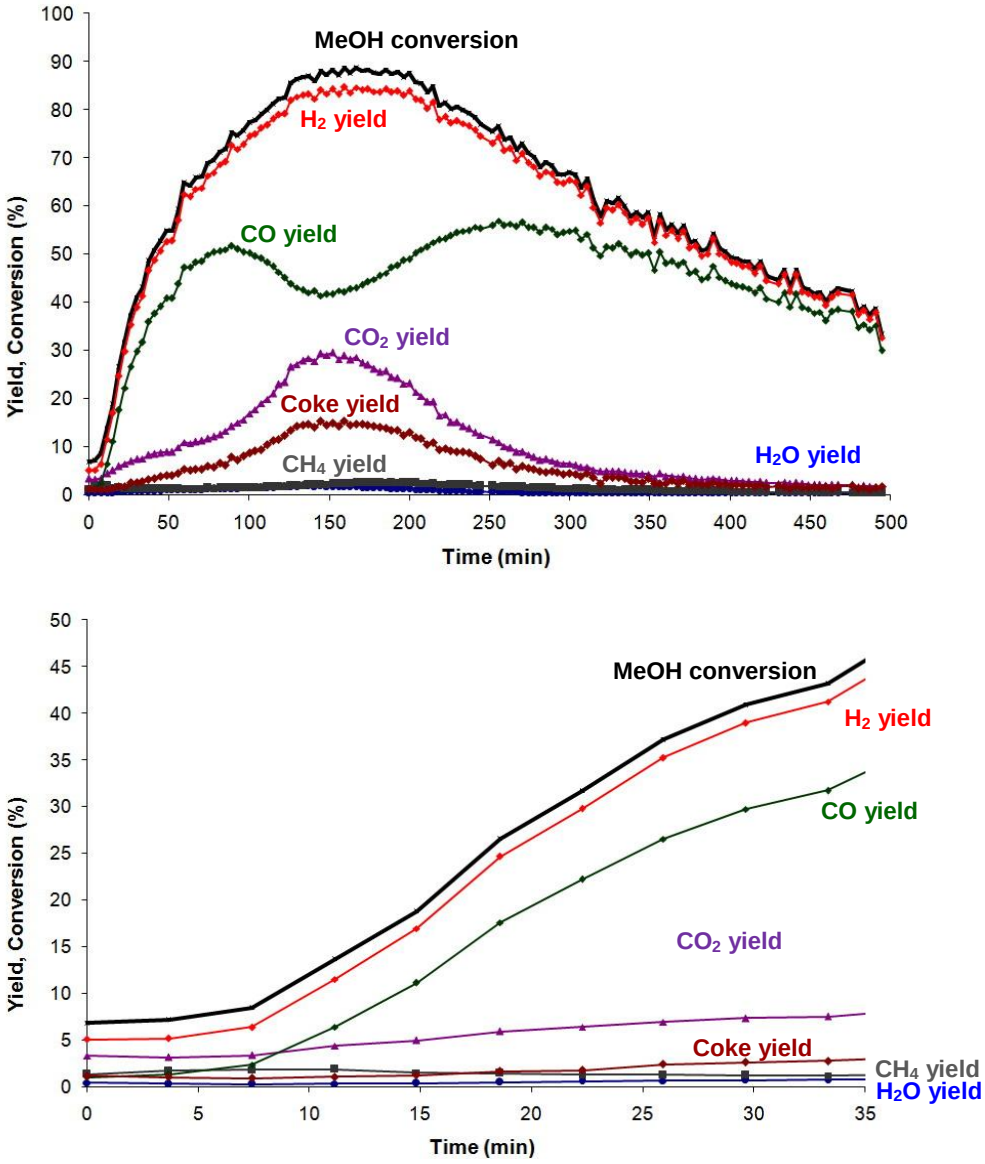

Figure 3-9. (Top) Methanol conversion and yields to products in function of the reaction time. Feed composition: 15.6mol% methanol, remainder N2; overall contact time 0.2 s; temperature 300°C. (Bottom): detail of the first 20 min reaction time. Catalyst CF750.

Along the entire range of tos examined (0-380 min tos), we did not observe the formation of either dimethoxymethane, formic acid or

formaldehyde. Methylformate was the only product formed, with 0.02% yield registered between 110 and 220 min tos.

The maximum spinel reduction degree was 82% only.

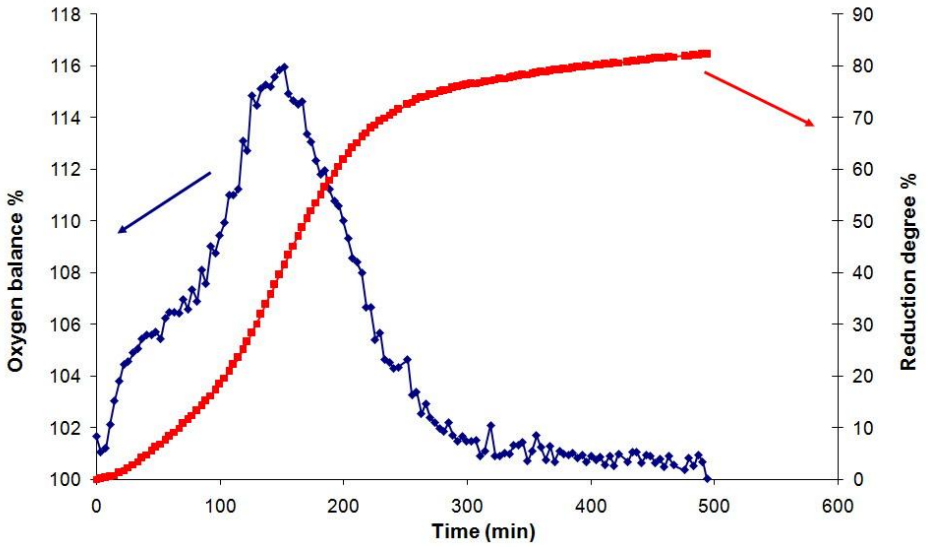

Figure 3-10. O balance and calculated degree of spinel reduction in function of reaction time. Conditions and catalyst as in Figure 3-9.

In overall, we can say that in the more crystalline CF750 sample, a lower concentration of highly reactive surface sites were present (which agrees with samples features previously reported[126]). Considering the overall extent of reduction measured during Zone I for the two samples (0.17% after 4' tos for CF750, 3.5% after 22' tos for CF450), it comes out that this discrepancy is not attributable only to the different surface area of the two samples, but also to the different surface features, for instance, to the different spinel crystallinity. In other words, these data confirm the presence of highly reactive (reducible) surface species in CF450, which instead are less exposed in the case of CF750.

In order to gain further information regarding the different behaviors observed, especially in regard to the initial reactivity (Zone I), we carried out a surface characterization by means of IR spectroscopy, contacting the samples with methanol.

Recently, another catalytic test has been carried out on a $CoFe_2O_4$ annealed at 320°C (sample CF320), in order to confirm the hypothesis just discussed. This sample is characterized by a higher surface area ($106 m^2/g$) compared to the CF450 and CF750 ones; the results of the catalytic test of complete reduction at 300°C is reported in Figure 3-11.

In the Zone I concerning the very beginning of the reaction, the sample shows a really high oxidizing power demonstrated by the high conversion of MeOH achieved during the first minutes of reaction (>40%) and the very high oxygen delivery from the solid material (Oxygen balance >130%). The consequence of this behavior is that the reduction degree after 4' is about 2,5% (instead of the 0,17% of CF750 and 0,8% of CF450). The surface area effect is shown in the second part of the Zone I where the conversion is always over 20% (CF450 shows an average conversion in this part comprised between 10% and 20% while CF750 shows a conversion degree <10%).

Actually, this sample is under further investigations and for this reason, data about the characterization are not yet available.

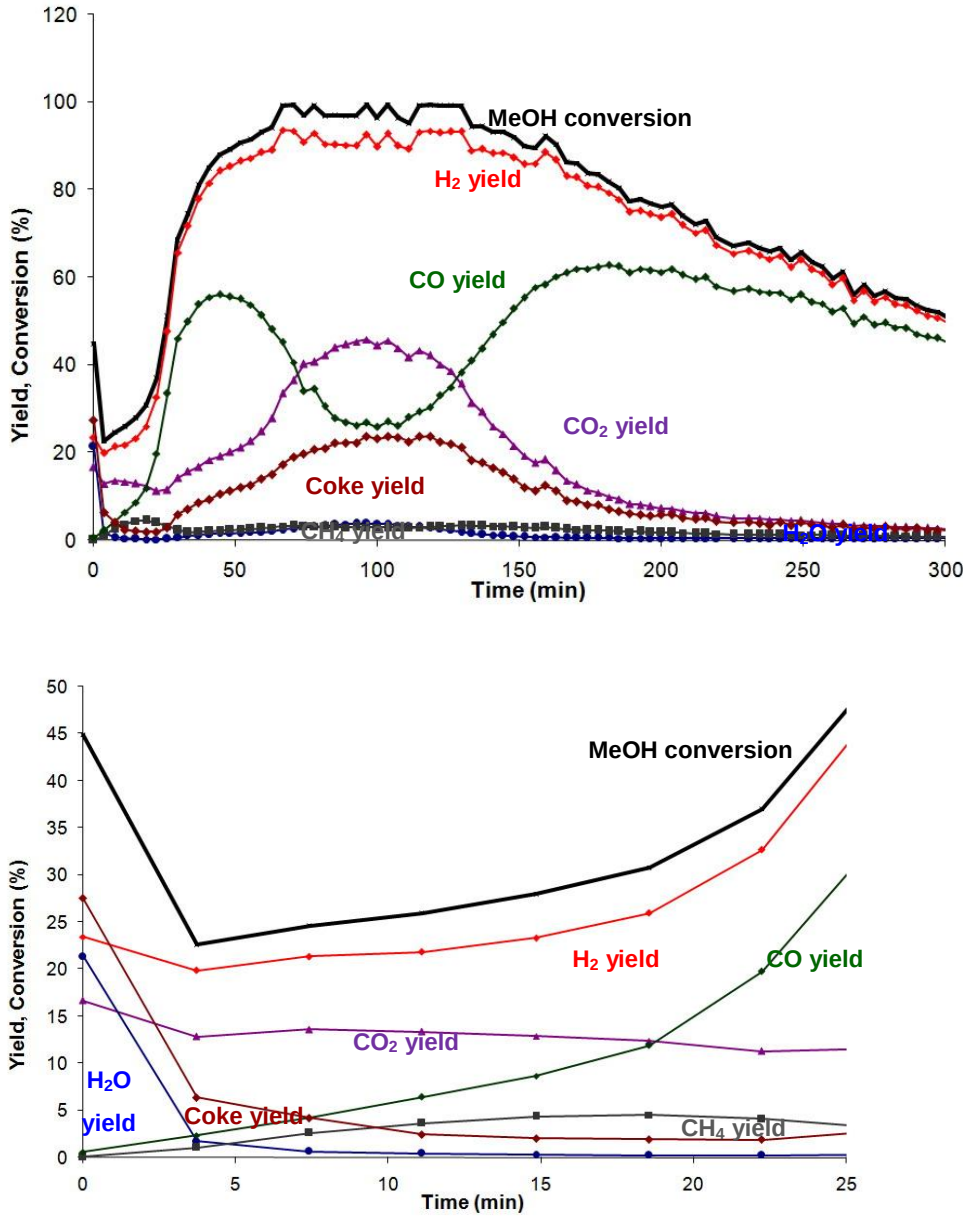

Figure 3-11. *(Top)* Methanol conversion and yields to products in function of the reaction time. Feed composition: 15.6mol% methanol, remainder N_2; overall contact time 0.2 s; temperature 300°C. *(Bottom)*: detail of the first 20 min reaction time. Catalyst CF320.

3.1.3 The effect of thermal annealing on surface characteristics: the interaction with methanol

The study of methanol adsorption has been carried out to gain information about the behaviour of the CF450 and CF750 materials during the initial period of the reaction. After methanol contact at RT with both systems [curves (1) in section (a) and (b) of Figure 3-12], a complex band can be observed in the 1550-1300 cm^{-1} range, produced by methanol interaction with the surface. As reference we can consider methanol adsorption on Aerosil 200 (commercial pyrogenic silica) activated at 150°C (dotted line). Pure silica is conveniently used as a reference system because of its scarce activity and null reactivity: it can interact with probe molecules only through surface OH-groups, giving rise to weak H-bonding interactions.

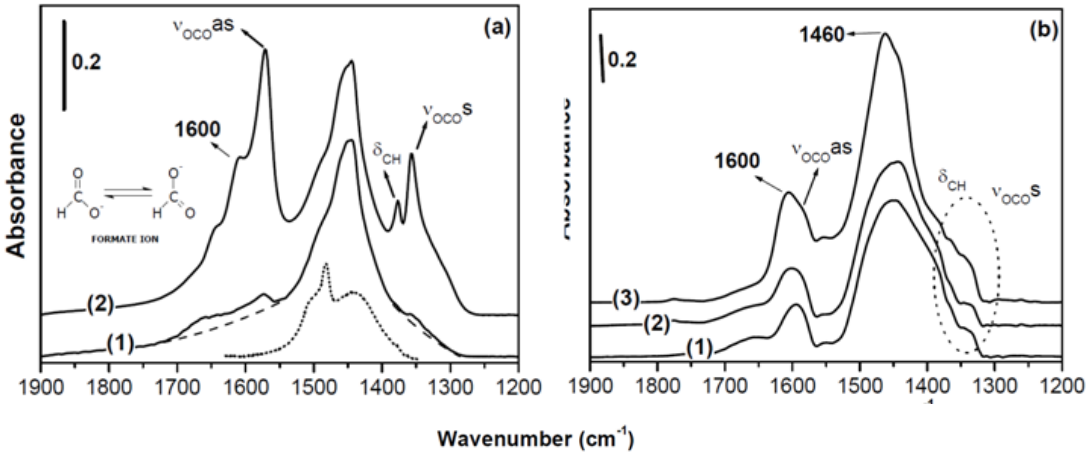

Figure 3-12. Absorbance differential spectra, normalized against the spectrum of the starting sample, of CF450 [section (a)] and of CF750 [section (b)] activated in vacuo at 350°C, after methanol contact at: BT [curves (1)], 150°C [curves (2)], and 250°C [curve (3)]

For what concerns the CF450 catalyst, increasing the temperature up to 150°C in methanol atmosphere, different signals appear in the spectrum [curve (2) in section (a)]. They can be confidently ascribed to adsorbed

formate ions, that give rise to a typical band triplet due to the following modes: asymmetric COO stretching (ν_{OCOas}; strong band at ~ 1570 cm^{-1}), CH deformation (δ_{CH}; weak sharp signal at ~1375 cm^{-1}) and symmetric COO stretching (ν_{OCOs}; medium band at ~1355 cm^{-1})[131]. Comparison between spectra (1) and (2) of section (a) indicates that minor amounts of the formate species form already at BT. Methanol at relatively low temperatures dehydrogenates to formaldehyde, that readily reacts to generate surface formate species; this process requires the reduction of the employed material to take place. The generation of formate ions thus confirms the capacity of methanol to reduce the material at relatively low temperatures.

Bringing the sample above 200°C in methanol atmosphere, it is possible to observe (not shown in a figure) the total loss of transparency of the solid sample to infrared radiation. This radical change of optical features can be attributed to the further reduction of the system. In fact, the reduction process may not be only a surface phenomenon, and involve the migration of O^{2-} ions from the bulk towards the surface, generating drastic mutations in the electronic characteristic of the material.

Turning now to methanol adsorption on the CF750 catalyst, the differential spectral pattern reported in section (b) of Figure 3-12 shows that the signals of formate species are weak and ill-defined, even after the increase of the temperature up to 250°C in methanol atmosphere. Another important difference is that, in the case of the CF750 material, the total loss of transparency of the solid to infrared radiation (indicating the possible complete reduction of the system) is observed upon heating the sample above 250°C in methanol atmosphere. This fact highlights that the reduction of this system needs higher temperatures and longer contact times with methanol than in the case of the CF450 catalyst. In

other words, the migration phenomena of O^{2-} ions from the bulk towards the surface are slower for the more crystalline oxide.

The IR study of methanol adsorption allows to state that this molecule is a good reducing agent for $CoFe_2O_4$ catalysts at relatively low temperatures; still, the CF750 system requires higher temperatures or longer times to reach the same reduction degree. Moreover, the information provided are in line with experimental results obtained during the initial reactivity of samples with methanol (initial period of Zone I, with the solid which is still oxidized): the presence of highly reactive surface species in the CF450 spinel, which are not observed (or are present in much less amount) with CF750.

3.1.4 Bulk characteristics of used catalysts

Catalytic and characterization results reported so far highlight that the surface and bulk reactivity of CF450 and CF750 spinels were different, because of the presence of highly reactive sites in the former oxide, which were only a minor fraction in the case of CF750. These sites were rapidly consumed during the very first minutes reaction time in methanol anaerobic oxidation carried out at 300°C (Zone I), and the degree of reduction achieved during this latter period was greatly different for the two oxides.

Since the use of the spinel as a catalyst for methanol transformation into H_2 would necessarily imply a regeneration step of the reduced solid, we were wondering whether the surface and bulk features of the solids were maintained after a reoxidation step with steam.

Table 3-1. Main characteristics of samples prepared shows the main bulk features of the reoxidized CF450 and CF750 samples, after partial and complete reduction; the reduction step was carried out at two different T levels, 300°C and 420°C. For example, in the case of the partially

reduced CF450, we stopped the reduction at 300°C after 30 minutes (which roughly corresponds to the end of Zone I, with a degree of spinel reduction corresponding to approximately the 4.5%), whereas the completely reduced (and strongly coked) sample was obtained by downloading the solid after 300 min (Zone IV). The data clearly indicate that the complete redox cycle did not cause any relevant modification of bulk features of CF750, whereas did profoundly affect the characteristics of CF450. In fact, the reoxidized CF450 showed a remarkable increase of the crystallinity and a concomitant decrease of the surface area; in other words, used-CF450 had characteristics very close to those of CF750. It is worth noting that this was not due to any high-temperature treatment, since both the reduction with methanol (an endothermal process) and the oxidation with steam (a mildly exothermal process) were carried out at temperatures not higher than 420°C.

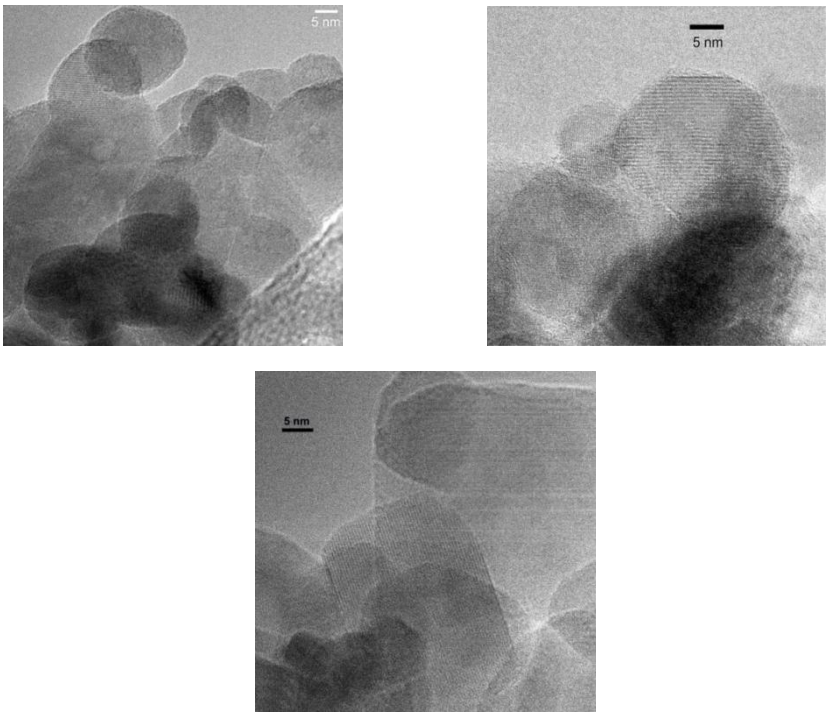

Figure 3-13. TEM images of used CF450 (top) and CF750 (bottom).

Figure 3-13 show the HR-TEM pictures of samples after contact with methanol at 420°C and reoxidation with steam; the images reveal an increase of crystallite size, with respect to the fresh samples, ranging now from ~10 to ~25 nm for CF450 and from ~30 to ~40 nm for CF750. Moreover, particles contours appear well-outlined and definitely more roundish if compared with those of fresh samples: a sintering (or aggregation phenomenon) is clearly present. All this confirms that CF450 undergoes irreversible morphological changes, whereas CF750 doesn't.

Figure 3-14, showing XRD patterns of samples after reduction at 420°C and reoxidation with steam, provides additional information; it is confirmed that the crystallinity of CF450 and CF750, which was very different for the freshly calcined samples, became similar after the redox cycle. Moreover, both samples still show some weak reflections attributable to metallic Co/Fe alloy and metallic Co, which are especially evident in the case of the used CF450.

In the IR spectrum of used CF450 (first completely reduced by interaction with methanol at 420°C for 180 min, and then reoxidized with steam at 420°), the component at ~620 cm^{-1} is no longer evident (see the dotted-line curve in Figure 3-3, top); this high-ν signal can be ascribed to the surface fraction of the Fe-O vibrational mode which considerably decreases as a consequence of the drastic decrease of surface area produced after the reduction/oxidation cycle. The band ascribable to Fe-O vibrations shifts from ~587 cm^{-1} (in the calcined sample) to ~578 cm^{-1}; also in this case, the shift is attributable to the increased particles size caused by sintering phenomena. In fact, a similar shift was observed in calcined samples, when increasing the calcination temperature from 450°C (CF450) to 750°C (CF750).

In the case of CF750, as the morphological changes of used sample are less important than those of used CF450, the position of the band at

~580 cm^{-1} remains virtually unchanged before and after the reduction/oxidation cycle [see the dotted-line curve in section (b)], even if in this case the use of the material as a reagent/catalyst reduces (to a fairly limited extent) the high-ν component of the overall Fe-O vibrational band.

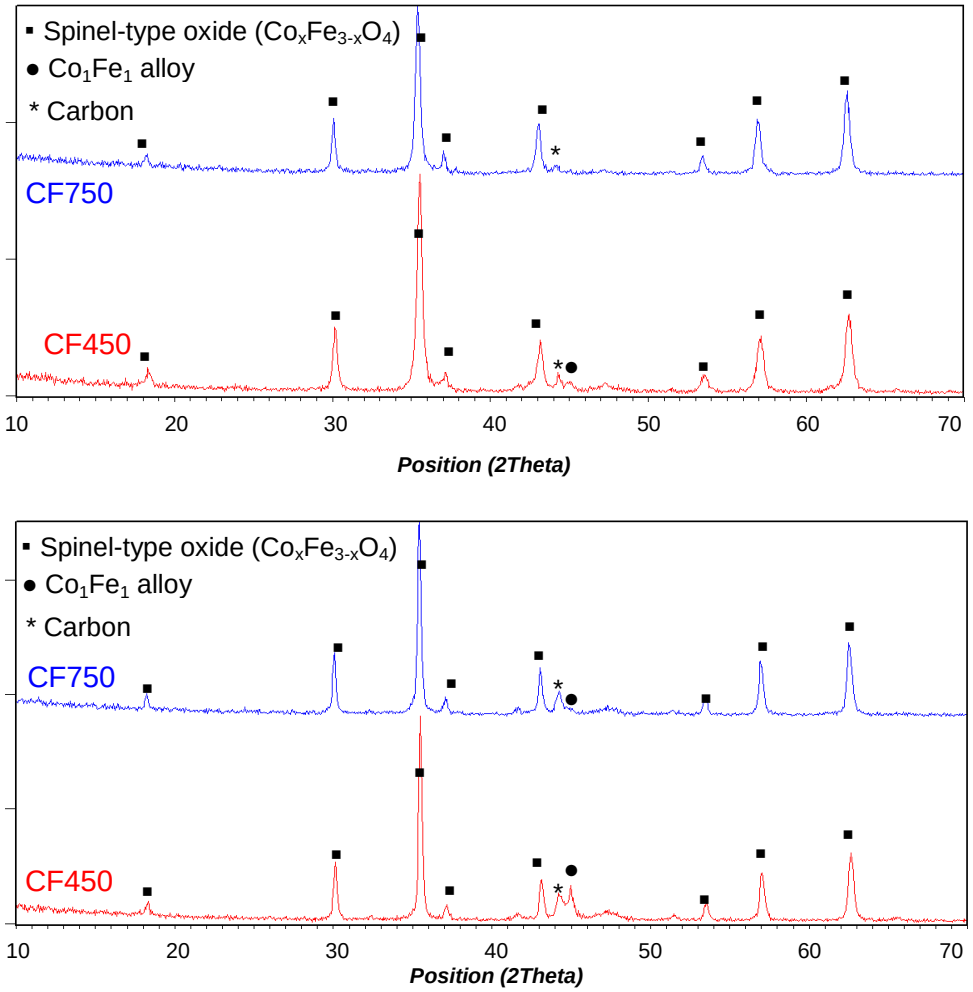

Figure 3-14. XRD patterns of CF450 and CF750 samples after reduction with methanol at 420°C for 30 min (τ 1 s) and then oxidation with steam at 420°C (Top Figure), and after reduction with methanol at 420°C for 180 min (τ 1 s) and oxidation with steam at 420°C (Bottom Figure).

In regard to the band resolved spectra (Figure 3-3, bottom, Section II), it is possible to observe that:

- the intensity of the bulk component remains unchanged in both fresh and used samples. This feature is actually the main basis of the band assignment;
- the surface component, on the contrary, decreases of ~30% after the employment in the redox cycle;
- the S/B integrated intensity ratio decreases for both samples after their employment in the redox cycle. This confirms that the surface area decrease produced during the redox cycle leads to the loss of an appreciable fraction of surface Fe-O modes, regardless of the starting SSA value.

In regard to the Me^{Oh}-O vibrations (Figure 3-4, top), in spectra collected in the far-IR region, the component at ~415 cm^{-1} is no longer evident in the spectrum of the CF450 material employed in the redox cycle (see the dotted-line curve). As in the case of the Fe-O modes, the high-ν signal component can be ascribed to the surface fraction of the Me^{Oh}-O vibrations, which noticeably decreases after the employment in reaction, due to the drastic decrease of surface area. In the case of used CF750, as the morphological changes are less important than those of used CF450, the shape of the Me^{Oh}-O band envelope remains virtually unchanged before and after the reduction/oxidation cycle [see the dotted-line curve in section (b), with respect to the solid-line one].

All the previous considerations can be confirmed by observing the band-resolved spectra reported in Figure 3-4 (bottom). The following can be stated:

- the surface component decreases of ~40% after the use in the reaction only in the case of the CF450 sample, whereas for the CF750, no changes of the S band are observed; for CF450, the

integrated absorbance of S component passes from 16 to 6 cm^{-1}, whereas for CF750 the integrated absorbance is 6 cm^{-1} in both calcined and used samples.

- the bulk components seem to increase slightly on passing from fresh to used CF450, whereas they remain virtually unchanged for CF750.

Taking into account all previous considerations, it is possible to state that:

- both samples lose a fraction of surface Fe^{Th} during the redox cycle;
- the fraction of surface Me^{Oh} remains unchanged in the case of CF750;

So, also FTIR analysis confirms that the two cobalt ferrites CF450 and CF750, originally morphologically quite different from one another, become very similar after (just one cycle of) employment as reagent/catalyst in chemical water splitting reaction.

3.1.5 TPR investigation

A further investigation about the possible recovery of the original structural features of CF450 has been made by TPR analysis; here we reported the reduction profile recorded during the first reduction of CF450 and CF750.

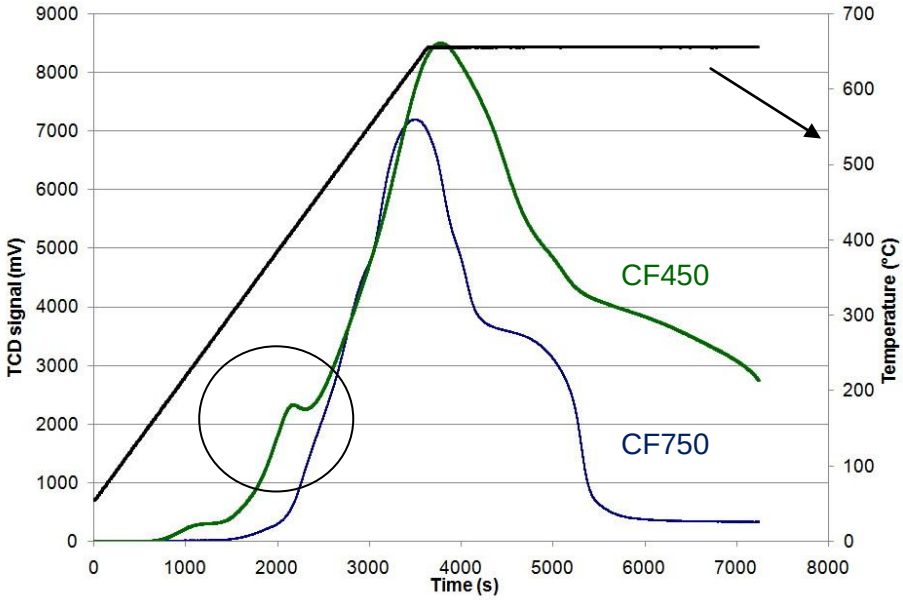

Figure 3-15. TPR comparison of CF450 and CF750

The main difference concerns the peak highlighted by the circle that is present only in the CF450 analysis. This peak can be ascribed to the highly reactive species identified by means of IR spectroscopy and catalytic tests (other analysis, not reported here, demonstrate that the low temperature peak is function of the annealing temperature).

So, TPR tests were carried out after the reoxidation of the sample in oxygen, in order to check whether the low-T reduction peak was maintained even after the first reduction (and reoxidation) step. Figure 3-16 reports the 1st and the 2nd reduction of CF450, both carried out at a maximum temperature of 450°C.

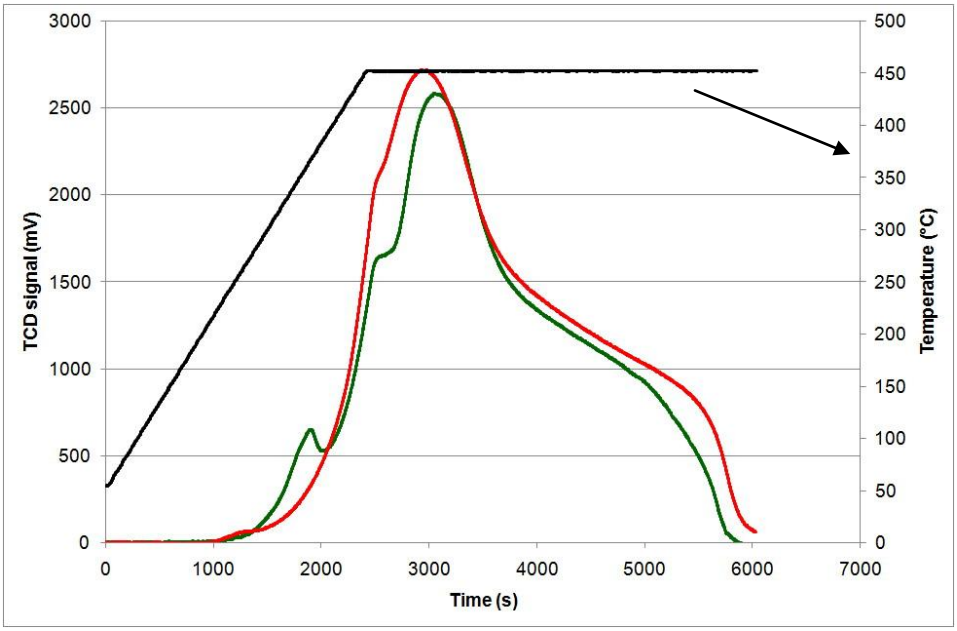

Figure 3-16. 1st and 2nd TPR on CF450 (between the two analysis TPO with oxygen was carried out)

As it's possible to see, in the second analysis the low temperature reduction peak is not present any more. Furthermore, we can say that the temperature effect is not here involved, because the maximum temperature reached during the TPRO experiment is the same as that used for the thermal treatment made on the fresh catalyst (450°C). The loss of the very reactive surface species is due to the fact that the redox cycle, carried out at 450°C, involving first a complete reduction and then a reoxidation of the solid, leads to a strong annealing of the crystallites, in the same way as it occurs when calcination temperature higher than 450°C are used. This means that in principle, it should be possible to limit the solid reduction at the very reactive surface sites, for example by carrying out the TPR experiment at the maximum T of 300°C only; at these conditions, the annealing phenomena should be avoided, and the reactive surface sites should be maintained. Results shown in

Figures 3-17 and 3-18 demonstrate that the hypothesis put forward was correct; we first carried out a TPR experiment up to 300°C, then a TPO up to 450°C, and finally a second TPR up to 450°C. Figure 3-17 shows that the reduction at 300°C only involves the surface active-species (red curve).

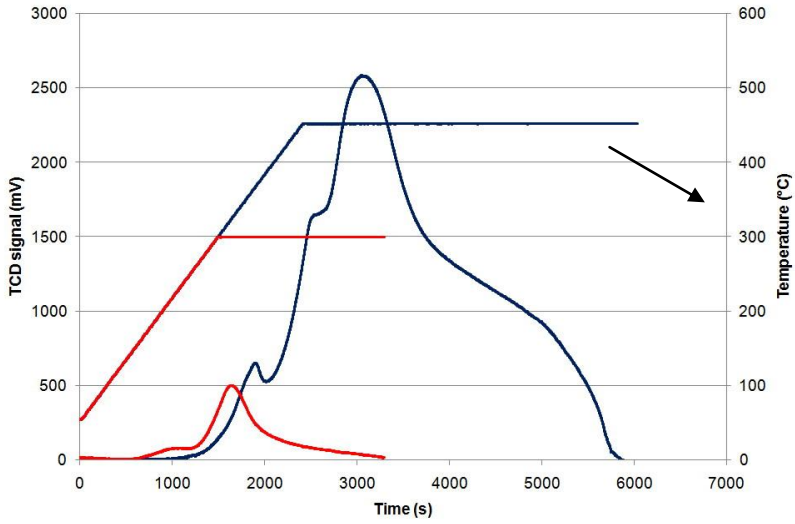

Figure 3-17. Comparison between the 1st 420° TPR (blue) and the first one of the 300°C TPR (red)

Figure 3-18 compares three consecutive TPR profiles (Tmax 300°C); the intermediate TPOs were carried out at 450°C. It is shown that the highly reactive species were still present during the 2nd and 3rd TPR experiments (as evident from the corresponding low-T hydrogen consumption).

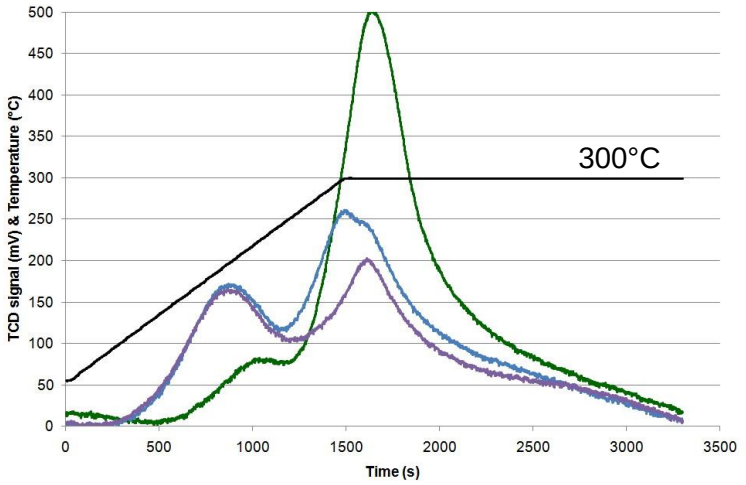

Figure 3-18. 1st (green), 2nd(blue) and 3rd(violet) reduction at 300°C on CF450. Reoxidation at 450°C

Finally, we repeated the TPR experiments, but using a maximum T of 300°C also for the intermediate TPOs; profiles are shown in Figure 3-19.

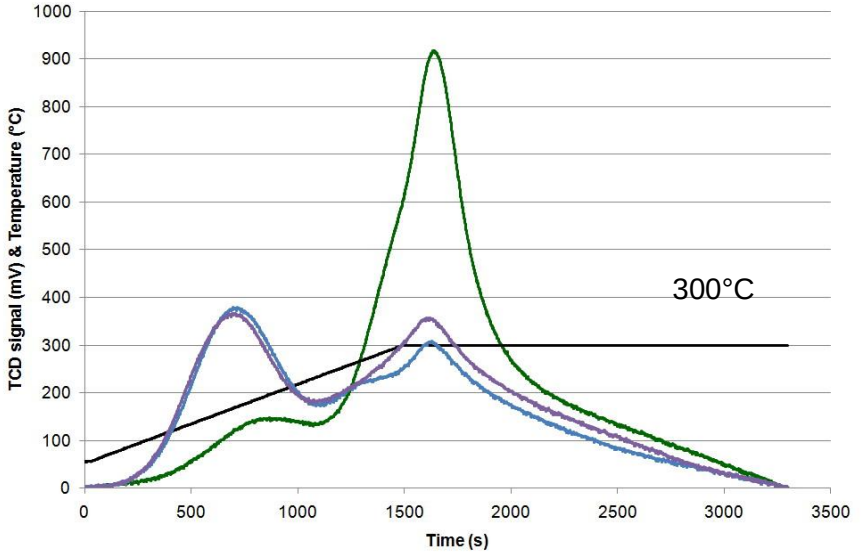

Figure 3-19. 1st (green), 2nd (blue) and 3rd (violet) reduction at 300°C on CF450. Reoxidation at 300°C

The reduction profile changes after the first redox cycle even if the reoxidation is performed at the lower temperature available.

In conclusion, modifications of the catalyst structure cannot be completely avoided even if the reduction degree is very low.

3.1.6 Conclusions on the chemical-physical properties of Cobalt ferrites

Chemical-physical properties of CF450 and CF750 have been analyzed by means of IR spectroscopy, TEM, BET, in-situ IR tests, catalytic tests, XRD characterization and TPRO investigations. All these characterization techniques showed differences between the two materials.

The characterization of synthesized compounds by means of FTIR, TEM, XRD and BET analyses evidence how the annealing temperature modifies the morphological properties of the cobalt ferrites. CF450 ($CoFe_2O_4$ annealed at 450°C) is characterized by higher surface area and smaller dimension of the particles, while CF750 (annealed at 750°C) evidenced a more crystalline structure.

These differences highlight a chemical reactivity of the smaller particles which is higher than that of the more crystalline (aggregated) domains. In catalytic tests of reduction of the cobalt ferrite with MeOH at 300°C, a different behavior of the two materials is evidenced especially during the first minutes or reaction, when the oxygen delivery from the material is strongly affected by the structural properties of the fresh calcined solid. Furthermore, in-situ IR spectra demonstrate that the interaction of CO with the two samples lead to the formation of different adsorbed species as a consequence of the presence of surface active sites in CF450 that are not observed in CF750. Finally, TPR analysis demonstrate that smaller particles (or surface active sites related to the defective sites in

the material) can be reduced at lower temperature, which is a further confirmation of the results obtained in catalytic tests and in-situ IR experiments. However, the reoxidation of CF450 with water or air cannot completely restore the original morphology of the oxide, even when the reoxidation is carried out at very low temperature (see TPRO investigations).

3.2 MeOH thermochemical reforming

Methanol thermochemical reforming was studied using three different mixed ferrites as oxygen vectors, which are:

- $CoFe_2O_4$
- $NiFe_2O_4$
- Fe_3O_4

As just discussed in the last paragraph, the annealing temperature of the material is one important parameter affecting the catalytic activity and selectivity to the various products. However this feature was not stable, as highlighted by means of the characterisation of the solid before and after the a Redox cycle (Paragraph 3.1). This motivation drove us towards the screening of different materials, all annealed at the same temperature, that is 450°C in air. This temperature was chosen because temperatures used for the catalytic tests were lower than this value (the higher one is 420°C, for the reoxidation step, that is the best compromise between thermodynamic and kinetic requirements). The samples will be identified using these labels:

- FF450 – Fe_3O_4 annealed at 450°C
- NF450 – $NiFe_2O_4$ annealed at 450°C
- CF450 – $CoFe_2O_4$ annealed at 450°C

3.2.1 Characterization of the synthesized materials

As described in the “Experimental part”, the characterization technique used were power-XRD, BET and TPR analysis, which allowed us drawing a complete picture of the structural and redox properties of the oxides.

XRD patterns of the fresh compounds are reported in Figure 3-20: the spinel phase was successfully synthesised in all cases.

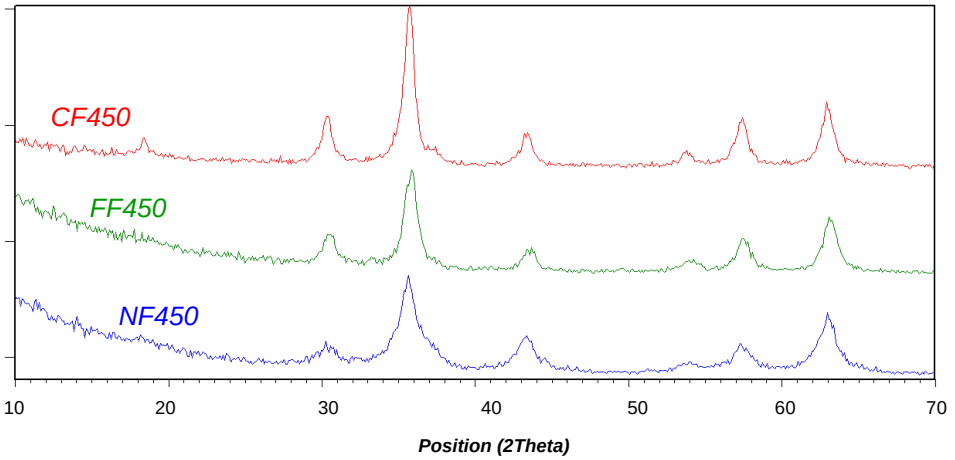

Figure 3-20. XRD pattern of the fresh material.
From the bottom: NF450, FF450, CF450

The Scherrer equation was also used for the calculation of the crystallite dimensions that is strictly related to the morphological features of the samples; results are reported in Table 3-2. Main characteristics of samples

Furthermore, the BET analysis was carried out in order to check for possible differences between the samples (Table 3-2); the results show that all the ferrites have similar SSA, which gives us the possibility to compare the chemical differences without any contribution from other features.

Sample	***SSA (m^2/g)***	***Crystallite size (nm)***
NF450	94	7
FF450	85	10
CF450	70	12

Table 3-2. Main characteristics of samples

Results reported in Table 3-2 show that there is an inverse proportional relationship between the surface area and the crystallite size..

Another important feature , useful for the interpretation of catalytic results, is the redox properties of each material. TPR analysis was carried out and reduction profiles are reported in Figure 3-21.

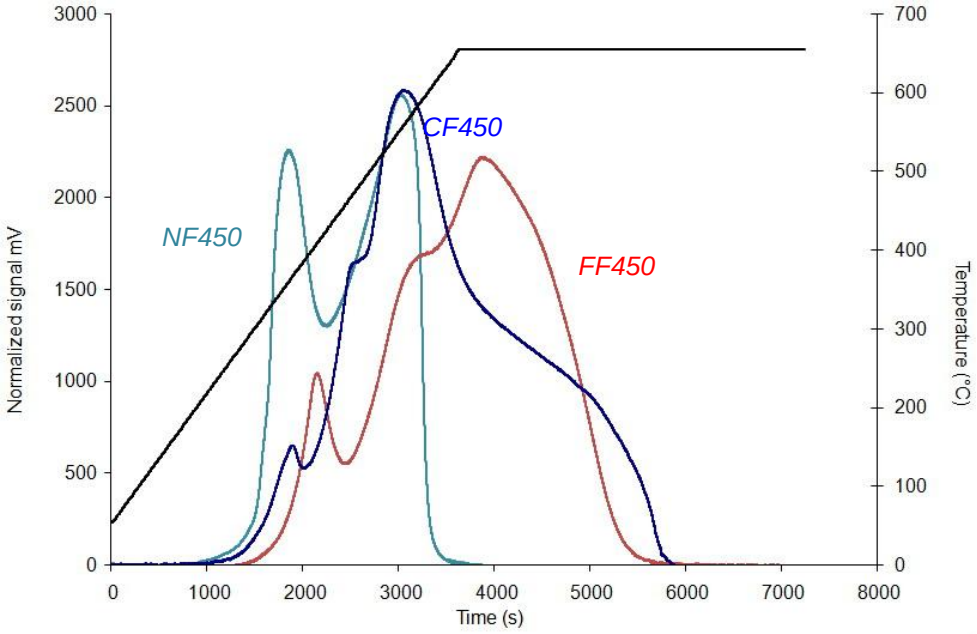

Figure 3-21. TPR analysis of NF450 (green), CF450 (blue) and FF450 (red); temperature (black) is referred to the secondary Y-axis.

As a matter of fact, the analysis shows that NF450 has a deep reduction at lower temperature than the other ferrites, which confirms the higher oxidizing power previously discussed (see paragraph 1.3.5.4).CF450 shows a TPR profile that suggests an intermediate behaviour, whereas FF450 is the compound reduced at the higher temperature, which agrees with thermodynamic comparison previously discussed.

Concerning TPR analysis of $CoFe_2O_4$, CF750 did not show the reduction peak at 300°C-350°C (see paragraph 3.1.5), which was instead observed with the CF450 sample; this peak was attributed to highly reactive

surface species. We also observed a similar effect with the other ferrites; therefore this feature can be assumed to be true for all the samples examined, in regard to the interpretation of catalytic results.

3.2.2 Catalytic tests: the complete reductions of ferrites

As reported for CF450 in paragraph 3.1.2, preliminary catalytic tests were carried out on the three mixed ferrites, in the aim of understanding the nature of structural changes occurring during reduction, as inferred from the reaction products formed. These initial tests were not finalized at the study of the reproducibility of the material in the so-called "steam-iron" loop, but were useful in the aim of defining the best conditions for the cycle tests.

3.2.2.1 Cobalt ferrite

Reduction with MeOH at 300°C

The results and the discussion about the catalytic test on CF450 at 300°C have been reported in paragraph 3.1.2 (see Figure 3-5 and Figure 3-6). Here, only the final considerations for each "Zone" of reaction are briefly summarized.

"Zone I" was limited to the first 22 min time-on-stream, and was characterized by a slightly increase of MeOH conversion. An initial high selectivity to CO_2 and H_2 was noticed, but after few minutes CO, CH_4 and coke selectivity began to grow up. The production of intermediate compounds such as methylformate, dimethoxymethane and formaldehyde was registered too, but with very low yields. The amount of oxygen released by the solid was comparatively very high during the first few minutes, then decreased, indicating a slower reduction rate for the ferrite. The reactions involved were:

$CH_3OH + Me^{n+}O \rightarrow CO_2 + 2\,H_2 + Me^{(n-2)+}$ (1)

$CH_3OH + Me^{(n-2)+} \rightarrow C + 2H_2 + Me^{n+}O$ (2)

$CH_3OH \rightarrow CO + 2H_2$ (3)

$C + 2H_2 \rightarrow CH_4$ (4)

$CH_3OH + 2Me^{n+}O \rightarrow CO_2 + 2\,H_2O + 2Me^{(n-2)+}$ (5)

$2\,CO \rightarrow CO_2 + C$ (6)

“Zone II” was between 22 min and 100 min tos, and was characterized by a rapid raise of both MeOH conversion and CO and H_2 yields, probably due to the progressive increase of the number of active species which catalyse MeOH dehydrogenation (reaction 3). Therefore CO_2 and coke yields increased too, because of reactions (1), (2) and (6) that still took place even though at a comparatively lower extent.

“Zone III” was comprised between 100 min and 210 min tos, and methanol conversion still remained high, reaching the top value of 88%. The yield of CO decreased, but all the other products yields increased (as the intermediate products also did); this was due to the main contribution of reaction (1), as also demonstrated by the rapid raise of the oxygen uptake.

“Zone IV” was the final part of the reaction (after 210 min tos), and was characterized by a continuous decrease of MeOH conversion and of all yields, except that to CO that showed an initial increase, due to methanol decomposition (due to the low oxidizing power of the highly reduced material), followed by a slight decrease, similarly to what observed for all the other products: this was due to the deactivation of the completely reduced material.

Reduction with MeOH at 420°C

The catalytic test carried out at 420°C was also described in paragraph 3.1.2 (Figure 3-7). This high-temperature test showed that all the four Zones described above were shortened, and occurred during only 1 hour tos; MeOH conversion was total during all the experiment. H_2O and CO_2 yields were very high during the first minutes of reaction (the higher yield was at 11 min), if compared to the experiment carried out at 300°C: this is because reaction (5) was strongly favoured by the higher temperature used, and by the oxidation state of the solid. After this initial period, a slow decline oxygen delivery by the solid oxide was observed, until the complete reduction of the material was finally reached (at about 70 min tos, see Figure 3-8).

On the other hand, CO and coke yields increases during the first 70 min f tos, because of reactions (3) and (6). Finally, a steady state was observed when the reduction of the oxide was completed; coke was the main product due to reaction (6), while CO_2 yield was lower than coke yield because of the contribution of the reverse WGS reaction:

$$CO_2 + 2H_2 \rightarrow CO + H_2O \qquad (7)$$

Reoxidation with water of totally reduced samples

The reoxidation tests on the samples reduced either at 300°C or 420°C was carried out, and the results are in agreement with considerations made in regard to the reduction step. Results are shown in Figs. 3-22 and 3-23.

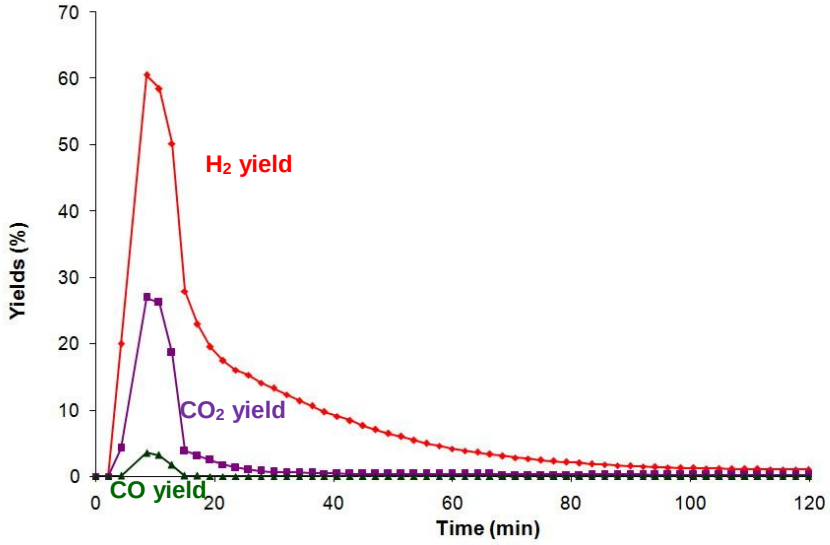

Figure 3-22. Reoxidation with water at 420°C of the CF450 reduced at 300°C (see Figure 3-5).

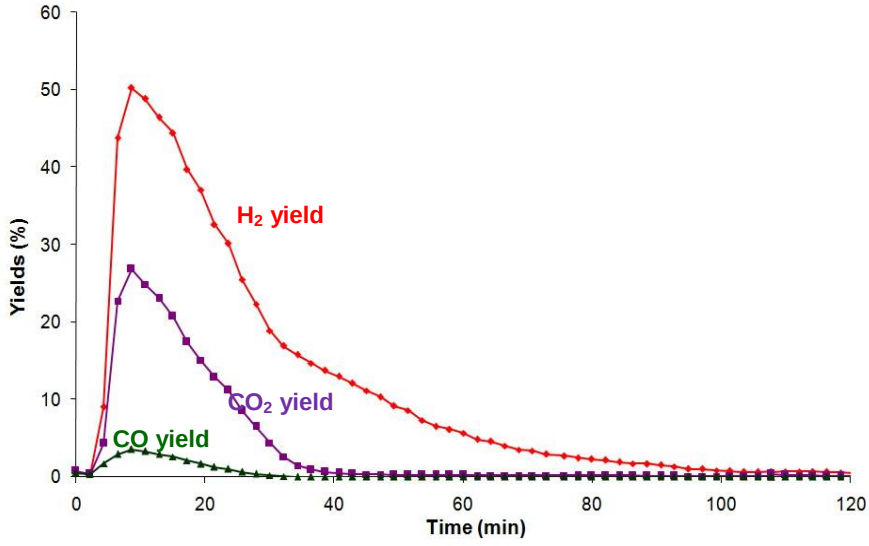

Figure 3-23. Reoxidation with water at 420°C of the CF450 reduced at 420°C (see Figure 3-7).

The products of reoxidation were H_2 and CO_x that derived from the reoxidation of the solid and from the gasification of deposited coke.

$$Me^0 + xH_2O \rightarrow MeO_x + xH_2 \quad (8)$$

$$C + xH_2O \rightarrow CO_x + xH_2 \quad (9)$$

As it is possible to see, CO yield was much lower than CO_2 yield, even if the amount of deposited coke was very high; this was probably due to the catalytic properties of Co and Fe in the water-gas-shift reaction.

Another comment about these graphs is about the integral values of the produced gases; the total amount of hydrogen evolved was higher in the catalytic test reported in Figure 3-23 than in Figure 3-22 (7,1 mmol *vs.* 5,5 mmol, respectively), probably because of the higher amount of coke deposited during the reduction at 420°C; furthermore, the total CO_2 evolved during the reoxidation step was greater, too (2,3 mmol *vs.* 1,1 mmol).

Concluding, it's possible to say that the reoxidation of a sample with a huge amount of coke deposited over it does not give interesting data, because the H_2 evolved is mainly derived from the gasification of deposited carbon compounds. Because of this reason, we decided to carry out the reoxidation step over the completely reduced samples in some specific cases only.

3.2.2.2 Nickel ferrite

Reduction with MeOH at 300°C

The NF450 was reduced at 300°C, and the results are reported in Figures 3-24 and 3-25.

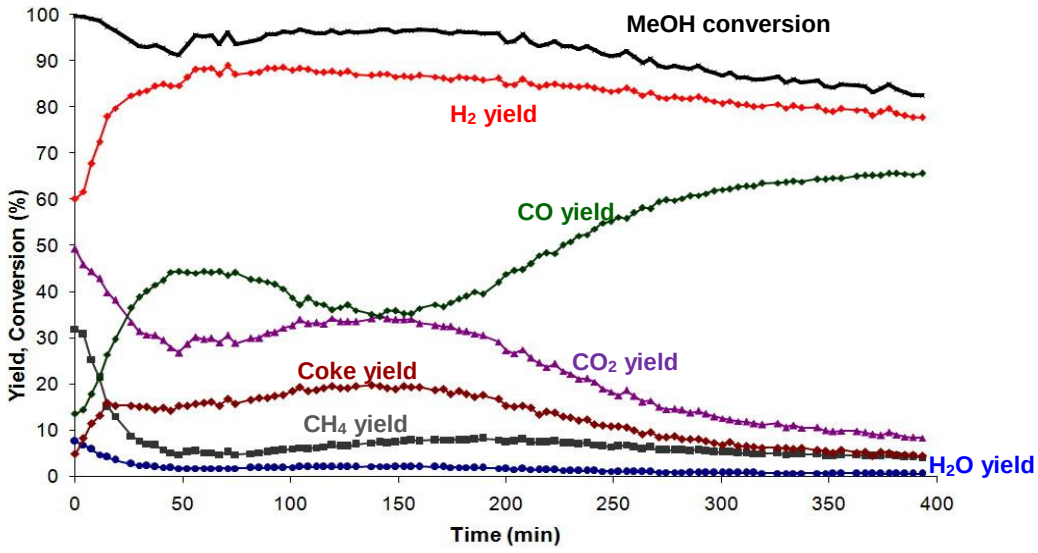

Figure 3-24. Product yields and MeOH conversion at 300°C with NF450.

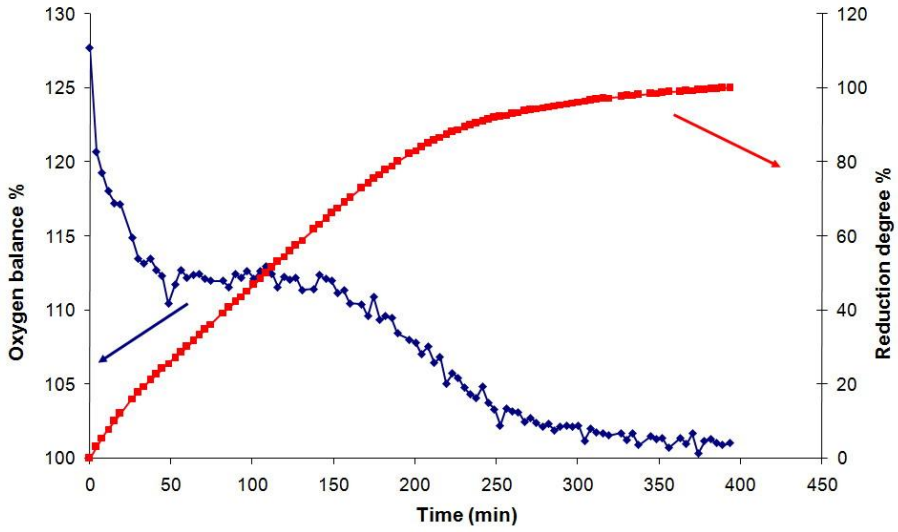

Figure 3-25. Oxygen balance (blue, left axis) and reduction degree of NF450 (red, right axis).

As in the CF450 case, we can identify several “Zones of reaction”, where the product yields changed a lot because of the modifications occurring

in the sample. The first part of the reaction is the most different one, when compared to the behavior shown by CF450.

With NF450, “Zone I” lasted until 50 min tos; MeOH conversion was total since the first instants of reaction, because of the higher oxidizing power of the material, and probably because of the higher surface area, too. This difference is also shown by the CO_2 and H_2O yields, that both were very high; they derived from the total oxidation of methanol.

$$CH_3OH + 2Me^{n+}O \rightarrow CO_2 + 2\ H_2O + 2Me^{(n-2)+} \quad (5)$$

Further proofs of this property are the H_2 and CO yield, which both were by far lower than that obtained with CF450. Anyway, MeOH decomposition (reaction 3) gave non-negligible yields to CO and H_2, because of the high conversion of the reactant.

$$CH_3OH \rightarrow CO + 2H_2 \quad (3)$$

Intermediate oxidation products such as methylformate, formic acid and formaldehyde were very low during this catalytic test if compared to the CF450 one; the highest yields recorded is 0,05% for methylformate.

The other important difference was the CH_4 yield, that started over the 30% (in CF450, the highest yield to methane was about 2,5%), as a consequence of the methanation of coke and CO:

$$C + 2H_2 \rightarrow CH_4 \quad (4)$$

$$CO + 2H_2 \rightarrow CH_4 + H_2O \quad (10)$$

This behavior was expected, because Ni is one of the most active species in these kind of reactions (for instance, reaction (10) is the reverse of Steam Methane Reforming, that is catalyzed with Ni in industrial plants, as reported in paragraph 1.2.3.1).

The product yields changed along with the increasing of tos, because of the progressive reduction of the solid that led to a lower oxidizing power. Coke, CO and H_2 yields rose until the end of Zone I (at 50 min), while CO_2 and H_2O yields decreased. In addition, CH_4 selectivity underwent a strong reduction, probably due to a selective deactivation of the active species involved in methanation.

The oxygen balance, reported in Figure 3-25, shows that the oxygen delivered by the material was remarkable since the very beginning of the reduction time (O balance > 110% during all “Zone I”). Another consideration is about the highly reactive species in the oxidized sample, previously observed in the CF450 sample (see paragraph 3.1.2). In the case of NF450, this type of surface active sites was also present. In fact, the rate of reduction (proportional to the oxygen delivery) during the first 4 min was much higher than that registered during the 4-12 min tos, which is a proof for the presence of these highly reactive sites in the fresh material.

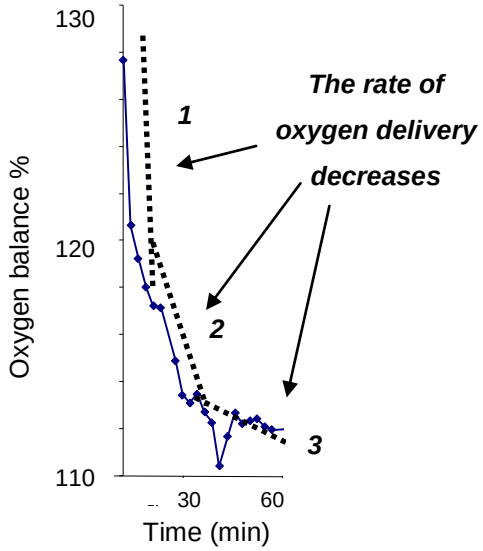

Figure 3-26. ZOOM of the 0'-50' Oxygen Balance graph

"Zone II" is related to the 50 min-150 min period, during which the trends are similar to those observed for "Zone III" of CF450. In this Zone, we can observe that CO yield decreases while CO_2 slightly increases, because of the partial oxidation of methanol:

$$CH_3OH + Me^{n+}O \rightarrow CO_2 + 2\ H_2 + Me^{(n-2)+} \quad (1)$$

This is also demonstrated by the oxygen balance graph, where the oxygen delivery is stable, which also means a steady oxygen uptake from the solid by MeOH.

"Zone III" is the ending Zone (like "Zone IV" in CF450), where the reduction of the solid is nearly complete and the reaction that mainly takes place is MeOH decomposition; a very slow deactivation phenomenon is observed in this sample too.

Reduction with MeOH at 420°C

The reduction test carried at 420°C is reported in Figure 3-27.

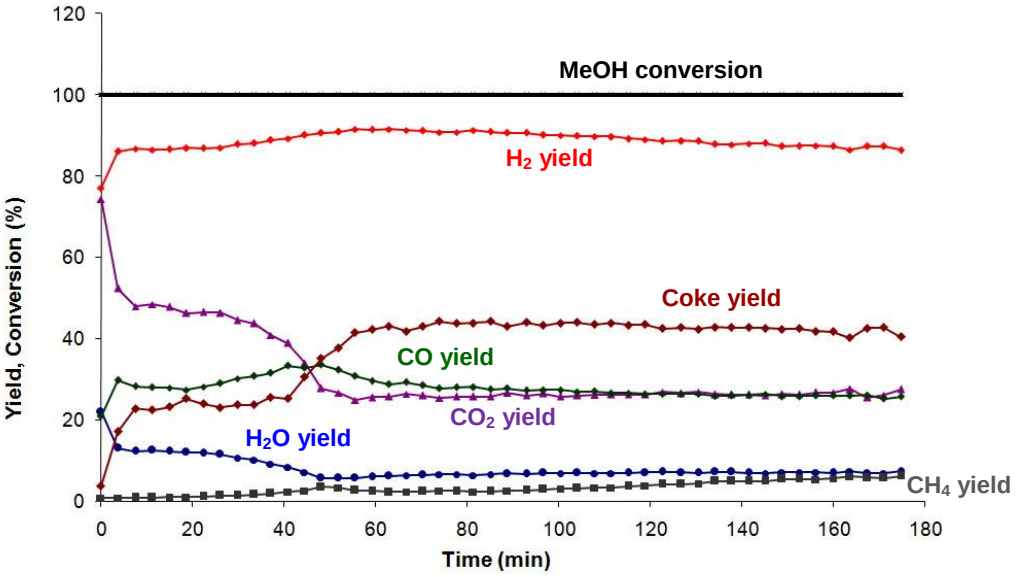

Figure 3-27. Product yields and MeOH conversion at 420°C using NF450.

Like in the CF450 test, the different “Zones” of reaction are condensed during the first 70 min tos; MeOH conversion is total during the entire test.

CO_2 and H_2O yields are very high at the beginning of the reaction; then, the loss of oxidizing power of the solid lead to a decrease of these products and to a raise of CO, H_2 and coke yields, until the end of the “Zone I” at about 70 min. After this period, experimental data show a steady state where decomposition of MeOH, disproportion of coke and reverse-WGS take place, like in the corresponding CF450 test.

Despite the very fast kinetics of reduction, the main difference between the Co- and Ni- ferrite, concerning the redox properties, are clearly evident from the experiment; in fact, CO_2 and H_2O yields at the very beginning are higher in NF450 than in CF450.

Reoxidation with water of totally reduced samples

The reoxidation was carried out only on the sample reduced at 300°C. The resulting graph is hereafter reported (Figure 3-28).

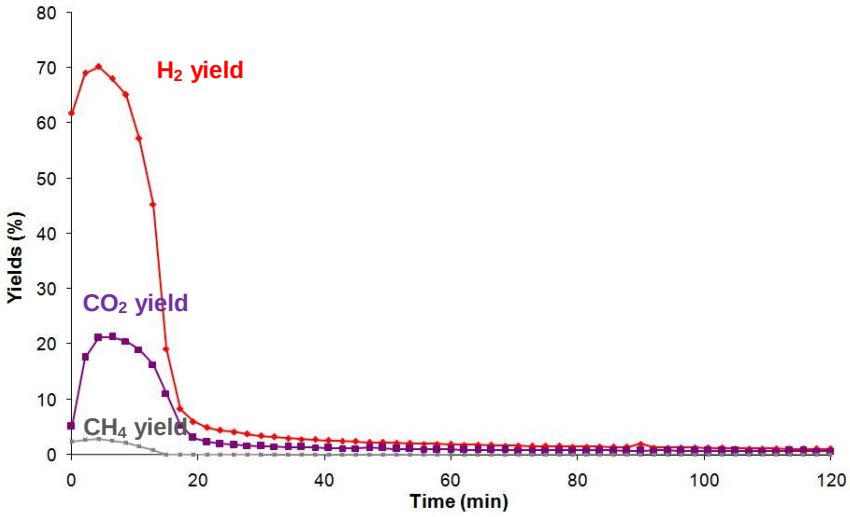

Figure 3-28. Reoxidation with water at 420°C of the NF450 totally reduced at 300°C (see Figure 3-24)

The main products were H_2 and CO_2, as expected; however, the main difference with respect to the CF450 test is that despite the very large amount of coke deposited on the catalyst (40%$_w$ of the reduced catalyst mass), no CO formed. The third product was CH_4, that is produced by the methanation of coke, which occurs because of the large amount of hydrogen produced during reoxidation.

3.2.2.3 Magnetite

MeOH reduction at 300°C

The third sample screened is the Fe_3O_4, which is known to be the worst oxidant compared to all the other iron spinel oxides. The results of the test are reported in Figures 3-29 and 3-30.

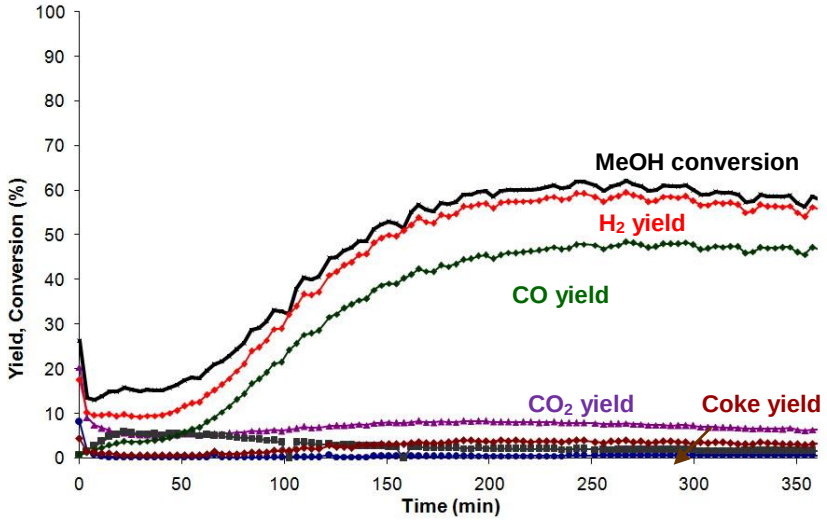

Figure 3-29 Product yields and MeOH conversion at 300°C using FF450.

In this case, the catalytic test period can be splitted into two Zones only.

“Zone I” is limited to the first 50 min tos. At the very beginning, the catalytic behavior of the material was similar to that one observed with

the other two compounds, where CO_2 and H_2O yields showed their higher values. After this first moment, characterized by a relative high MeOH conversion too, the trends experimentally observed were strictly dependent upon the progressive reduction of the iron oxide, that led to the production of CO and H_2 as products of MeOH decomposition.

"Zone II" included all the remaining part of the catalytic test. MeOH conversion started to rise, like in the case of CF450, but the growth was very slow; this occurred because of the kinetic limitations characterizing this material under anaerobic oxidation reactions. The consequences of this property are the very low yield to oxidation products, such as CO_2 and H_2O, and the largely prevailing contribution of MeOH decomposition:

$$CH_3OH \rightarrow CO + 2H_2 \qquad (3)$$

Carbon dioxide and coke were the secondary products, with a very low yield obtained during the entire experiment (except for CO_2 yield, which was high during the very first 5 min tos).

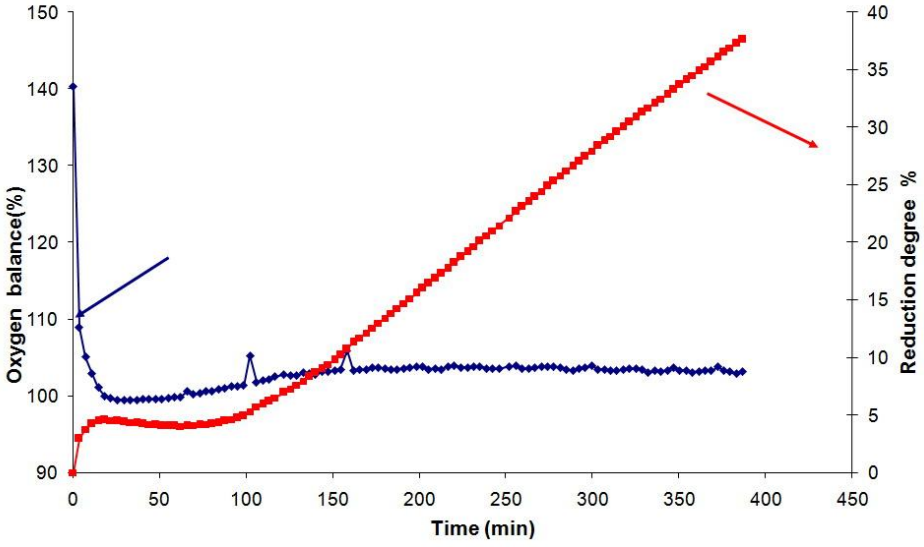

Figure 3-30 Oxygen balance (blue, left axis) and reduction degree of the catalyst (red, right axis), with FF450.

During “Zone I”, the oxygen balance showed a high initial uptake from the solid, followed by a stabilization at about 100% in “Zone II”; this means that after the reduction of the highly reactive species (like in the other ferrites), the bulk reduction was very low, and after 6 hours only the 35% of the oxygen present in the oxide had been removed.

In regard to the nature of the highly reactive species, we can attribute it to low-coordination atoms present on the surface (like in the case of CF450 and NF450), but also to oxidized species deriving from the oxidation of Fe^{2+} to Fe^{3+} in air, at RT. In other words, the initial high reactivity might be due to the presence of a Fe_2O_3 layer covering the spinel. This thin layer might form during the stocking of the material, and it cannot be revealed by means of XRD analysis because it is not a crystalline bulk phase.

Reduction with MeOH at 420°C

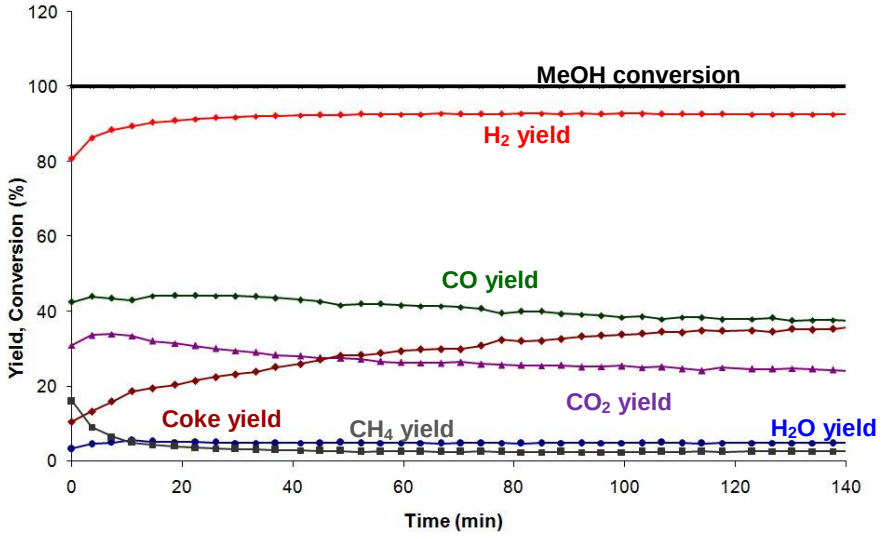

Figure 3-31 Product yields and MeOH conversion at 420°C using FF450.

The test carried out at higher temperature (420°C, Figure 3-31) showed the same behavior of the other compounds, with a decrease of CO_2 yield

and the progressive increment of the coke yield during the increasing tos. The main difference, compared to the NF450 and CF450 test, is that the yield to CO_2 was lower than that to CO during all the experiment time, demonstrating again the very low oxidizing power of this material, also at high temperature. Consequently, the time required for the complete reduction of the material at this temperature was more than two hours, nearly twice as much that needed with the other spinels.

Reoxidation with water of totally reduced sample

In this case the total reduced sample was obtained only at 420°C; here we report about the reoxidation of this material (Figure 3-32).

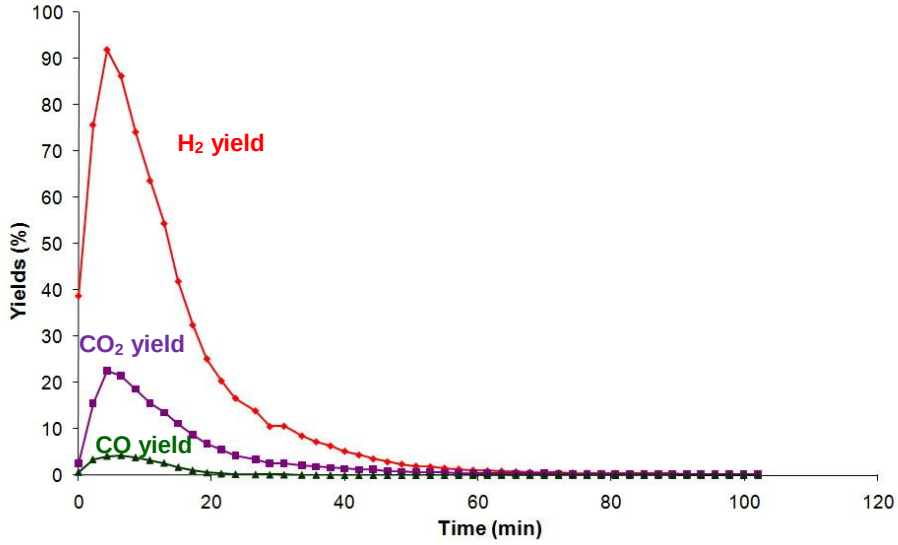

Figure 3-32 Reoxidation with water at 420°C of FF450 totally reduced at 420°C.

As in the other cases, H_2 and CO_2 were the two main products. Carbon monoxide was also observed during the reoxidation, as in CF450, due to a very large amount of coke deposited during the reduction step.

3.2.3 Catalytic tests: the repeated cycles

In order to carry out repeated redox cycles, alternating the methanol and water feeds, first it is necessary to define the best reaction conditions for each step, especially for the reduction one.

3.2.3.1 Definition of the parameters for the repeated cycles

Reduction step

The most important parameter to set is the reduction degree of the solid to achieve during the first step, because a low degree of reduction will give low water conversion and consequently low hydrogen concentration (and low overall amount of hydrogen produced) during the second step. For this reason, we have established a minimum reduction degree of 10%, that can be compared to the reduction of a supported system containing only the $10\%_w$ of the active oxide on the support.

The second important aspect is the temperature of the first step, that can reasonably be comprised between 300°C and 420°C, as demonstrated by the complete reduction tests. At 300°C, the conversion of MeOH (and, correspondingly, the extent of reduction achieved) was strongly related to the redox properties of the material, while at higher temperature a complete conversion of the reactant was soon achieved with all samples. Furthermore, we have discussed how the reactions which led to the oxide reduction (partial oxidation and total oxidation, reactions (1) and (5)) took place mainly at the beginning of the reaction time, while the extent of methanol decomposition, an undesired reaction, with all samples rapidly grew up after “Zone I”.

For CF450 and NF450, the temperature chosen is 300°C, which allows us to monitor structural modifications of the samples (at higher temperature, the high reduction rate could hide changes occurring during

the cycles). For FF450, instead, this temperature is too low for the reduction step (it took more than 3h to reach 10% of reduction degree), while at 420°C the reduction was very quick, as it was for the other ferrites. Because of this, a middle temperature of 360°C was used, because at this temperature the catalytic behavior should be comparable to that one of the other materials. In order to counterbalance the drawback derived from the increased temperature, the reduction steps were carried out until a higher reduction degree of the oxide was reached, that finally led to a greater hydrogen productivity.

Finally, taking in account all these considerations, the reduction conditions were chosen as follows:

- CF450
    - T = 300°C
    - Time = 60’
    - Reduction degree expected for the 1st cycle = 10%
- NF450:
    - T = 300°C
    - Time = 30’
    - Reduction degree expected for the 1st cycle = 17%
- FF450:
    - T = 360°C
    - Time = 60’
    - Reduction degree expected for the 1st cycle = 35%

All the consecutive cycles were carried out while maintaining the temperature and the reaction time for the reduction step constant, in order to check whether the reduction degree was changing along with the increasing cycle number.

Reoxidation step

The reoxidation step was carried out at 420°C, because of the too slow kinetics at lower temperatures. In this case, it was decided that the parameter monitored for the interruption of the reoxidation step was the hydrogen concentration: for all the samples, the reoxidation was stopped when a hydrogen concentration as low as 0,1%$_v$ was reached.

3.2.3.2 CF450 repeated cycles

CF450 has been used for six complete redox cycles; integral results concerning the repeated reduction steps are reported in Figure 3-33.

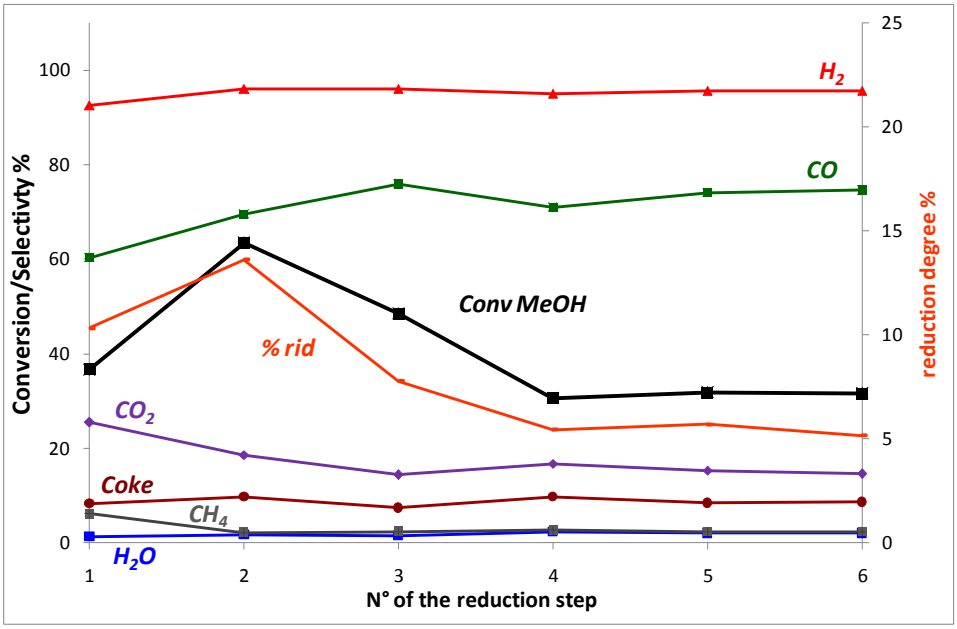

Figure 3-33 . Integral values of the repeated reduction steps on CF450 at 300°C.

To better understand the results reported, it's important to notice that for each one of the six reduction steps (on the x-axis), only the integral values are reported (for the definition of "integral value", see paragraph 2.3.2). This visualization is useful in the aim of understanding if the solid

characteristics are changing. Of course, the instantaneous yields were calculated too, but the experimental trends were similar to those reported in the previous paragraphs, where a wide discussion on the different reduction "Zones" for each material are reported. Furthermore, the reoxidation step was carried out after each reduction, to complete a cycle, but the results of these steps will be shown later; now, it is important to underline that an oxidation step took place in between two consecutive reductions.

Changes occurring between the first and the second step were quite remarkable: MeOH integral conversion showed an increase from 40% to 60%, H_2 and CO average selectivity also raised, while CO_2 and CH_4 decreased. These trends provide a clear demonstration of the loss of oxidizing power. These two considerations agree each other; in fact, if we hypothesize that the reoxidation with water after the 1st reduction has not been able to fully recover the original oxidation state of the oxide, we should observe a reduction step at the 2nd cycle that corresponds to a less oxidant solid (for instance, the reaction might start from "Zone II" and not from "Zone I"). As a consequence of this, a higher conversion of methanol due to the presence of sites active in alcohol decomposition would be observed (see discussion in paragraph 3.1.2 about "Zone I" and "Zone II").

After this difference, the following steps were characterized by a progressive decrease of MeOH conversion and of the reduction degree achieved during the same reduction time. This phenomenon is related to a deactivation phenomenon that will be better discussed later on, by means of the characterization of the used solid (possible sources for deactivation are sintering, deposition of coke that cannot be gasified during reoxidation with water, structural modifications).

One further comment is about the value of the reduction degree reached during the last three cycles, which was a constant value of about 5%. The fact that finally a steady and reproducible value is reached is a good result; however, the value should be improved, in order to increase the productivity of the system.

Figure 3-34 shows the integral amount of hydrogen produced (red curve) during the six oxidation steps, and the reduction degree (orange curve) reached during each one of the six reduction steps.

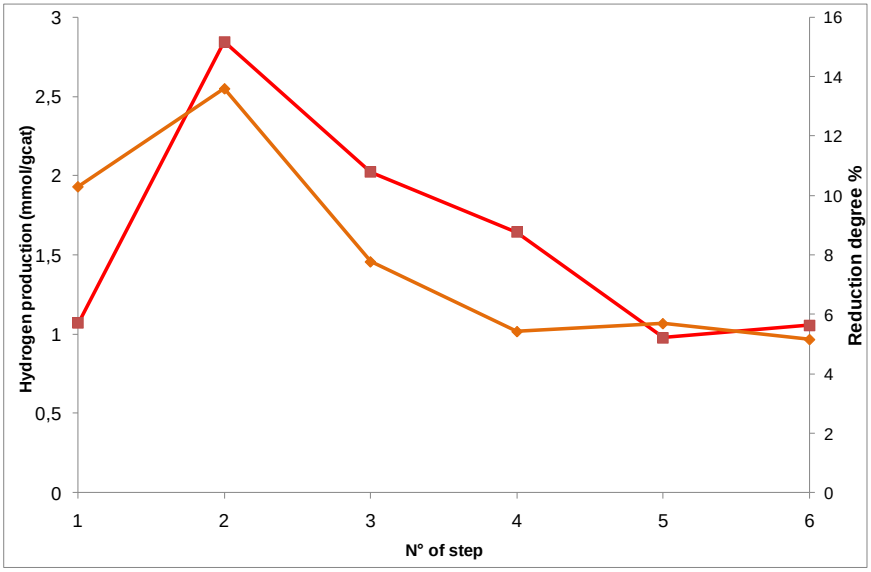

Figure 3-34. Reoxidation of CF450 after each reduction step. Hydrogen produced (mmol/g_{cat}, red plot, square symbols) and reduction degree reached during the reduction step before each oxidation (%, orange curve, rhombs).

It is shown that the two parameters were strictly related; the first reoxidation step demonstrates that the hydrogen produced was lower than that obtained during the other steps which also supports the hypothesis of an incomplete reoxidation of the solid during the first cycle.

Another important result is about the formation of CO_x: during the reoxidation, only CO_2 formed, and no CO was produced. This is explained by the very high catalytic activity of Co and Fe in Water-Gas-Shift, that may justify the complete gasification of coke to CO_2. However, in the complete reduction of the material a very huge amount of coke were deposited and CO was consequently produced (see Figure 3-22and Figure 3-23); so, this result demonstrates that limiting the formation of coke during the reduction step lead to the gasification of coke with no Co production.

3.2.3.3 NF450 repeated cycles

NF450 has been tested for five complete redox cycles; results obtained during the reduction steps are reported in Figure 3-35.

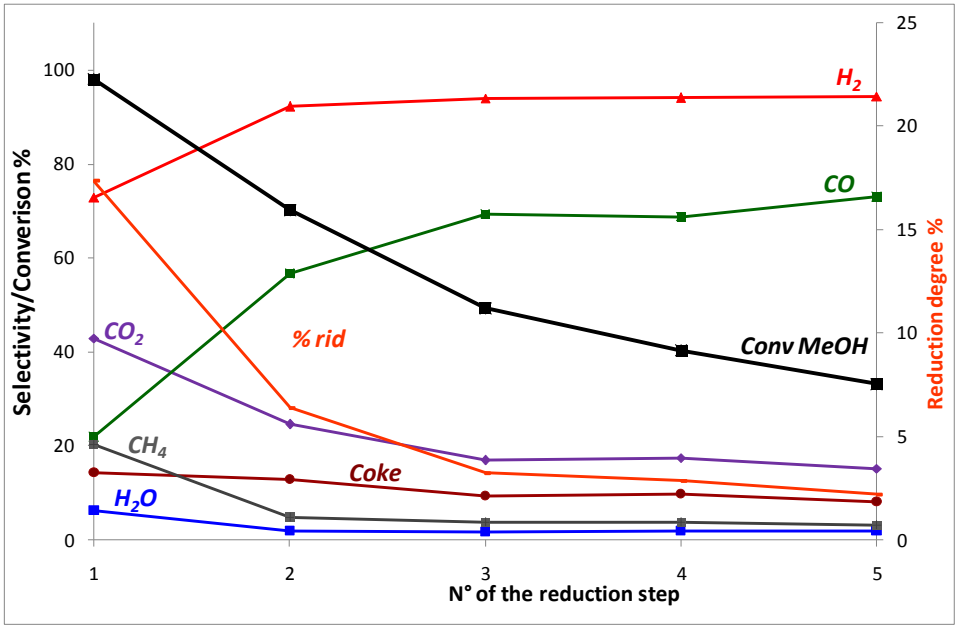

Figure 3-35 Integral values of the repeated reduction steps with NF450 at 300°C.

MeOH conversion, CO_2, H_2O selectivity and reduction degree all showed a progressive decrease along with the increased cycle number, while CO and H_2 selectivity increased. This is the consequence of the loss of oxidizing power of the solid, that in the end was even lower than that of CF450 (however, a longer reduction time, as in the case of CF450, might drive to a similar reduction behavior for the two oxides).

In the final cycle, a very low methanol conversion (about 35%) and reduction degree (<3%) make the results obtained during the reoxidation step hard to be quantified; therefore, the graph in Figure 3-36 is not showing the 5th oxidation step.

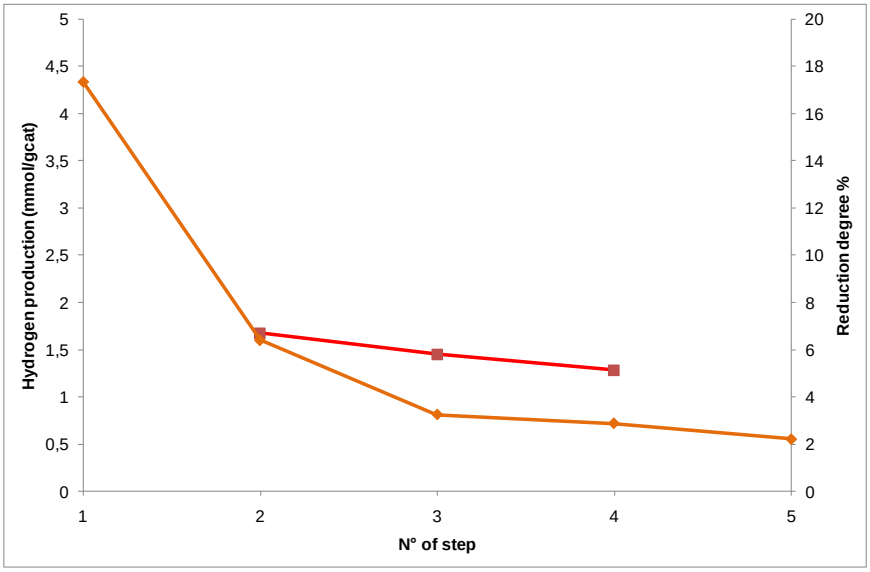

Figure 3-36. Reoxidation of NF450 after each reduction step. Hydrogen produced (mmol/g_{cat}, red plot, square symbols) and reduction degree reached during the reduction step before each oxidation (%, orange curve, rhombs).

Unfortunately, the total amount of hydrogen produced during the first reoxidation step could not be calculated, because of experimental problems. However, it is possible to notice similar values for the two parameters when compared to the corresponding ones obtained with

CF450 (results reported in Figure 3-34): 6-8% reduction degree gave a 1,7-1,8 mmol/g hydrogen production with both samples.

Same as before, no CO was registered; only a 0,05% yield to CH_4 during the 3rd reoxidation step.

3.2.3.4 FF450 repeated cycles

The third compound tested was FF450; it is important to remind that this compound was tested at 360°C because of the very low reduction rate taking place at lower temperatures.

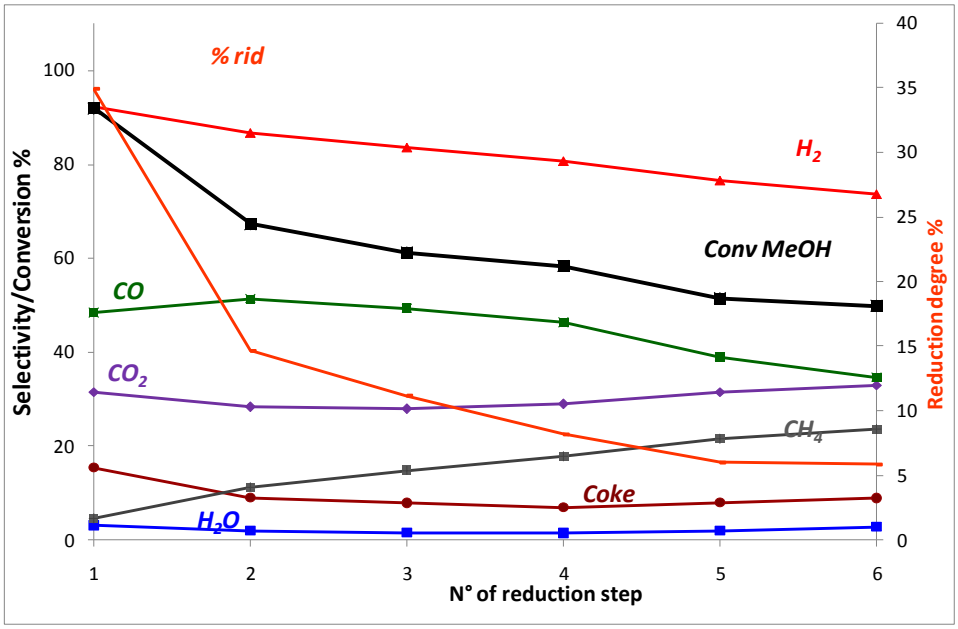

Figure 3-37. Integral values of the repeated reduction steps with FF450 at 360°C.

The first cycle was characterized by a higher conversion of the reactant and a higher reduction degree, if compared to CF450 and NF450, due to the higher temperature used (360°C vs 300°C for CF450 and NF450); for this reason, the comparison of this point with the other compounds is not

meaningful. After the first cycle, the performance fell down and the catalytic behavior became comparable to that of NF450 and CF450.

However, one difference concerns the H_2 and CO selectivity; with both CF450 and NF450, selectivity to these products increased while increasing the cycle number, and CO_2 continuously decreased. The trend observed with FF450 was opposite, because both H_2 and CO were consumed by the methanation reaction; in fact, CH_4 selectivity progressively increased up to 20% in the last cycle.

However, MeOH conversion also decreased, and this was probably related to a modification of the structure, that will be analyzed in the next paragraph. Finally, the reduction degree decreased along with the increasing number of cycles, up to a final value of about 6% (Figure 3-38); this demonstrates that FF450 is a very poor oxidizing oxide if compared to CF450 and NF450, which reached the same reduction value after 4/5 cycles but at 60°C lower temperature.

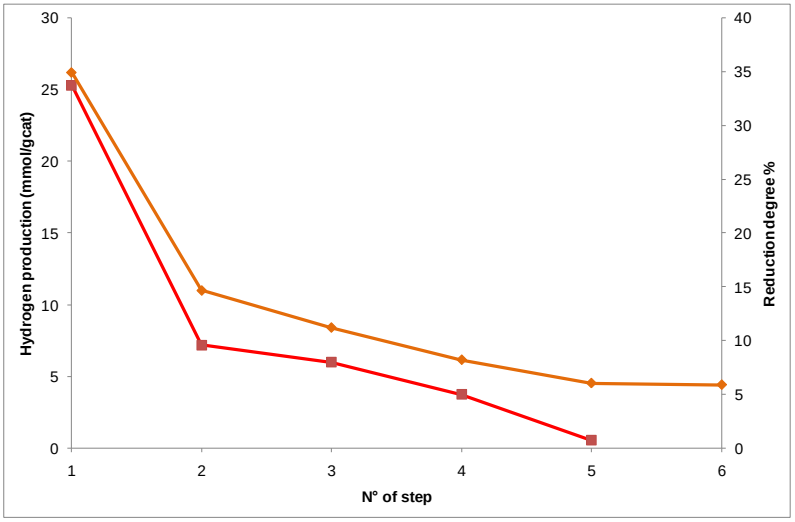

Figure 3-38. Reoxidation of NF450 after each reduction step. Hydrogen produced (mmol/g_{cat}, red plot, square symbols) and reduction degree reached during the reduction step before each oxidation (%, orange curve, rhombs).

FF450 showed a big difference concerning the CO_x production during the repeated reoxidation steps; H_2 and CO_2 were the main products, but CO formed at non-negligible concentration (up to 4% of yield in the 4th cycle). This is probably due to the high coke deposition that took place at relatively higher temperature (360°C), especially during the first reduction step, where a 90% MeOH conversion and a 15% selectivity to coke led to the deposition of 30 mg of coke on the reduced catalyst (for comparison: NF450 after the 1st reduction, 10 mg of coke, CF450 4 mg of coke).

For a deeper discussion on coke deposition during the repeated cycles, look at paragraph 3.2.4.2.

3.2.3.5 Characterization of the used materials

With all materials, a deactivation phenomena was observed. Structural characterization was essential in order to understand the reason for these changes. Hereafter, the XRD and the BET analysis of the three materials investigated are reported.

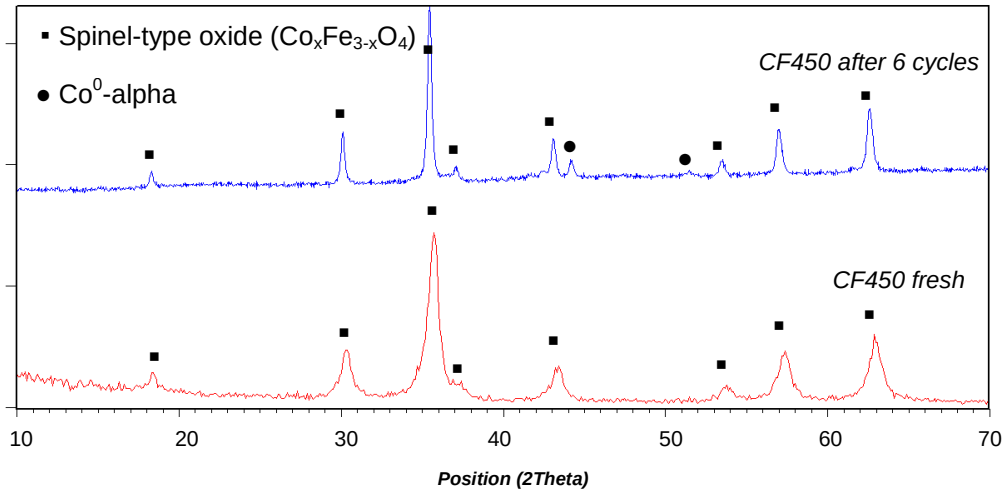

Figure 3-39 XRD patterns of fresh and used materials: CF450

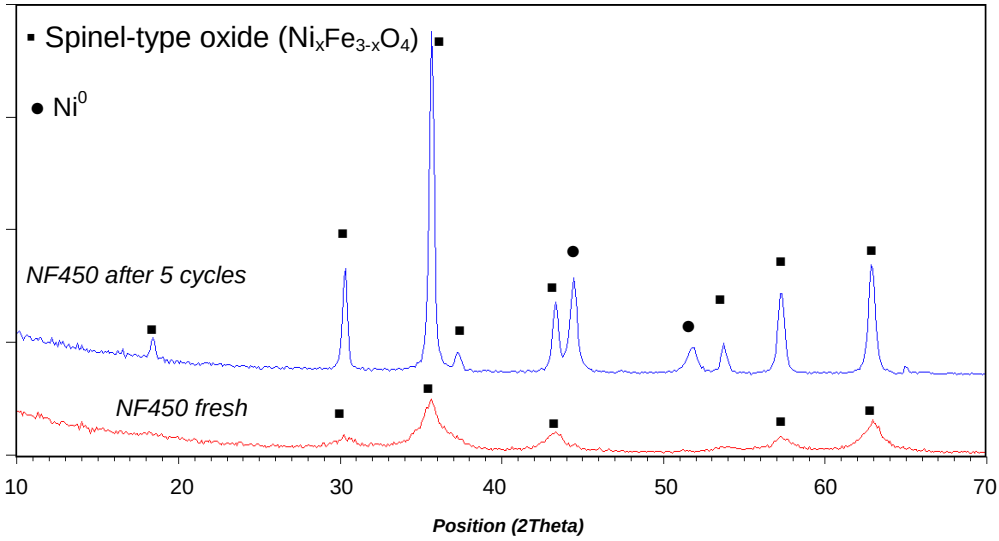

Figure 3-40. XRD patterns of fresh and used materials: NF450

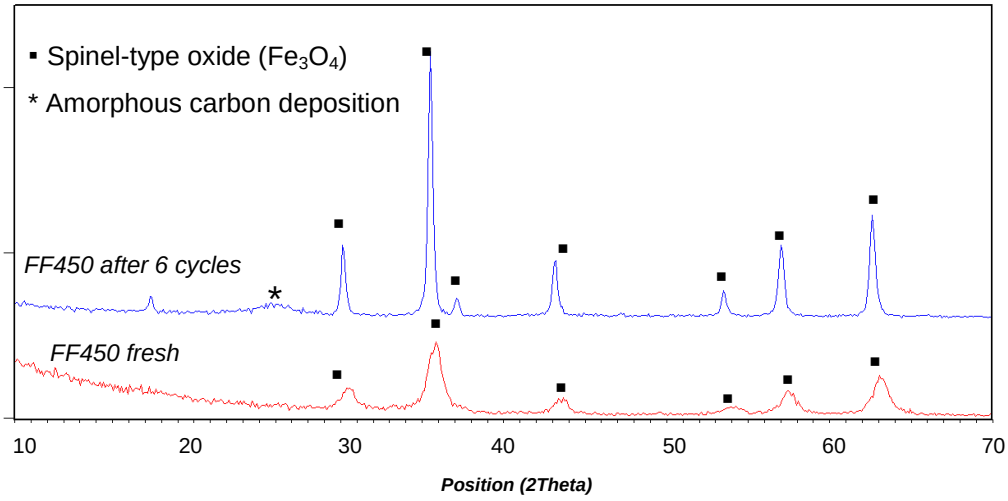

Figure 3-41. XRD patterns of fresh and used materials: FF450

XRD patterns show that Co^0 and Ni^0 were present in used CF450 and NF450, respectively: this is an unexpected phenomenon, because from the thermodynamics a Co/Fe alloy with the right composition is oxidizable by water to the corresponding mixed ferrite oxide. Therefore, it is

possible to hypothesize either the presence of a non stoichiometric reduced phase, or a incomplete reoxidation of the reduced CF450 and NF450 samples.

In FF450, the carbon deposited was not completely gasified during the second step; this is demonstrated by the very large peak at around 26° in the XRD pattern, which is attributable to amorphous carbon.

The other modification that occurs with all samples was a sintering phenomenon, as demonstrated by the sharper diffraction reflections in the used compounds patterns; the crystallite dimensions calculated from the Scherrer equation are reported in Table 3-3.

The additional consequence of the sintering was the decrease of the specific surface area; BET results are also reported in the Table 3-3.

Sample	***SSA (m2/g)***		***Crystallite dimension (nm)***	
	fresh	*used*	*fresh*	*used*
CF450	72	<5	12	35
NF450	94	<5	7	38
FF450	85	37*	10	55

Table 3-3. SSA and crystallite dimension of CF450, NF450 and FF450 as-synthesized and after use in repeated cycles. *=relatively high surface area due to the residual coke.

The two phenomena just discussed are in agreement with the catalytic results obtained with the three oxides:

- CF450 showed a decreasing of the oxidation power between the 1st and 2nd cycles, which was due to the lower oxidation state, demonstrated by the presence of the Co^0 specie (see paragraph 3.3.3.2 for deeper investigation) from the second cycle onwards, a progressive decrease of the activity of the material was the consequence of the sintering phenomenon.

- NF450 is the oxide showing the most drastic changes in catalytic results: the segregation of Ni led to the formation of Fe_3O_4; this explains the considerable decrease of MeOH conversion because of the lower oxidizing power of this oxide (see paragraph 3.2.2.3).
- FF450 is the only oxide that showed a linear decrease of the activity along with the increased number of cycles, which is explained by taking into account sintering phenomena. BET analysis showed that the surface area did not decrease too much (from 85 to 37 m^2/g), but this final value was probably due to coke, which was still present even after the reoxidation step. Indeed, deposition of coke was evident simply by handling the oxide: the solid blots all the surfaces like a "pencil.

3.2.3.6 Conclusions about the repeated cycles

The results reported offer promising perspectives but also show some drawbacks.

Catalytic experiments with the three samples tested have shown results which are in agreement with those reported in literature, about the redox properties of the samples (oxidizing power rank: NF450>CF450>FF450). Reactivity tests showed that the products distribution is function of the chemical composition of the ferrite, both during the reduction step (for instance, with the nickel ferrite the methanation reaction was favored) and the reoxidation one (with CF450 and NF450, no CO formed from the gasification of coke). This result can be useful for the design of a ferrite based catalyst able to produce a CO/H_2 ratio in the lean gas from the 1^{st} step which is affected by the solid composition.

On the other hand, two main drawbacks were noticed.

Firstly, the repeated cycles demonstrate that the decrease of hydrogen productivity is a consequence of modifications involving the solid.

Secondly, with CF450 we observed the development of a steady behavior (from 4th cycle onwards), but the hydrogen produced was very low; moreover, coke deposition was not completely avoided even when the conversion of MeOH was low, because of the large decrease of the oxidizing activity.

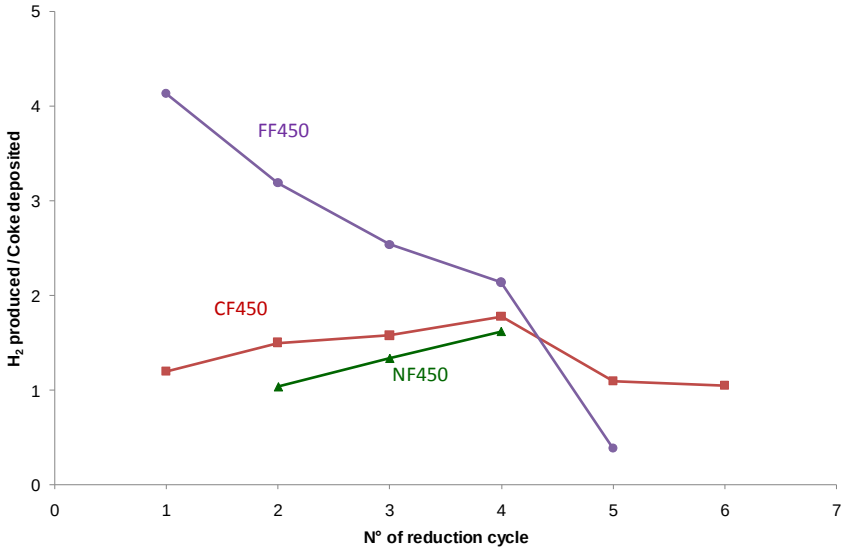

Figure 3-42. H_2 produced during the reoxidation step in relation to the coke deposited during the corresponding reduction step, in function of the cycle number, for CF450, NF450 and FF450.

Therefore, hydrogen productivity and H_2/coke ratio is the second problem to solve, in order to optimize these looping systems. A low H_2/coke ratio (Figure 3-42) means that coke gasification is the main H_2-producing reaction, while the target of the process is to use the material redox cycle for hydrogen production.

In the next paragraph, a preliminary screening of different solutions aimed at finding a solutions for these problems is reported.

3.2.4 A preliminary screening of possible improvements for thermochemical MeOH reforming

3.2.4.1 Reoxidation in air of used samples

One of the problems met during the repeated cycles of the spinels is the segregation of metallic Ni and Co, observed in used NF450 and CF450 samples. From a stoichiometric standpoint, the presence of Ni^0 and Co^0 suggests that the spinel phase is definable as $(A^{2+}_x\ Fe^{2+}_{1-x})\ Fe^{3+}_2O_4$ (A=Ni,Co); therefore the presence of Fe^{2+} shows that the sample is not completely oxidized by means of the treatment with water. This can be due to two possible reasons:

1- Segregation of Ni (Co) during the reduction step, with formation of domains that are not reoxidizable with water at this temperature.
2- Incomplete reoxidation of the two samples because of thermodynamic limitations.

It is known that the reoxidation step of the reduced oxide with water is an exothermic reversible reaction (see paragraph 1.3.5.4), thermodynamically favored at low temperature. This is the reason why the reoxidation step has to be performed below a certain temperature. The maximum conversion allowed for this type of reaction decreases when the temperature is raised (see Figure 3-43). On the other hand, the kinetics of the reaction is usually proportional to temperature, as long as conversion is far from the equilibrium value, but it will decrease when the thermodynamic limitation is approached. The isokinetic curves ($-r_a/C_{A0}$) reported in Figure 3-43 are function of both the temperature and the "distance" from the equilibrium conversion. This means that if we are near to the equilibrium conversion, the reaction rate will be very slow and the time necessary to complete the reaction will be very long.

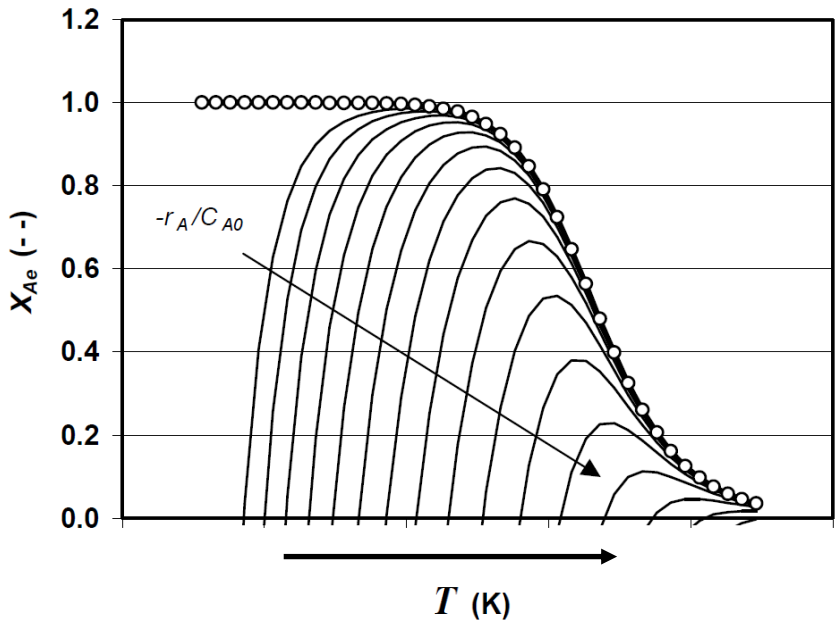

Figure 3-43. Exothermic reversible reaction: equilibrium conversion as a function of the temperature and isokinetic curves ($-r_a/C_{a0}$)

In our case, this means that the operating temperature of the reoxidation steps (420°C) could be low enough for FF450 so allowing to reach the complete reoxidation (no Fe^0 was observed in the XRD pattern of used sample), but it could be too high for CF450 and NF450. The consequence is that the equilibrium conversion of these two samples could be lower than 100%; furthermore, the reoxidation rate at the end of the reoxidation step could be very low because of kinetic reasons.

An additional evidence further confirming the hypothesis of a thermodynamic limitation, is shown in Table 3-4: in fact, the rank relative to the extent of solid reoxidation achieved during the reoxidation step was the opposite of the rank relative to the extent of reduction obtained during the reduction step (both referred to the 1st cycle). This confirms that the two steps, reduction and reoxidation, were limited by thermodynamics.

Sample	***Thermodynamic trend***	
	1st Reduction step	*2nd Reoxidation step*
NF450	+++	+
CF450	++	++
FF450	+	+++

Table 3-4. Extent of solid reduction or reoxidation (both achieved during the 1st cycle) of NF450, CF450 and FF450. Legend: +++ complete; ++: almost complete; + partial.

In order to demonstrate that no segregation phenomenon of metallic species took place (which might be another reason for the incomplete reoxidation with water of reduced samples), we carried out the reoxidation of reduced oxides with air, instead of water. In such a way, any thermodynamic barrier should be overcome, and the original spinel oxide should be obtained.

The annealing in air of used NF450, CF450 and FF450 was carried out using the same procedure described for the calcination of the freshly precipitated spinel precursors, using a maximum temperature of 450°C. The materials obtained were analyzed by means of XRD and BET surface area; the results obtained are hereafter reported (Figures 3-44 and 3-45, Table 3-5).

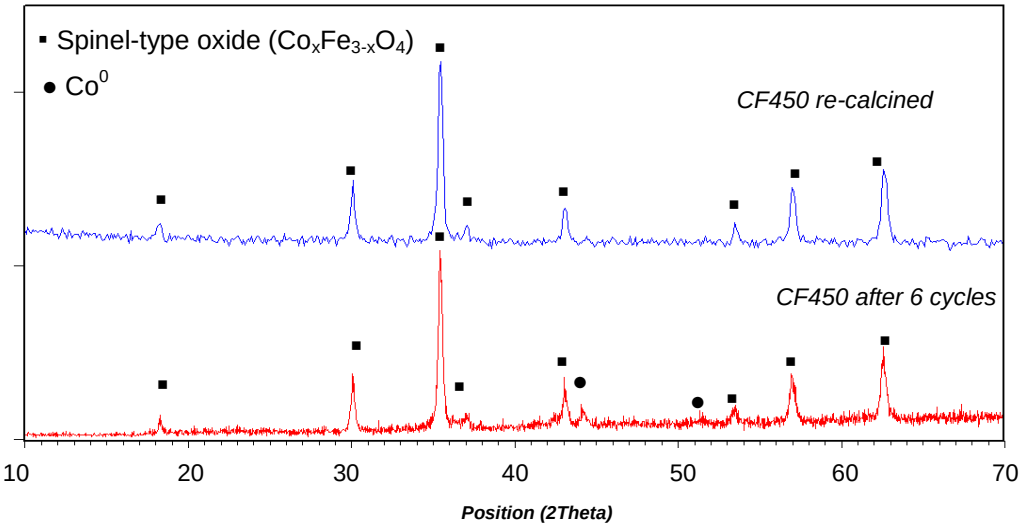

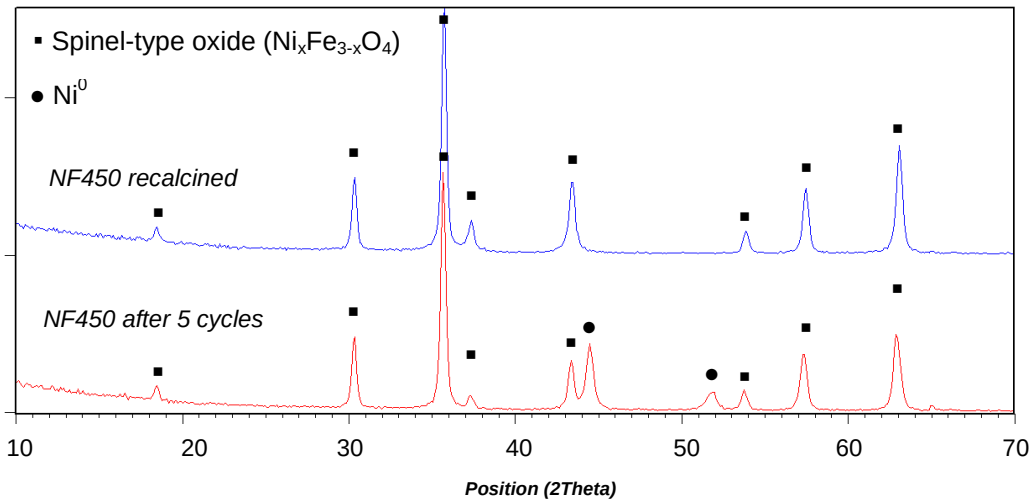

Figure 3-44. XRD pattern of (top) CF450 and NF450 (bottom) first used in 6 RedOx cycles, and then calcined in air.

Sample	SSA (m^2/g)		Crystallite dimension (nm)	
	After cycles	Re-calcined	After cycles	Re-calcined
CF450	<5	13	35	36
NF450	<5	10	38	41
FF450	37*	15	55	54

Table 3-5 . SSA and crystallite dimension of CF450, NF450 and FF450 used in repeated cycles and then re-calcined in air.

The surface area of CF450 and NF450 slightly increased, which demonstrates that the re-calcination in air of the samples did not change the morphology of the oxide.

Concerning FF450, calcinations were carried out in order to check whether the coke deposited could be burnt at relatively low temperature; from the BET analysis, showing a decrease of SSA compared to the sample reoxidized with steam, it can be inferred that the oxidation of coke took place.

Catalytic test with NF450 regenerated in air

For a better understanding, the NF450 re-calcined in air will be now identified with the code NF450_reg.

The NF450_reg sample was tested in one catalytic experiment carried out using the same conditions of the repeated cycles. The result is reported in Figure 3-46 (6th cycle, carried out after the reoxidation in air).

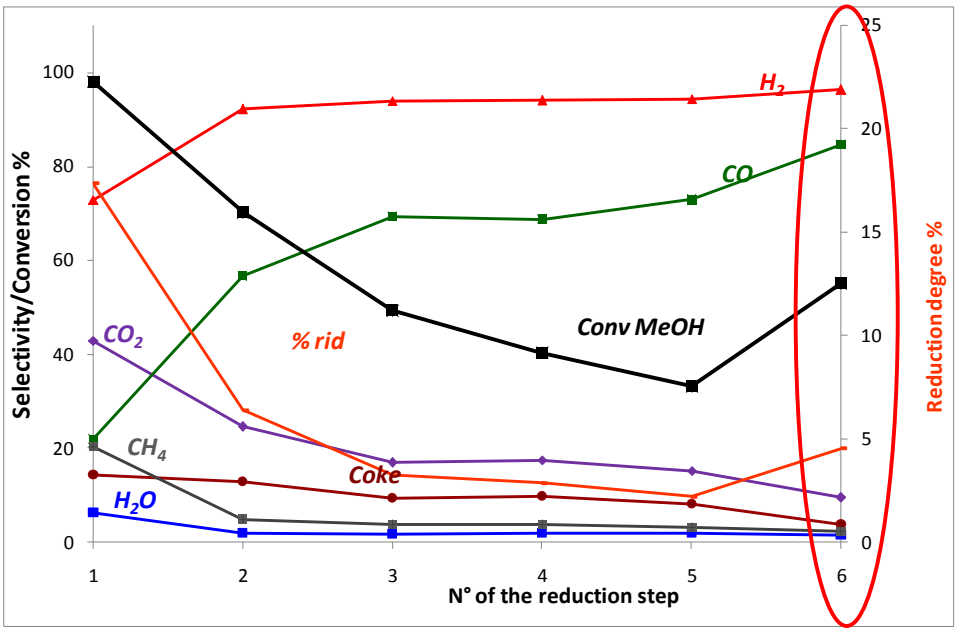

Figure 3-45 . Integral values of the repeated reduction steps with NF450 at 300°C (taken from Fig. 3-35), plus an additional 6th cycle with NF450_reg.

From the catalytic result, we can see that the activity of the sample increased with respect to that shown by the sample at the 5th cycle, but the oxidizing power was not completely recovered: actually, the CO selectivity rose while CO_2 selectivity decreased. However, a lower amount of coke was also observed.

If we compare the 3rd cycle with the 6th one, the same MeOH conversion and reduction degree were reached, which however are still too low for practical purpose.

Conclusions on the reoxidation with air

In conclusion, we can say that the incomplete reoxidation of the material with water could be the main problem for the reproducibility of the process along several cycles. A further reoxidation with air demonstrates a possible recovery of the original solid composition.

Many other solutions can be proposed, such as:

- Extend the duration of the second step, but this will reduce too much the total productivity of the process because more time would be needed;
- After the reoxidation step at 420°C, decrease the temperature till the temperature for the reduction step is reached, while keeping on feeding water, in order to help the reoxidation from a thermodynamic point of view
- Add an air-reoxidation step (3rd step of the cycle) to the chemical loop, in which the sample is put in contact with air to complete the reoxidation, and also remove all the carbon still deposited on the catalyst.

Sintering phenomena cannot be solved with this approach, and other solutions will have to be taken into account in order to hinder it or to improve the productivity.

3.2.4.2 High-temperature repeated cycles on CF450, to increase the H_2/coke ratio

From the analysis of Figure 3-42, we can infer that during the first three cycles carried out on FF450, a high H_2/coke ratio was obtained. Taking into account the redox properties of this oxide, it can be reasonably concluded that this behavior was a consequence of the temperature at which the reduction step was carried out. Probably a higher temperature would lead to a higher overall coke deposition but, if we consider the first minutes reaction time, the reduction rate might be much faster than coke deposition.

To demonstrate this hypothesis, CF450 was used for 6 consecutive redox cycles at 420°C, both for reduction step and the reoxidation steps; catalytic results are shown in Figure 3-47; Figure 3-48 shows the results obtained during the reoxidation steps.

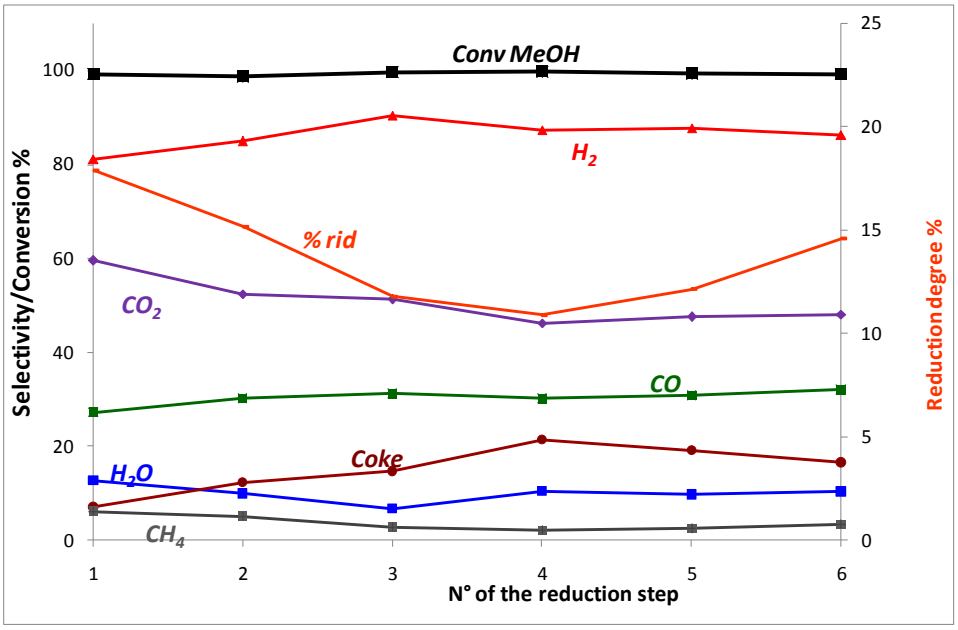

Figure 3-46. Integral values of the repeated reduction steps with CF450 at 420°C.

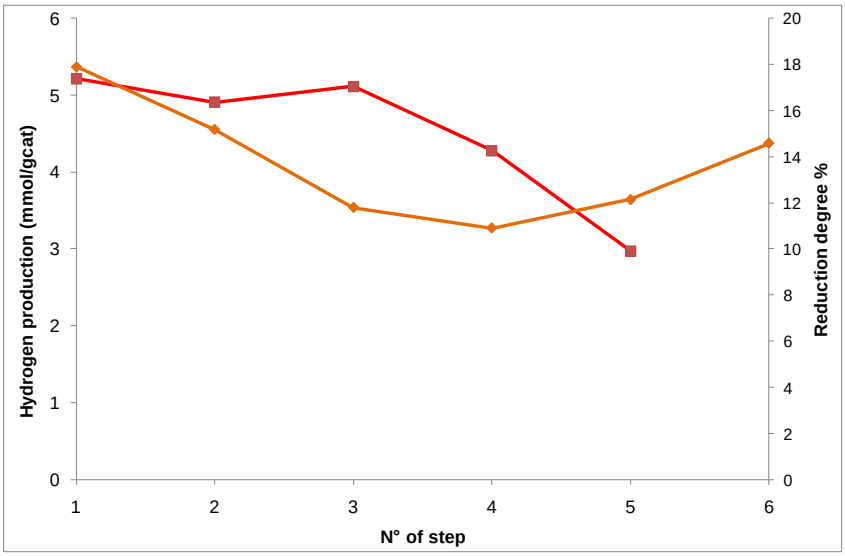

Figure 3-47. Reoxidation of CF450 after each reduction step (the latter at 420°C). Hydrogen produced (mmol/g_{cat}, red plot, square symbols) and reduction degree reached during the reduction step before each oxidation (%, orange curve, rhombs).

As in the previous cases, the reduction time was basically defined on the reduction degree desired; in this case, 20% of reduction was reached in about 10 min tos.

A complete conversion of MeOH was reached during each reduction step (as described in the part related to the “long” catalytic test at 420°C, reported in paragraph 3.1.2), and the oxidizing power of the material was higher probably because of the faster ionic oxygen diffusion inside the material lattice. Figure 3-48 shows that the hydrogen production was greater than that previously obtained with reduction at 300°C, but also in this case it slightly decreased during the six cycles.

Figure 3-49 reports the H_2/coke values in function of the cycle number, compared with the values previously discussed (Figure 3-42).; it can be noticed that using a reduction temperature of 420°C led to much higher values of H_2/coke.

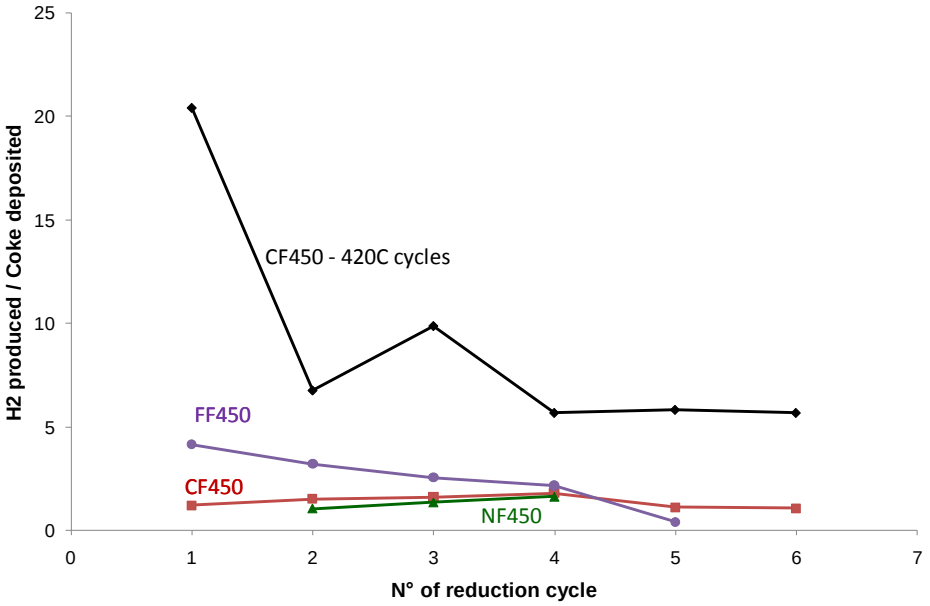

Figure 3-48. H_2 produced during the reoxidation step in relation to the coke deposited during the corresponding reduction step, in function of the cycle number, for CF450, CF450_420, NF450 and FF450.

We can conclude that even though the coke deposition during the low temperature test on CF450 was quantitatively lower (4% yield) compared to the 420°C test (10-15% yield), the reduction degree remained greater than 10% during all the high-temperature cycles. As a consequence of this, the ratio between the H_2 produced during the second step and the coke deposited during the corresponding first step greatly improved. This demonstrates that the oxidizing power of the solid is not the only parameter that has to be taken into account for the final optimization of the process.

From the XRD pattern of the used sample (Figure 3-50), we can notice that the amount of Co^0 raised compared to the corresponding used samples after 300°C-reduction cycles. This is probably due to the greater sintering effect that takes place during reduction at 420°C; the lower

surface area led to a slower reoxidation rate. Comparison of SSA and crystallite dimensions of used samples is shown in Table 3-6.

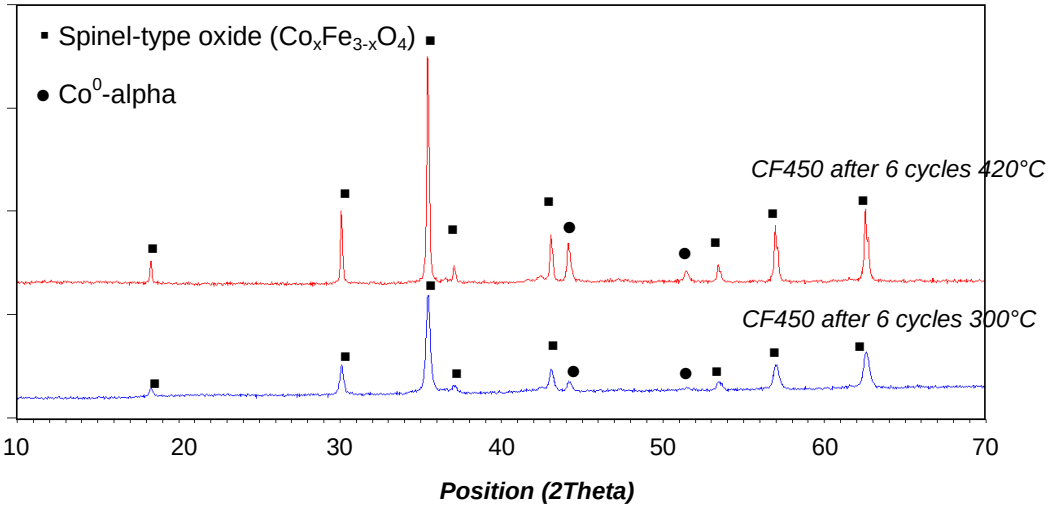

Figure 3-49. XRD patterns of used CF450 after reduction at different temperatures

Because of the incomplete oxidation of the sample as probed by XRD analysis, the used sample has been annealed at 450°C. This thermal treatment led to the recovery of the mixed spinel phase, without any residual Co^0, which means that a regeneration with air is still possible also in this case.

Sample CF450	***SSA (m^2/g)***		***$D_{crystallite}$ (nm)***	
	fresh	*used*	*fresh*	*used*
Cycles (R420-O420) + air	72	13	12	85
Cycles (R300-O420) + air	72	<6	12	36

.Table 3-6. Comparison of SSA and crystallite dimension of used CF450 samples.

Conclusions on the high-temperature tests

In conclusion, increasing the temperature could help to increase the H_2-to-coke ratio and the overall H_2 productivity too, because the time needed to reduce the sample is now 10 min and not 60 min, like in the case of reduction tests carried out at 300°C, with CF450. Another advantage is the temperature difference between the two steps which becomes nil; because both the reduction and the reoxidation steps were carried out at 420°C.

3.2.5 *Conclusions on the MeOH thermochemical reforming*

In this paragraph a deep analysis of reaction conditions for the steam-iron process, with MeOH as the reducing fuel, has been made.

The oxidizing power scale of the ferrites is $NiFe_2O_4$>$CoFe_2O_4$>Fe_3O_4, but after just one cycle all the oxides undergo deactivation. We have carried out an investigation on the causes responsible for this effect, by means of XRD and BET analysis. Two main effects contribute to the deactivation experimentally observed::

1. An incomplete reoxidation of NF and CF materials, probably due to thermodynamic limitations; so, the incomplete recover of the original spinel led to the formation of Fe_3O_4, which is less active than the starting compounds.
2. Sintering/aggregation phenomena which led to a decrease of SSA and hence to a decrease of the reaction rates.

Another drawback is the deposition of coke during the first step of the cycle. The Hydrogen produced-to-coke deposited ratio made evident to us that the temperature of 300°C may not be the best choice for an efficient performance of the repeated cycles.

Two solutions have been proposed:

1. An increase of the reduction temperature; cycles carried out with a reduction temperature of 420°C, with CF450, showed that the $H_2^{prod}/Coke_{dep}$ ratio can be strongly improved by changing this parameter.
2. A third step of oxidation with air, to be carried out after the 2nd step of water dissociation; this may help to completely restore the original oxidation state of the spinel.

Finally, the last problem that has to be solved in order to further improve the overall productivity of the process concerns the sintering phenomena, which can be probably avoided either by adding physical promoters or by supporting the active phase on specific oxides, as already reported in the literature[101,120].

3.3 Investigation on $CoFe_2O_4$ modifications during the redox process

A further investigation on the modifications occurring in $CoFe_2O_4$ during the redox cycle was carried out in collaboration with Dr.Millet of IRCE-CNRs in Villeurbanne-Lyon, where I spent a three-months period focussed on a more in depth characterization of fresh and used materials. This deeper analysis was made by means of Mössbauer spectroscopy, which was integrated with the XRD and SSA results previously obtained. In some cases, XPS spectroscopy was also carried out.

This paragraph will be divided into four parts, which concern the analysis of synthesized, of reduced, of reoxidized and of recalcined solids, in order to follow the same logical sequence of the paragraph 3.2, dealing with the thermochemical methanol reforming.

3.3.1 Characterization of synthesized compounds

Firstly, the main characteristics of the fresh samples were analysed. XRD patterns of CFp, CF450 and CF750, already discussed in paragraph 0, are reported again in Figure 3-50. The three samples are, respectively: the cobalt iron mixed oxide obtained after coprecipitation and drying at 120°C (CFp), after calcination at 450°C (CF450) and after calcination at 750°C (CF750). It is shown that a spinel type oxide was obtained in all cases; moreover, the increasing crystallite dimension was directly related to the increasing of annealing temperature, which led to a more relevant sintering of particles.

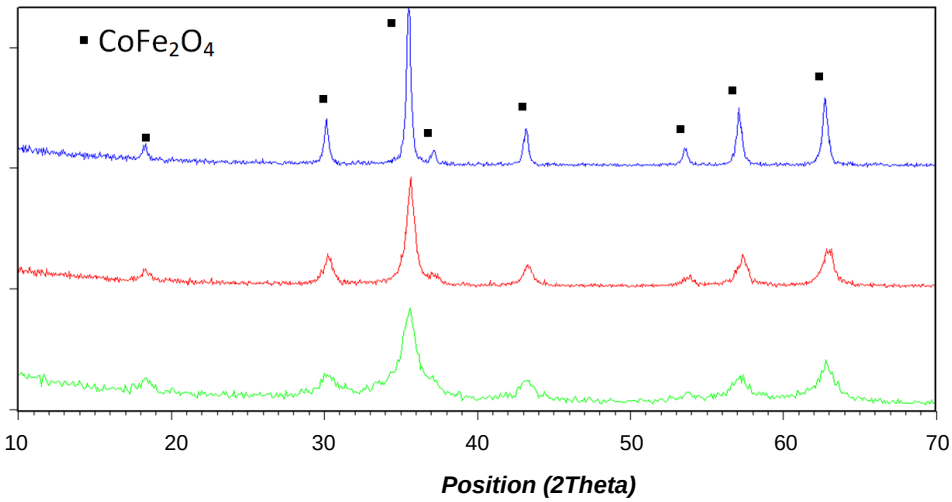

Figure 3-50. XRD patterns of fresh compounds (from the bottom, CFp, CF450 and CF750)

SSA and crystallite dimensions are reported in Table 3-7, which confirm the relationship between sintering phenomena and annealing temperature.

Sample	Treatment of the sample	SSA (m^2/g)	Crystallite size (nm)
CFp	Only dried 120°C	180	-
CF450	Calcined at 450°C	70	12
CF750	Calcined at 750°C	10	36

Table 3-7. SSA and crystallite size from Scherrer equation of fresh samples.

TPR analysis also demonstrates how the chemical activity of the two samples is affected by these differences, as reported in paragraph 3.1.5.

Mössbauer spectra were registered on these samples, and the morphological differences previously discussed were also evidenced using this technique. Experimental data and Lorentzian functions used for the fitting of the spectra are reported in the following pages, for the three samples examined.

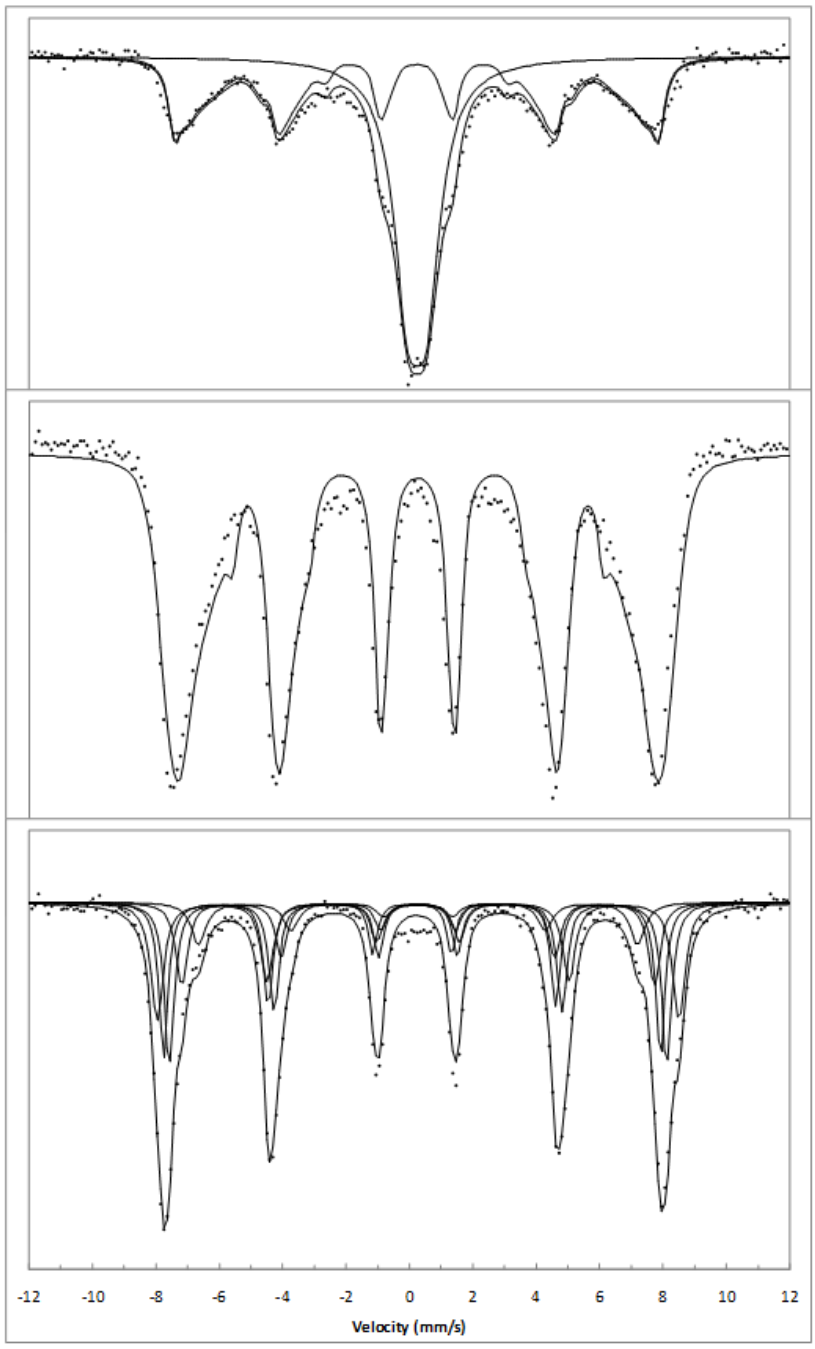

Figure 3-51. From the top: Mössbauer spectra of CFp, CF450 CF750 recordered at room temperature. Solid lines are derived from least-square fits.

The three spectra were quite different, because of the magnetic characteristics of the $CoFe_2O_4$, which are strongly dependent upon the size of the particles (Figure 3-52).

CFp shows the presence of two components in the fitting curve, a doublet and a sextet. The doublet component was due to the superparamagnetism behavior of the sample, which is a consequence of the small dimension of the particles; magnetization randomly changed under the effect of the temperature and only the effect of the electric field gradient at the nucleus is observed which gives rise to a doublet in the total spectra. Isomer Shift and Quadrupole Splitting were respectively equal to 0.33 mm/s and 0.69 ,mm/s, values that are in accordance with other authors[132,133,134]. As reported in those papers, a higher counting time during the spectra recording would have probably allowed to distinguish two different contributions to the doublet, related to Fe^{3+} in octahedral and tetrahedral sites, respectively. Besides a doublet, a distribution of sextets is needed to fit the total spectra that derives from the larger ferromagnetic particles that are amorphous. The distribution of Internal Magnetic Fields observed is shown in Figure 3-53. Both sub-spectra (doublet and sextet distribution) contribute for about 50% of the total fitting, if similar f-factor is assumed for the two components.

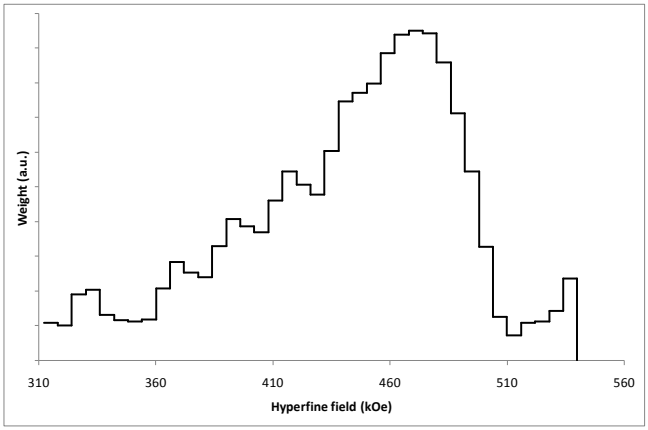

Figure 3-52. Hyperfine field histogram accounting for the magnetic sextet in CFp compound.

In CF450, the superparamagnetic doublet is not observed anymore because of the larger size of the particles in this sample. However, the middle temperature annealing (450°C) drove to an incomplete crystallization of the oxide and a distribution of Internal Magnetic Fields was still needed to fit the spectrum. According to the literature[133], Isomer Shift is 0,3 mm/s and the Internal Magnetic Fields are comprised between 36T and 51T, which is approximately what has been observed in this study with 0.2 mm/s and magnetic fields comprised between 33 and 52 T.

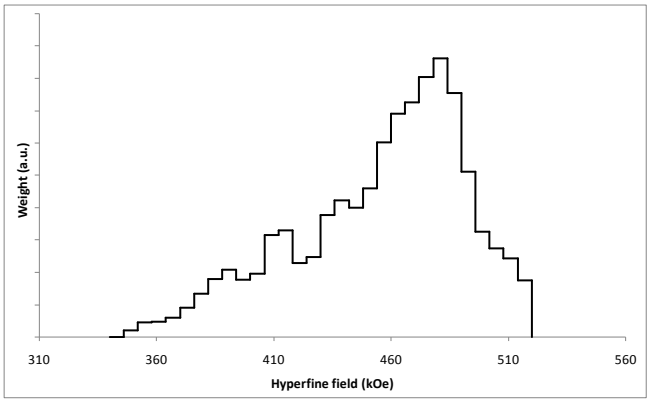

Figure 3-53. Hyperfine field histogram accounting for the magnetic sextet in CF450 compound

CF750 is the most crystalline compound; neither superparamagnetism doublet nor Internal Magnetic Field distribution were needed to fit the spectrum. As shown in Figure 3-51, the spectrum has been fitted with five different sextets. Each one of these sextets correspond to a given environment for the ferric cations in the ferrite compound referred to a different Fe^{3+} in the structure, in accordance with Sawatzky et al.[135,136].

These five different environments have been explained by the inverse spinel configuration of $CoFe_2O_4$, where half of the octahedral sites are occupied by Co^{2+} cations and the other half by Fe^{3+} ones. On the opposite hand, tetrahedral sites are completely filled by Fe^{3+} in the so-called high-spin field distribution.

The generic formula is:

$$(Co^{II}_{1-\delta}Fe^{III}_{\delta})^{Th}(Fe^{III}_{2-\delta}Co^{II}_{\delta})^{Oh}\ O_4 \qquad 0<\delta<1$$

where δ is the inversion degree of the oxide

Experimentally, a high inversion degree is usually obtained[137] with an annealing treatment followed by a slow cooling ramp[138], but the complete inversion is rarely observed. Consequently, the atoms in A (*Th*) and B (*Oh*) sites are a distribution of Co and Fe atoms that changes the internal magnetic field as a function of the chemical composition of the different unit cells. Only six tetrahedral nearest neighbors surround octahedral sites, so the composition of *Oh* environment is relevant in the total magnetic field. On the other hand, the iron ions in the tetrahedral sites are surrounded by twelve octahedral positions and the chemical composition of these sites does not affect a lot the internal magnetic field. For these two motivations, one of the five components in the fitting curve is referred to iron atoms in tetrahedral positions, while the other four components are referred to Fe^{3+} in the octahedral sites, with different chemical composition of the surrounding atoms: this interpretation is called “next-nearest neighbors’ theory”. Furthermore, in this work the interpretation has been made using the same isomer shift for the iron atoms in the octahedral sites in order to reduce the number of parameters adjusted in the fitting calculation. This is required because a very high number of freedom degrees could drive to values with no chemical-physical meaning. To better fit the spectrum, different isomer shifts have been assumed and fixed for the B sites, and the one with the lower value of χ^2 (variance of the final fitting) was considered to be the good one, as reported in the following table.

The inversion degree of the spinel is calculated as the double of the Fe^{3+} in A site considering a f-factor similar for all the iron species involved in the fitting.

IS	X^2	A			B1		B2		B3		B4		δ
		%	H(T)	IS	%	H(T)	%	H(T)	%	H(T)	%	H(T)	
0,37	813	24	48,4	0,18	24	50,8	26	48,5	16	46,1	10	42,8	48
0,4	920	35	48,4	0,19	21	50,9	21	48,5	13	46,1	10	42,9	70
0,41	742	39	48,4	0,2	20	50,9	19	48,5	13	46,0	9	43,0	78
0,43	857	45	48,4	0,2	18	51,0	17	48,5	10	46,0	10	43,0	90

Table 3-8. Mössbauer parameters computed from the spectra of CF750, recorded at 25 ° C; x isomer shift; H: internal magnetic field. Quadrupole Splitting is fixed to 0 in each fitting result

The relative ratios of the B sites derived from their relative spectral area is in agreement with the probability distribution to find an Fe^{3+} in B site with *m*Fe^{3+} in the next-near environment which is defined by the equation

$$P(m) = \frac{6!}{m!\,(6-m)!} * \boldsymbol{\delta}^{m}(1-\boldsymbol{\delta})^{6-m}$$

where m is the number of the surrounding Fe^{3+} and δ is the inversion degree of the spinel. For a 78% of inversion, we obtain the values reported below, that are in good agreement with Ferreira et al.[138].

B	m	P(m)	Fitting %
1	6	22,5	32,8
2	5	38,1	31,1
3	4	26,9	21,3
4	3	10,1	14,8
	2	2,14	
	1	0,24	

3.3.2 Characterization of reduced materials

The first step of the steam iron process studied in this thesis involves the reduction of the spinel oxide with MeOH. Here we will analyse reduced cobalt ferrites at different temperatures and with different reduction degrees of the material. The aim of this approach is to study the kinetics of CF450 and CF750 transformation, the species which are thermodynamically favoured and the relation between the material characteristics and the product distribution during catalytic tests.

It's important to underline that in some experiments here reported, the reduction has been carried out using τ=1s, in order to decrease the reduction rate and better evaluate differences between the two samples. Therefore, in every graph the residence time and the reduction temperature used are specified.

3.3.2.1 Different reduction degrees

The progressive reduction of the spinel is a function of both temperature and time-on-stream. Hereafter we report the XRD patterns of CF450 and CF750, reduced by means of different conditions.

The X-ray diffraction patterns show that the main reduced phase was the CoFe alloy, while other intermediate oxides such as FeO, CoO or Co^0 were not observed. Moreover, the patterns show that reduction in CF750 was slower than in CF450, under the same reaction conditions. This different chemical activity is more evident at low temperatures (300°C and 360°C), and it's the direct consequence of the different morphological features, such as surface area and crystallite dimension. These characteristics change the activity of surface species and the rate of the oxygen diffusivity from the bulk to the surface, a necessary process for the reduction of the core material. At 420°C, the reduction

degree was quite similar in the two samples (see the alloy reflections at 2Θ 65-66°), probably because at that temperature the oxygen diffusivity rate was no longer the rate determining step.

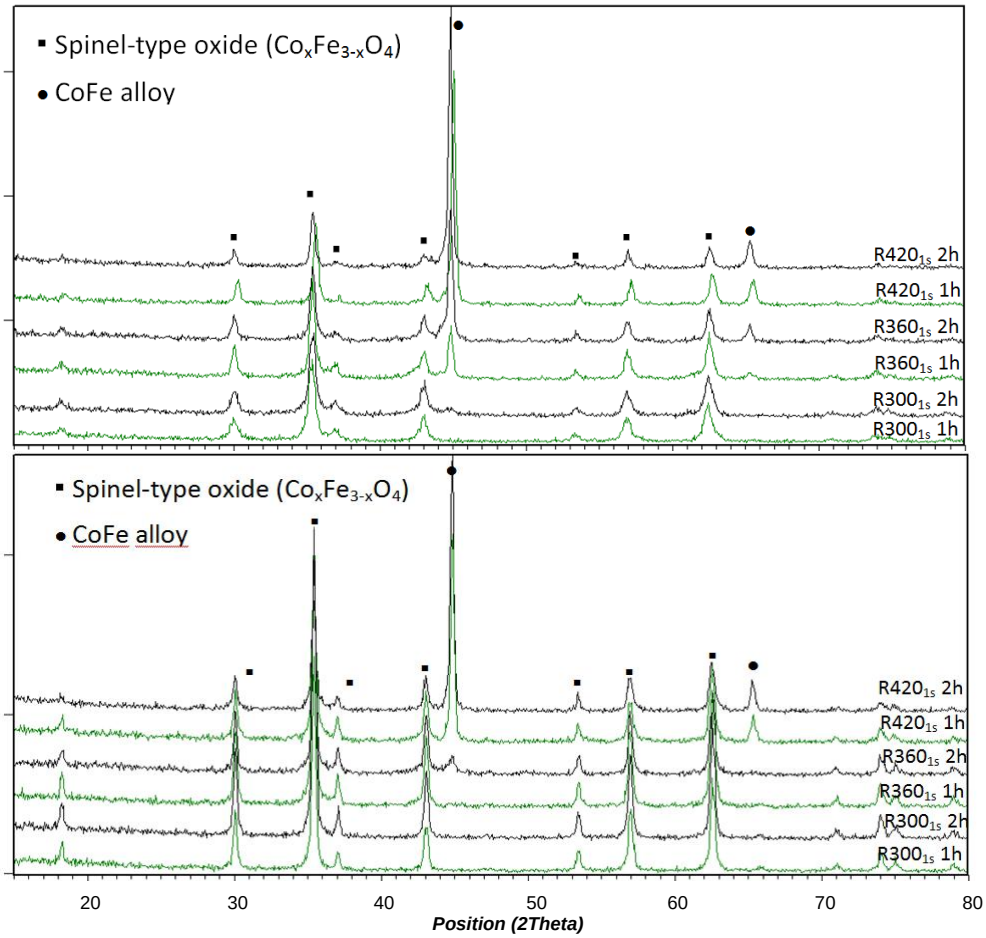

Figure 3-54. XRD patterns of CF450 (top) and CF750 (bottom) recorded at different reduction degrees.
Reduction was carried out with residence time equal to *1s*

Mössbauer spectra have been registered on the same samples, and results are shown in Figure 3-56, for samples CF450 and CF750; the tables after the figures report the hyperfine parameters derived from the fitting of the spectra. Concerning iron in the B sites, only one IS value for the four species is considered (as discussed in the previous paragraph).

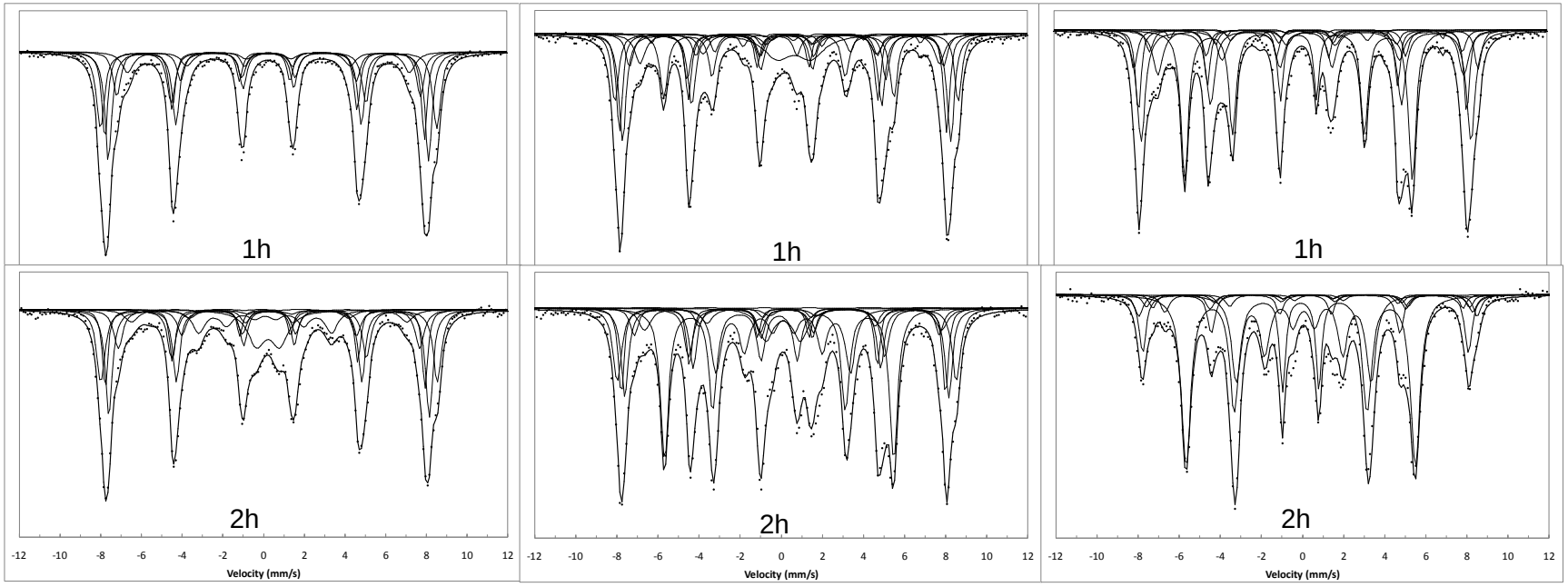

CF450_R300$_{1s}$ ***CF450_R360$_{1s}$*** ***CF450_R420$_{1s}$***

Sample	Fe^{3+} A site			Fe^{3+} B sites*				$Fe^{2,5+}$			Alloy			Fe_3C %			Doublet		
	%	H (kOe)	IS	%a	%b	%c	%d	%	H (kOe)	IS	%	H (kOe)	IS	%	H (kOe)	IS	%	QS	IS
1h 300°C 450	21	486	0,17	30	15	9	42	-	-	-	-	-	-	-	-	-	-	-	-
2h 300°C 450	15	486	0,18	21	26	12	6	-	-	-	1	338	0,002	9			10	1,15	0,32
1h 360°C 450	18	493	0,194	14	24	8	2	10	450	0,545	14	345	-0,003	6			4	1,17	0,316
2h 360°C 450	11	488	0,2	14	15	4	1	6	447	0,682	28	344	-0,007	14			6	1,66	0,217
1h 420°C 450	13	494	0,196	7	27	4	1	13	460	0,635	32	342	0,004	2					
2h 420°C 450	12	490	0,245	5	5	1	-	5	460	0,7	47	344	0,005	25					

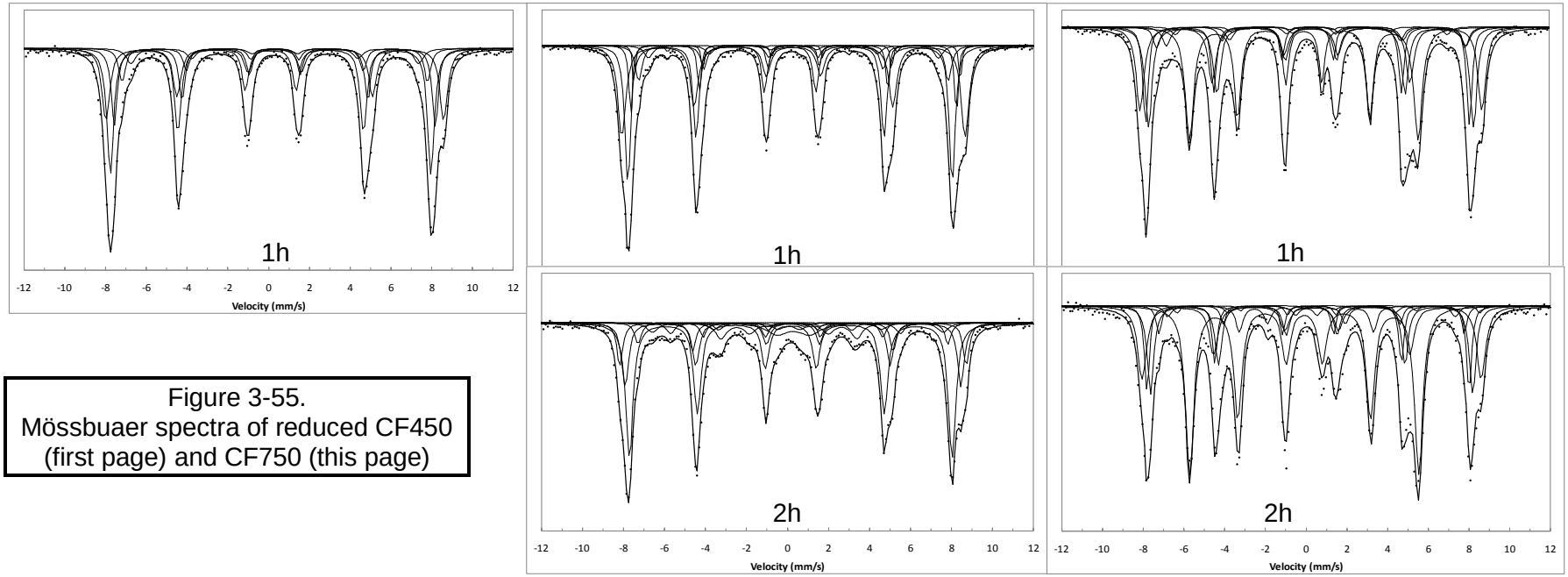

Figure 3-55.
Mössbuaer spectra of reduced CF450 (first page) and CF750 (this page)

CF750_R300$_{1s}$ ***CF750_R360$_{1s}$*** ***CF750_R420$_{1s}$***

Sample	Fe^{3+} A site			Fe^{3+} B sites*				$Fe^{2,5+}$			Alloy			Fe_3C %			Doublet		
	%	H (kOe)	IS	%a	%b	%c	%d	%	H (kOe)	IS	%	H (kOe)	IS	%	H (kOe)	IS	%	QS	IS
1h 300°C 750	26	486	0,178	28	10	7	52	-	-	-	-	-	-	-	-	-	-	-	-
1h 360°C 750	25	489	0,197	31	28	9	4	-	-	-	2	357	0	-			1	0,9	0,31
2h 360°C 750	43	487	0,257	11	19	6	0	4	438	0,595	4	346	-0,06	7			5	1,58	0,387
1h 420°C 750	16	493	0,195	21	22	5	2	5	456	0,622	30	348	0,012	0					
2h 420°C 750	12	489	0,19	18	17	4	2	1	446	0,85	40	347	0,002	5					

* Isomer Shift of 0,366 mm/s and Internal magnetic field of the four components comprised between 510 and 430 kOe.

In the case of CF450, it is shown that even after 1h of reaction at 300°C, some modifications occur, which contrasts with what inferred from the XRD pattern. The experimental data are now fitted with five sextets while a distribution of Internal Magnetic Field was needed to fit that of the fresh compound which was presenting a low crystallinity. This means that the highly-reactive oxygen species observed by means of both TPR (see paragraph 0) and catalytic tests (see paragraph 3.1.2), were delivered by the solid, leading to the formation of a better crystallized material.

The reduced main phase is the CoFe alloy, as inferred from XRD pattern; fitting of Mössbauer spectra shows that the average of Internal Magnetic field for the CoFe alloy is around 34,5-35,0T. The trend of this parameter as a function of the composition of the CoFe alloy, has been described by Johnson et al. in 1963[139] and for this value the Cobalt concentration in the alloy should be around 40%, suggesting a segregation process during the reduction step (from 33% Co and 66% of Fe in the original spinel, to a Co-rich reduced phase) that involves approximately the 5-10% of the Co atoms. Therefore, the hypothesis of a segregation process put forward to explain the incomplete reoxidation observed during the second step (see paragraph 3.2.3.5) is demonstrated by this result. Further investigations focussed on this topic are required, in order to clearly explain the phenomena involved during the overall redox process.

A new sextet characterized by an IS of mm/s and an Internal Magnetic Field of has been evidenced. Because of its isomer shift value in between a Fe^{3+} and a Fe^{2+}, it has been attributed to a mixed valence species $Fe^{2,5+}$. This specie which may correspond to a very low amount of Fe_3O_4 as the intermediate reduced phase arise form a quick electron exchange between the Fe^{3+} and the Fe^{2+} cations occupying neighboring octahedral sites in a so-called electron-hopping phenomenon, firstly described by Sawatzky et al. in 1969[140]. This electron exchange is faster

than the time required for the Mössbauer effect, and an intermediate specie called $Fe^{2,5+}$ is observed. For further description about this phenomena, read the following paragraphs.

Another observation concerns the iron carbide formation, in both CF450 and CF750. This compound is formed by reaction between CO, produced by MeOH decomposition, and iron reduced specie, as reported in many articles in the literature[141,142,143,144,145]. After two hours of reduction, at all the temperatures tested this compound was found in a non-negligible amount; this means that the reduced iron and the high CO concentration led to the disproportionation of carbon monoxide to iron carbide and CO_2. In paragraph 3.2, dealing with the discussion on catalytic tests, we identified coke as one product of the reaction, but now it is possible to say that this reaction is driving to the formation of the iron carbide specie. The main difference between CF450 and CF750 is the ratio between Fe_3C and CoFe alloy, which is lower for CF750. This is probably another consequence of the higher SSA of CF450, because the carbide formation takes place on the catalyst surface, where coke and reduced iron are in contact; therefore, the different SSAs could explain this difference. Consequently, the total reduction degree of the sample is obtained from the sum of Fe^0 and carbide specie; the analysis evidence that a higher reduction degree was reached for CF450 than for CF750, further confirming the different behaviours of the two materials.

Another point concerns the fact that low reduced compounds are well fitted only considering a doublet besides the other sextets to fit the spectra. A superparamagnetic ferric iron oxide phase is formed from reduced Fe nanoparticles upon oxidation by air during the stocking period at room temperature. In order to optimize the visualization of the result in the next graphs, the very low contribution (<5%) of this doublet since it should derive from the oxidation of metallic nanoparticles, has been added to that of the Fe alloy specie (Fe^0).

All these considerations regarding the origin of the different species found in the spectra, can be summarized in a picture as shown in Figure 3-57.

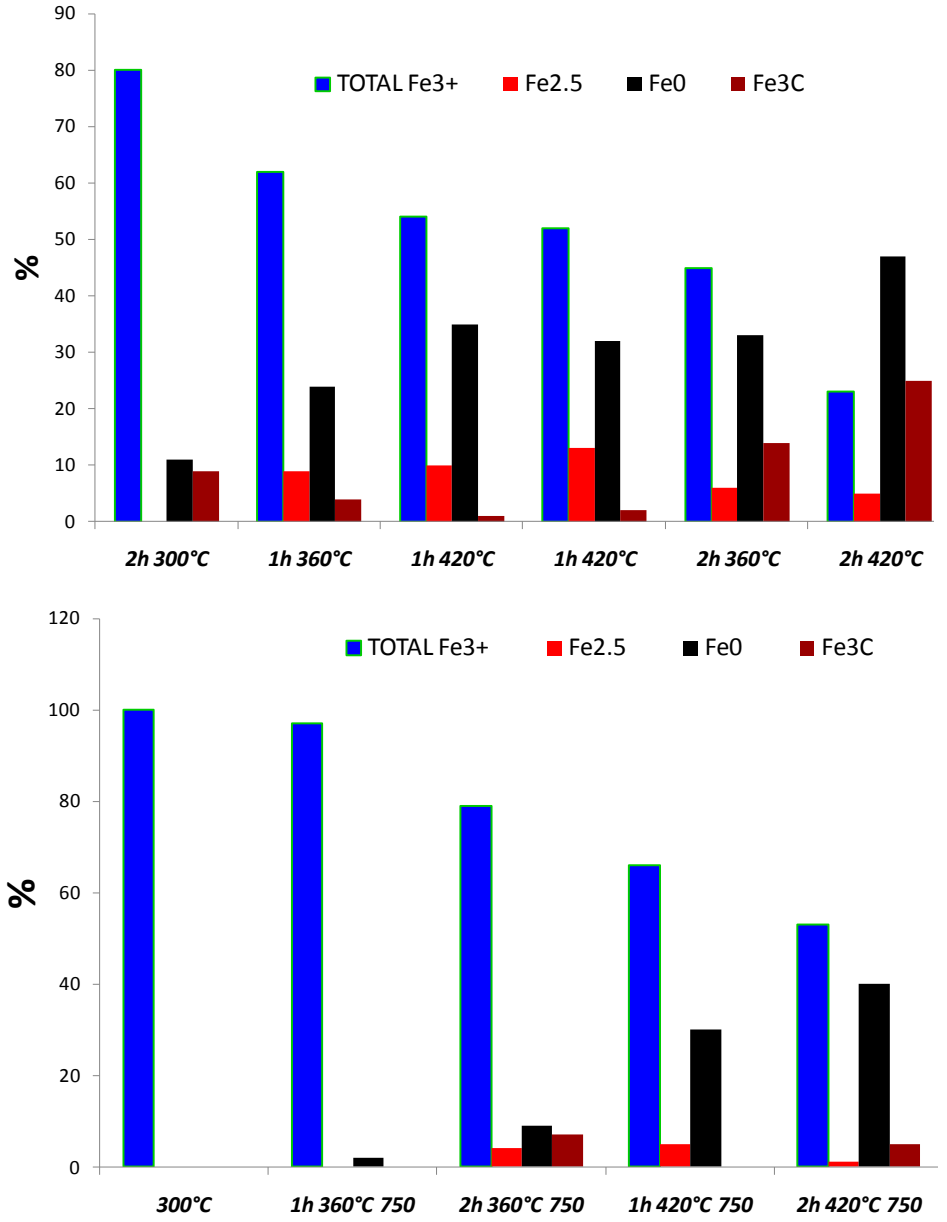

Figure 3-56.Nature and relative amounts of the phases present during the reduction of CF450 (top) and CF750 (bottom), as found by means of Mössbauer spectroscopy.

It is possible to observe that:

1. the reduction rate of CF750 was lower than that of CF450
2. Iron Carbide-to-CoFe alloy ratio was lower in CF750 presumably because of the lower SSA
3. The presence of Fe_3O_4 as an intermediate compound of the reduction process is evident mainly in CF450, probably because its formation was proportional to the SSA (as it was the iron carbide specie).

Finally, we can state that the initial structural features of the samples affect the reduction of the oxide by MeOH. Therefore, the maintenance of these characteristics along the repeated cycles is an important feature, in order to maximize the material performance in the steam iron process.

3.3.2.2 Low reduced compounds

As reported in the previous paragraph, spectra of samples with low reduction degree are well fitted adding to the normal inverse spinel configuration a low intense doublet. To further investigate this particular behavior, four samples have been specifically prepared and analyzed by Mössbauer spectroscopy. Figure 3-58 also shows the results of the reduction test of CF450 with MeOH, carried out at 300°C, in order to better show how the 4 samples having different degree of reduction were obtained.

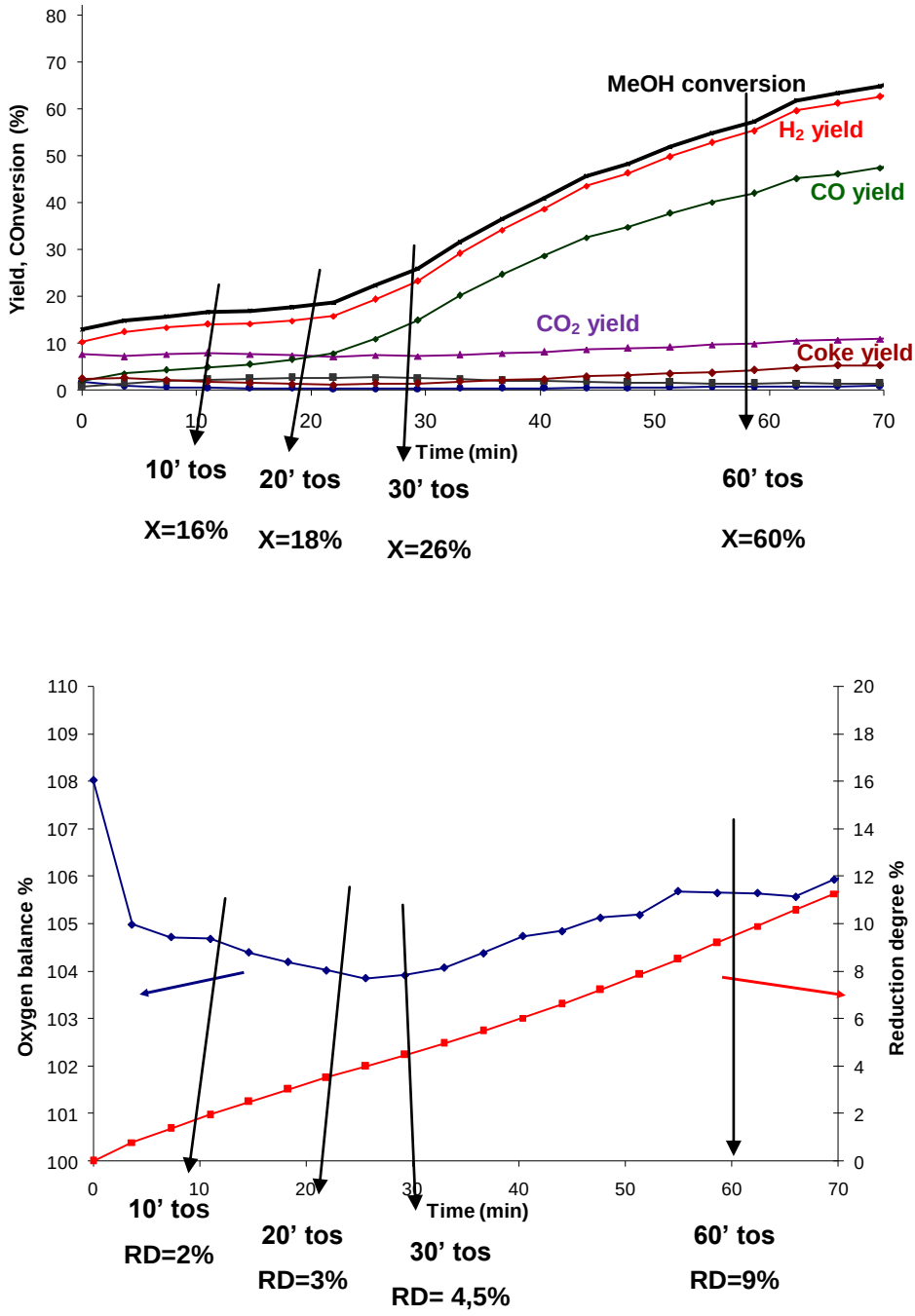

Figure 3-57. Definition of the four low-reduced samples
(X= methanol conversion; R.D. = Reduction degree)

From the spectra reported in Figure 3-59, it can be observed that the relative intensity of the doublet component increases with the reduction. In the first two sample (after 10 and 20 min of reduction), it is difficult to fit the total spectra by adding a doublet, because a very high quality fitting is obtained only considering one inverse spinel configuration (classical five sextets). But in the samples reduced for 30 and 60 min, the fitting of the total spectra can be improved by adding the doublet; however, the fitting optimization performed leaving the hyperfine parameters of this doublet free always rejected it. We had thus to impose its line width to have it taken into account.

In the 60 min reduced sample (the more reduced one, bottom-left figure) the sextet corresponding to CoFe alloy is hardly visible which shows that this phase starts to form only after 1 hour of reduction at 300°C.

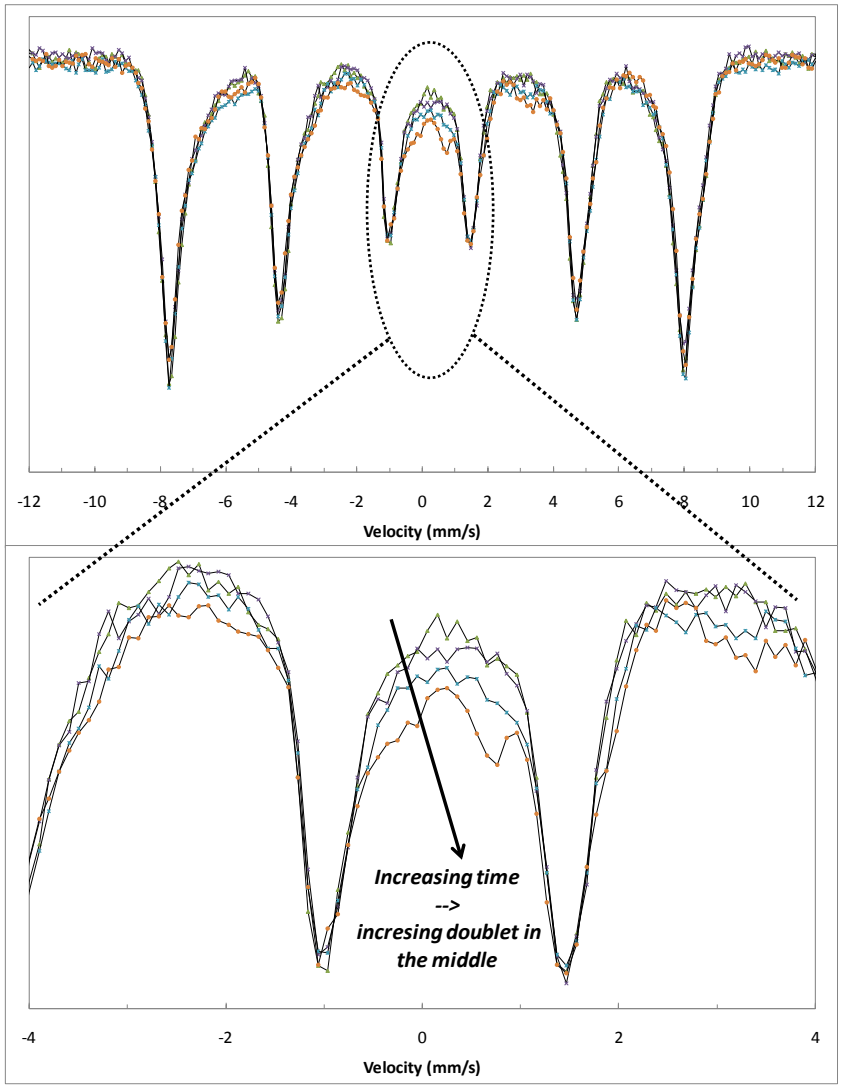

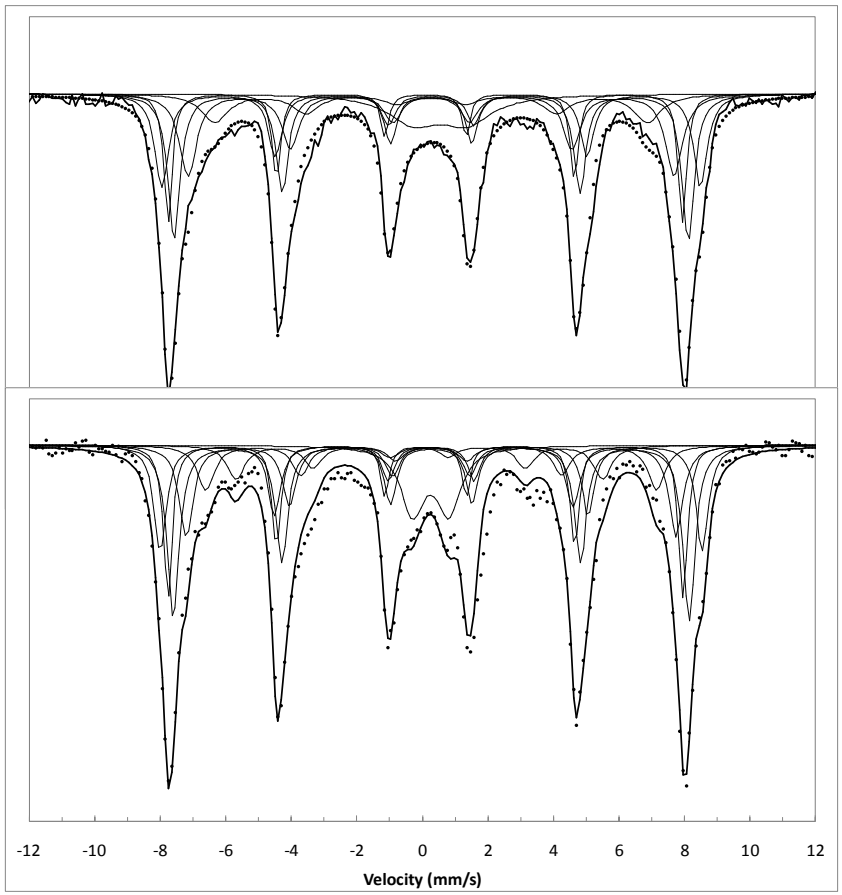

Figure 3-58.
Left: Mössbauer spectra of low reduced samples
Right: 30' and 60' reduced spectra ("manual" fitting)

From these analyses, we can say that the increase of MeOH conversion from 20% to 60% during the second half hour of reaction time (the “Zone II” described in paragraph 3.1.2), can be ascribed to the development of a reduced phase. Since this reduction can hardly be seen by Mössbauer spectroscopy, which is a bulk technique, we have used X-ray photoelectron spectroscopy (XPS)which is a surface technique to better evidenced this reduction. The 20 min and 60 min reduced compounds have thus been characterized by XPS. The results obtained are gathered in Table 3-9.

Info	***Fe***	***Co***	***O***	***C****	***Fe / Co***	***% Fe+Co***
Fresh	11.9	6.5	49.5	32.1	***1.83***	***18,4***
Red 20 min	13.7	10.5	47.3	28.5	***1.31***	***24,2***
Red 60 min	12.9	10.1	48.6	28.5	***1.27***	***23***

Table 3-9 . Results of XPS analyses of 20 min and 60 min reduced CF450 samples . * see “Experimental part” for explanation

It is shown that a slightly higher concentration of Fe and Co (and a correspondingly lower concentration of O) in the reduced samples compared to the fresh one may confirm the hypothesis put forward. However, the most interesting consideration is about the Fe/Co ratio: the fresh compound shows a ratio close to the theoretical value for the spinel phase (1.83 *vs.* 2), whereas the surface of reduced samples is characterized by a higher concentration of Co, which confirms the segregation phenomena discussed above.

The binding energies of $Fe2p_{3/2}$ and $Co2p_{3/2}$ slightly decrease (from 711,4eV to 710,4eV and from 780,6eV to 779,8eV respectively) demonstrating the presence of reduced species on the surface too. No metallic species are observed neither for iron nor for cobalt, probably

because the stocking period lead to a reoxidation of the completely reduced particles by air.

So we can conclude that the change of conversion and products distribution experimentally observed along with the increasing reduction time are strongly affected by both bulk features (formation of the reduced phase) and surface characteristics (higher metal concentration and higher Co/Fe ratio).

3.3.2.3 Complete reduction of CF450

As in the catalytic test paragraph, a complete reduction of CF450 has been carried out with methanol, using a residence time of 0,2s; the resulting spectrum is shown in Figure 3-60.

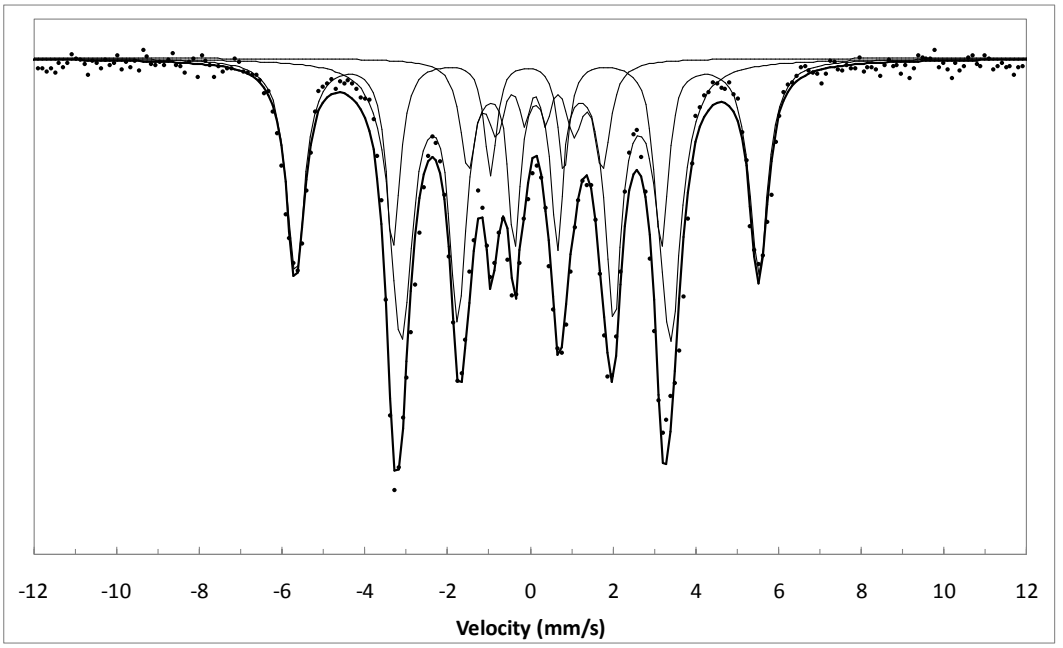

Figure 3-59.Mössbauer spectra of CF450 completely reduced at 420°C, with residence time 0,2s.

Sample	CoFe alloy			Fe_3C			Hagg carbide		
	%	H(kOe)	IS	%	H(kOe)	IS	%	H(kOe)	IS
70' 420°C CF450	34	346	0,022	52	201	0.23	14	101	0.22

Table 3-10. Fitting data for the reported spectra.

The figure shows the total absence of Fe^{3+} and $Fe^{2,5+}$ species which confirms the complete reduction obtained at 420°C in 70 min only (see paragraph 3.2.2.1). Anyway, the fitting spectrum evidenced three species which correspond to the CoFe alloy, Fe_3C, also observed in the samples with lower reduction degree, and Fe_5C_2, another carbide phase known as Hagg carbide[146,147]. The molar ratio between Fe and C in this phase is 2.5, with a resulting higher concentration of carbon compared to the classical iron carbide; this justifies its formation at only very high reduction degree, when the concentration of reduced Fe species and CO deriving from methanol decomposition were the highest (see paragraph 3.1.2).

3.3.3 Samples after complete redox cycles

Complete redox cycles were carried out on fresh materials. Firstly, cycles characterized by a complete reduction of the solid have been made; then, CF450 has been used for one cycle with lower reduction degree. Finally, analyses of samples used for six consecutive cycles are reported.

3.3.3.1 One redox cycle with complete reduction of the solid

As in the paragraph 3.2.2, the CF450 was first totally reduced at different temperatures, and then reoxidized with water at 420°C: the spectra of the final materials are reported in Figure 3-61.

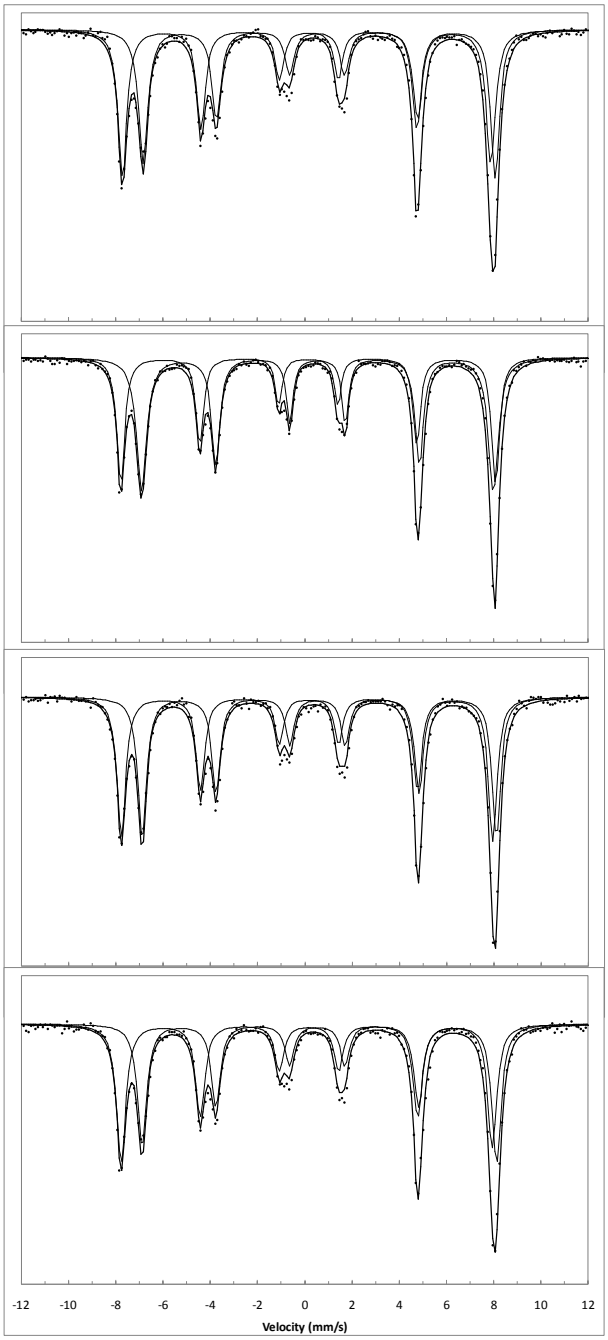

Figure 3-60.Mössbauer spectra of samples after complete reduction and reoxidation with water.

Sample	$Fe^{2,5+}$ Oh			Fe^{3+} Th		
	%	H (kOe)	IS	%	H(kOe)	IS
CF450_R300$C_{0,2s}$_O420C	49	455	0,618	51	488	0,274
CF450_R420$C_{0,2s}$_O420C	58	460	0,637	42	490	0,245
CF750_R300$C_{0,2s}$_O420C	51	459	0,627	49	491	0,265
CF750_R420$C_{0,2s}$_O420C	47	458	0,623	53	492	0,274

Table 3-11. Fitting data for the reported spectra.

After one cycle, the spectra of the materials were very different from the original ones shown in Figure 3-51. As introduced in paragraph 3.3.2, the presence of only two sextets characterized by Internal Magnetic Field of about 45,5T and 49T identifies the magnetite Fe_3O_4. The two sextets can be attributed to $Fe^{2,5+}$ and Fe^{3+} species. The former one is due to the fast electron hopping between the Fe^{2+} and Fe^{3+} in neighbouring octahedral sites whereas the Fe^{3+} is referred to iron in tetrahedral sites.

In this case, we observe an amount of about 50% for both ions, which means that Fe^{3+} is preferentially located in the octahedral cavities, and not equally distributed in both sites as in pure Fe_3O_4. This is because the magnetite contains cobalt in octahedral sites which derives from the reoxidation with water of the reduced material, where the original oxidation state of iron atoms was not completely recovered (as discussed in paragraph 3.2.3.5); so, the spinel phase is characterised by the general formula $Co_xFe_{3-x}O_4$, that justifies the ratio between the Fe^{Oh} and Fe^{Th}.

Furthermore, it's possible also to estimate the composition of the spinel (the x value) using the ratio between A and B site, and considering a complete inversion of the structure (which is only an approximation, as concluded in the discussion reported in paragraph 3.3.1 about CF750). Secondly, the approximation derives from the fact that iron in octahedral sites has been fitted considering only $Fe^{2,5+}$ specie, while it's demonstrated in the literature[148] that the best fitting for $Co_xFe_{3-x}O_4$ it's

obtained considering other contributions from Fe^{3+} ions with different environment due to the neighbour Co^{2+} that are distributed in *Oh* sites too (the same as for the interpretation of crystalline CF750 fresh compound).

For x=1

$CoFe_2O_4$ = no $Fe^{2,5+}$, no electron hopping

1. Fe^{3+} =100%

For x=0,75

$Co_{0,75}Fe_{2,25}O_4$ = ¾$CoFe_2O_4$ + ¼Fe_3O_4

1. Fe^{3+} (100% x ¾) + (33% x ¼) = 83%
2. $Fe^{2,5+}$ (0% x ¾) + (66% x ¼) = 17%

For x=0,5

$Co_{0,5}Fe_{2,5}O_4$ = ½$CoFe_2O_4$ + ½Fe_3O_4

3. Fe^{3+} (100% x ½) + (33% x ½) = 66%
4. $Fe^{2,5+}$ (0% x ½) + (66% x ½) = 33%

For x=0,25

$Co_{0,25}Fe_{2,75}O_4$ = ¼$CoFe_2O_4$ + ¾Fe_3O_4

5. Fe^{3+} (100% x ¼) + (33% x ¾) = 50%
6. $Fe^{2,5+}$ (0% x ¼) + (66% x ¾) = 50%

Finally, it is possible to estimate that only the 25% of the material was completely reoxidized, while the remaining 75% of the spinel was

magnetite. It is better to underline again that this calculation is an approximation, because the spinel was not completely inverted and the fitting is not performed considering a distribution for the *Oh* sites; indeed there was a certain amount of Fe^{2+} in the tetrahedral sites that could overlap with one of the two species, changing the ratio between them.

XPS spectrum of CF450_R420C$_{0,2s}$_O420C$_{0,2s}$ sample (the second sample in Figure 3-60) was recorded in order to evaluate how the surface composition is affected by this strong modification of the bulk.

	Fe	Co	O	C	Fe / Co
CF450	11.91	6.52	49.45	32.12	**1.83**
CF450 R420C$_{0,2s}$_O420C$_{0,2s}$	5.20	19.75	39.59	35.36	**0.26**

Table 3-12. Results of XPS spectroscopy analyses

Analysis shows that the surface composition was deeply altered after just one redox cycle. The Co concentration on the surface changed from 6.5% to nearly 20%, whereas Fe concentration decreased from 12% to 5%: this is a further confirmation of the segregation phenomenon that took place during the reduction step (see paragraph 3.3.2.2). In addition, this analysis shows that the starting composition of the material cannot be fully recovered by the water reoxidation step. Concerning the energy values, a slight decrease of both the Co2p$_{3/2}$ and the Fe2p$_{3/2}$ bonding energies compared to the fresh compound (from 780,6eV to 780,1eV and from 711,4eV to 710,8eV respectively) shows a decreasing of the oxidation state of both the elements. Again, this is a further demonstration that the sample undergoes to Co-segregation phenomena that lead to an incomplete reoxidation of the solid.

3.3.3.2 One redox cycle with low reduction degree

The complete reduction of the material has many drawbacks, such as the high formation of coke, as reported in the paragraph 3.2, and the incomplete reoxidation (or segregation) after the second water-dissociating step. In order to understand the influence of this parameter on the overall cycle, low reduction degree tests followed by reoxidation with water were carried out with CF450. The Mössbauer spectra collected on the used samples are reported in Figure 3-62.

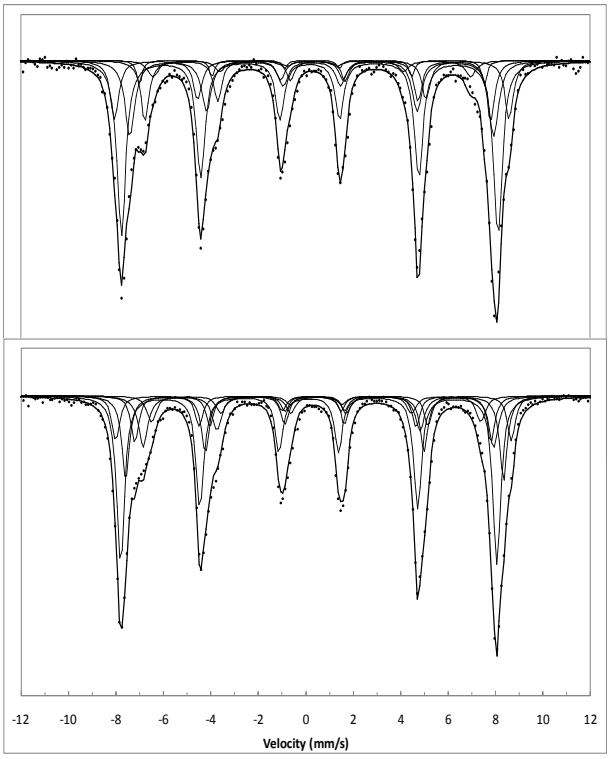

CF450_R300C$_{0,2s}$_O420C

CF450_R420C$_{0,2s}$_O420C

Figure 3-61.Mössbauer spectra of samples after low reduction, and reoxidation with water

Sample	Fe^{3+} Th			Fe^{3+} Oh sites				$Fe^{2,5+}$ Oh		
	%	H (kOe)	IS	%a	%b	%c	%d	%	H (kOe)	IS
R300_O420	43	491	0.177	14	21	3	5	14	451	0.528
R420_O420	39	490	0.223	10	19	10	7	14	457	0.631

Table 3-13. Fitting data for the reported spectra

The spectra can be fitted the same way as before, but here the fraction of *Oh* sites occupied by the $Fe^{2,5+}$ specie is only 14%. The calculations done in the previous paragraph are not meaningful now, because in this case the inversion degree of the spinel contributed to the fitting of the spectra in a non-negligible amount (see Fe^{3+} *Oh* sites in the table).

Anyway, we can notice that even after a low reduction cycle (10-20% of CF450 reduction), an incomplete reoxidation took place; this is a further demonstration of the kinetic and thermodynamic limitations of the water reoxidation at 420°C, as discussed in paragraph 3.2.4.1. In that case, a 3rd step involving a re-calcination in air was proposed to recover the original spinel composition at every cycle.

3.3.3.3 Repeated cycles on CF450

The materials used in the repeated cycle's experiments (see paragraph 3.2.3.2) were analyzed by means of Mössbauer spectroscopy, and the results are shown in Figure 3-63.

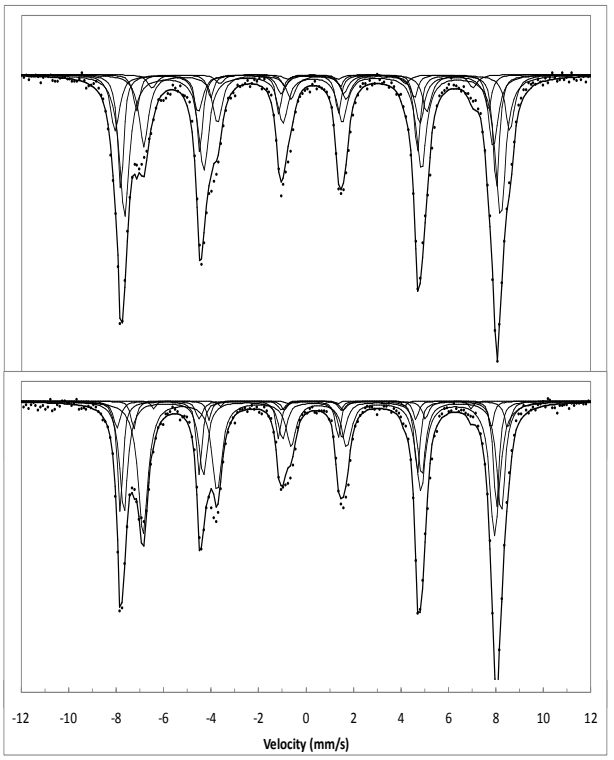

CF450_R300C$_{0,2s}$_O420C x6

CF450_R420C$_{0,2s}$_O420C x6

Figure 3-62. Mössbauer spectra of samples after low reduction and reoxidation with water

Sample	Fe^{3+} Th			Fe^{3+} Oh sites				$Fe^{2,5+}$ Oh		
	%	H (kOe)	IS	%a	%b	%c	%d	%	H (kOe)	IS
R300_O420 x6	41	490	0.223	11	18	13	4	12	454	0.669
R420_O420 x6	18	490	0.193	6	30	5	1	41	458	0.639

Table 3-14. Fitting data for the reported spectra

Again, the presence of magnetite demonstrates the incomplete reoxidation of the samples. From the second spectrum it is possible to notice a strong contribution of $Fe^{2,5+}$ to the fitting curve, evidencing that at higher temperature other modifications occur. This is probably due to the greater sintering, which reduces the oxidation rate because of the loss of SSA in the sample, as reported in .Table 3-6. Comparison of SSA and crystallite dimension of used CF450.

3.3.4 Reoxidation in air of used CF450

In paragraph 3.2, we concluded that a reoxidation step with air (after the oxidation with water) should help to recover the original oxidation state of the spinel oxide. Hereafter we report the analysis made on CF450 after these reactions:

1. Complete reduction with MeOH at 420°C (see paragraphs 3.3.2.3 and 3.2.2.1 for Mössbauer spectra and catalytic results, respectively).
2. Reoxidation with water at 420°C (see spectra at paragraph 3.3.3.1).
3. Reoxidation in air at 450°C for 3h.

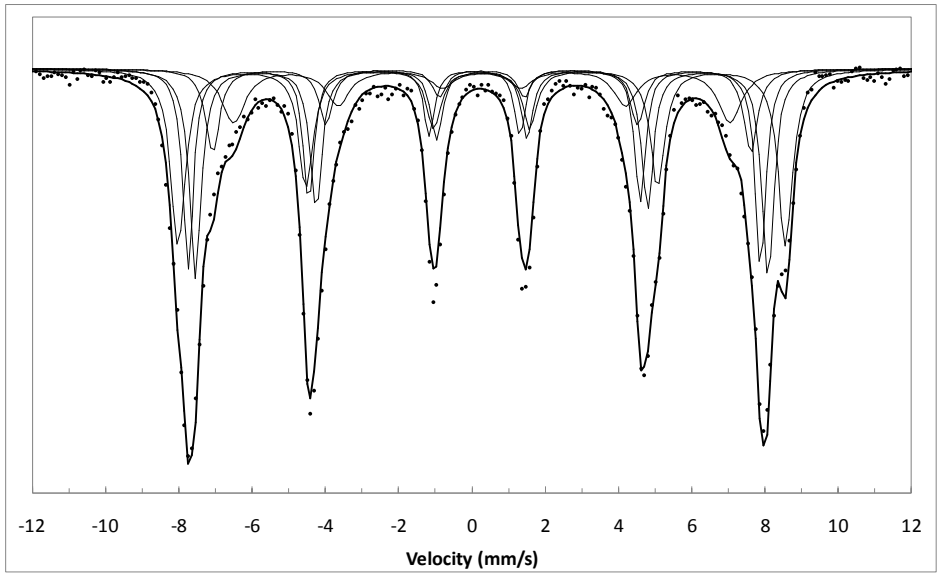

Figure 3-63. Mössbauer spectra of CF450 after MeOH+Water+Air

Sample	Fe^{3+} Th			Fe^{3+} Oh sites				$Fe^{2,5+}$ Oh		
	%	H (kOe)	IS	%a	%b	%c	%d	%	H (kOe)	IS
R300_O420 x6	22	483	0.188	27	26	12	13	-	-	-

Table 3-15. Fitting result of the reported graph

As it's possible to notice, the reoxidized sample spectrum was completely fitted considering only one $CoFe_2O_4$ spinel phase, while the $Fe^{2,5+}$ specie was not present anymore. This result further confirms the conclusions made in paragraph 3.2, about the reoxidation step with air, which seems to be useful in order to recover the original oxidation state of the material. Moreover, the step with air can completely reoxidize the oxide even after a high reduction degree cycle, whereas only the 25% of the original spinel composition could be recovered by means of water reoxidation (see 3.3.3.1).

3.3.5 Conclusions about transformations of CF450 occurring during the steam-iron process

Mössbauer spectroscopy of iron atoms has been a very powerful technique to understand the structural modifications occurring.

Spectra of CFp, CF450 and CF750 as-synthesized materials showed that morphological differences, such as crystallite dimension, strongly affect the magnetic properties of the oxides. Therefore, the Mössbauer spectroscopy can be usefully employed to analyze the characteristics of materials obtained by different synthetic methods.

Concerning the reduced materials, a different reduction ratio between CF450 and CF750 is observed, due to the different structural properties of the initial oxides. The thermodynamically favored reduced phase obtained from the reduction of $CoFe_2O_4$ with MeOH between 300°C and 420°C is the cobalt-iron alloy, followed by the formation of iron carbide and Fe_3O_4 in lower amount. Low reduced compounds showed first the appearance of a reduced phase, evidenced by the increased contribution of a doublet in the spectra, which is probably due to superparamagnetic

Fe_xO_y nanoparticles derived from the oxidation of CoFe during the stocking period in air at RT.

Samples used for complete redox cycles demonstrate that an incomplete recovery of the original oxidation state is always obtained, both in low reduced compounds and in completely reduced ones. This is evidenced by the presence of Fe_3O_4 phase in the Mössbauer spectra of all samples after the water dissociation step.

XPS analysis has been used to analyze the modifications occurring on the surface during reduction and reoxidation steps. Low reduced compounds demonstrate that during the first step with MeOH, the surface is enriched in metal ions because of the progressive reduction of the solid, and that Co/Fe ratio continuously increases also, probing a segregation of Co on the surface. This trend was also confirmed by the analysis of a reoxidized sample (CF450 R420$C_{0,2s}$_O420$C_{0,2s}$), where the Co/Fe ratio changed from 1.83 in the fresh compound to 0.26 in the used one, demonstrating that the accumulation of Co on the surface was not affected by the second step.

However, the treatment in air of the used sample led to the recovery of the original oxidation state of the oxide, as already discussed in paragraph 3.2.4.1.

4 Conclusions and perspectives

The first part of the thesis was focused on the characterization of the chemical-physical properties of CF450 and CF750, also by means of in-situ IR after CO adsorption, and how they affect the chemical activity during MeOH anaerobic oxidation. It was concluded that the starting materials show very different properties depending on the annealing temperature of the spinel $CoFe_2O_4$. A further demonstration also derived from Mössbauer spectroscopy, where the different magnetic properties of the materials in function of the average particle size strongly affected the resulting spectra of the materials. However, after just one redox cycle the original chemical-physical features could not be recovered.

Secondly, the reactivity of three different spinel ferrites in the steam-iron process with MeOH has been investigated. Catalytic results showed that the different nature of the chemical elements constituting the materials affected the products distribution during the two steps of the process. For instance, methane selectivity in nickel ferrite was higher than with the other systems, because of the catalytic properties of this element in methanation and reforming reactions. Moreover, the Co ferrite did not show the production of CO, resulting from the gasification of coke deposited during the first step of the reaction. Therefore, catalyst choice strongly affects the products distribution, a feature that can be used to select the proper composition of the solid in function of the nature of the desired products; for instance, the H_2/CO ratio of the lean gas deriving from the first step of reaction can be greatly affected by the choice of the spinel type.

The oxidizing properties of the materials, as inferred from the preliminary characterizations and the catalytic results, are summarized as follows:

$NiFe_2O_4$>$CoFe_2O_4$>Fe_3O_4, which is perfectly in agreement with the literature data.

Repeated cycles on CF450, FF450 and FF450 carried out with a low temperature of reduction (300°C) show that the materials undergo modifications that lead to the decrease of hydrogen productivity during cycles. This deactivation phenomenon is justified by both an incomplete reoxidation process in $CoFe_2O_4$ and $NiFe_2O_4$, because of thermodynamic limitations, and by a sintering phenomenon registered with all samples.

Possible improvements for the process have been identified and tested. Catalytic tests on CF450 carried out by increasing the reduction temperature from 300°C to 420°C show that the $H_2^{prod}/Coke_{dep}$ could be strongly improved. Furthermore, the time needed for the reduction of the material during the first step decreases remarkably, giving a higher productivity of the overall process. Another optimization could derive from adding a third step of air-reoxidation which can drive to the complete recovery of the original spinel composition.

In the last part of the thesis, a deep investigation of CF450 and CF750 evolution during the steam iron process is discussed. The characterization of synthesised and reduced materials demonstrates again that the chemical physical differences of the two materials affect the reduction rate of the solids. Furthermore a better identification of the phases generated because of the progressive reduction has been obtained. From these analyses also, an incomplete reoxidation of the material with water has been evidenced in the used materials. The integration of these results with XRD and XPS spectroscopy demonstrates that a Co segregation at the catalyst surface took place during the reduction step; the water reoxidation reaction could not recover the original composition, giving a material characterized by a composition like $Co_xFe_{3-x}O_4$ ($x<<1$) in the core and Co^0 on the surface.

Again, the analysis with Mössbauer spectroscopy of one sample after air regeneration evidenced the possible recover of the original spinel composition, $CoFe_2O_4$.

From all these analysis a possible schematization of the CF450 reduction mechanism is proposed in Figure 4-1.

The future perspective for the development of the steam iron process are based on a three-step cycle, as originally proposed in ENI patent[95], where a third step of air regeneration can lead to the recovery of the original composition of the material avoiding segregation phenomena. Higher reduction temperatures are preferred because of the higher productivity of the overall process and the increase of the H_2/Coke ratio. Concerning the material design, both the supporting of the active phase and the addition of promoters for the structure stability are required, in order to maintain the structural properties which can affect the efficiency of the system.

All these suggestions mainly derive from the analysis of the material properties, and therefore they should be taken into account whatever is the reducing fuel employed. In conclusion, a wide knowledge of all the aspects of these reactions might lead to the development of a very flexible process, which can be useful for a future switch towards new kinds of biomasses.

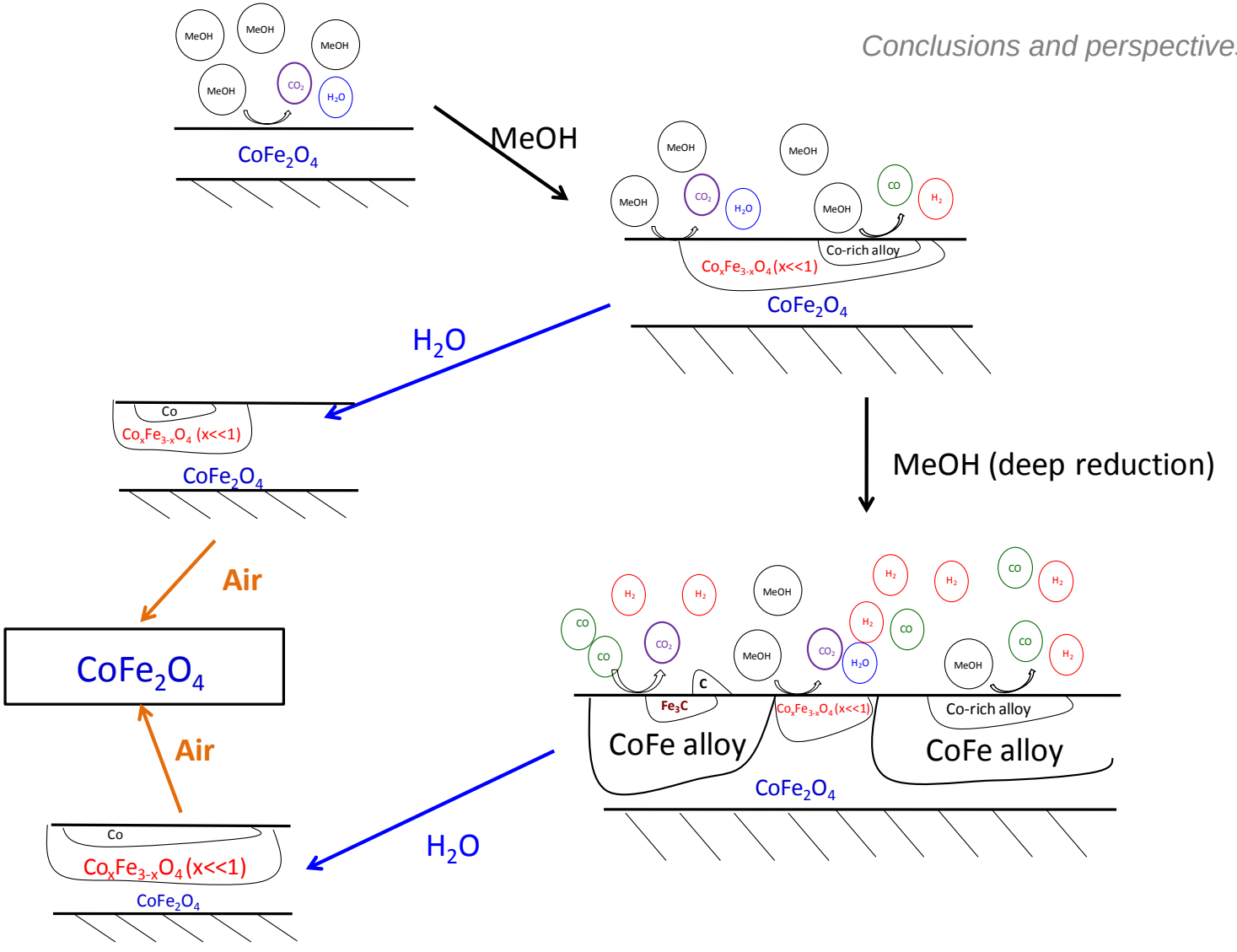

Figure 4-1. Reaction mechanism in CF450

5 Bibliography

[1] US Department of Energy and US Department of transportation. *Hydrogen posture plan.* **2006**.

[2] European commission. *Framework programme n°5 (Energy, environment and sustainable development) and n°6 (Sustainable*

[2] European commission. *Framework programme n°5 (Energy, environment and sustainable development) and n°6 (Sustainable energy systems).* **1998-2006.**

[3] Yang, J.; Sudik, A.; Wolverton, C.; Siegel, D. J. High capacity hydrogen storage materials: attributes for automotive applications and techniques for materials discovery. *Chem. Soc. Rev.* **2010**, *39*.

[4] US Department of Energy, Office of Energy Efficiency and Renewable Energy, FreedomCAR and Fuel Partnership. *Targets for Onboard Hydrogen Storage Systems for Light-Duty Vehicles***. 2009,** www.eere.energy.gov accessed 01/2012.

[5] Ahluwalia R. K.; Hua T. Q.; Peng J. K. and Kumar R. System Level Analysis of Hydrogen Storage Options*, 2010 DOE Hydrogen Program Review*, Washington, DC, June 8–11, **2010**.

[6] AA.VV. Fuel cell basics. In Stolten D., *Hydrogen and Fuel cells: fundamentals, technologies and applications*. Wiley-VCH, **2010**, ISBN 978-3-527-32711-9.

[7] HyCologne project, *http://www.hycologne.de/* accessed 01/2012, **2006**

[8] International Energy Agency*. Energy Technology Essentials*, *Table n°1* **2007**.

[9] AA.VV. Industrial Gases*.* In *Chemical Economics Handbook*, SRI Consulting, **2007**

[10] *Hyvolution project*, FP6 EU programme, Sustainable Energy System, **2006** www.biohydrogen.nl/hyvolution accessed 01/2012

[11] Zhang, Y.-H. P.; Sun, J.; Zhong, J.-J. Biofuel production by in vitro synthetic enzymatic pathway biotransformation. *Current Opinion in Biotechnology* **2010**, *21*, 663–669.

[12] Strik, D.; Bert, H.; Snel, J.; Buisman, C. Green electricity production with living plants and bacteria in a fuel cell. *International Journal of Energy Research* **2008**, *32*, 870–876.

[13] REN21 (Renewable energy policy network for the XXI century), *"Renewables 2011: Global Status Report,* **2011**

[14] Ren, N.; Wang, A.; Cao, G.; Xu, J.; Gao, L. Bioconversion of lignocellulosic biomass to hydrogen: Potential and challenges. *Biotechnology Advances* **2009**, *27*, 1051–1060.

[15] Zinoviev, S.; Müller-Langer, F.; Das, P.; Bertero, N.; Fornasiero, P.; Kaltschmitt, M.; Centi, G.; Miertus, S. Next-Generation Biofuels: Survey of Emerging Technologies and Sustainability Issues. *ChemSusChem* **2010**, *3*, 1106–1133.

[16] Olah, G. A. Beyond Oil and Gas: The Methanol Economy. *Angewandte Chemie International Edition* **2005**, *44*, 2636–2639.

[17] Knoef H.; *Handbok of biomass gasification*, Biomass technology group BTG, Enschede, **2005**

[18] Schaadt A.; Rapp S.W.; Hebling C. Reforming and gasification – biomass. In Stolten D., *Hydrogen and Fuel cells: fundamentals, technologies and applications*. Wiley-VCH, **2010**, ISBN 978-3-527-32711-9.

[19] Briens, C.; Piskorz, J.; Berruti, F. Biomass Valorization for Fuel and Chemicals Production -- A Review. *International Journal of Chemical Reactor Engineering* **2008**, *6*.

[20] Hofbauer H., *Necessary conditions for a successful market introduction of gasification technologies,* 3rd Conference on application of biomass gasification, **2009**, Stuttgart

[21] *www.nnfcc.co.uk/ - www.fao.org/* (accessed 01/2012)

[22] Palo, D. R.; Dagle, R. A.; Holladay, J. D. Methanol Steam Reforming for Hydrogen Production. *Chem. Rev.* **2007**, *107*, 3992–4021.

[23] Sá, S.; Silva, H.; Brandão, L.; Sousa, J. M.; Mendes, A. Catalysts for methanol steam reforming—A review. *Applied Catalysis B: Environmental* **2010**, *99*, 43–57.

[24] Holladay, J. D.; Hu, J.; King, D. L.; Wang, Y. An overview of hydrogen production technologies. *Catalysis Today* **2009**, *139*, 244–260.

[25] Navarro, R. M.; Peña, M. A.; Fierro, J. L. G. Hydrogen Production Reactions from Carbon Feedstocks: Fossil Fuels and Biomass. *Chem. Rev.* **2007**, *107*, 3952–3991.

[26] Hohn, K. L.; Lin, Y. Catalytic Partial Oxidation of Methanol and Ethanol for Hydrogen Generation. *ChemSusChem* **2009**, *2*, 927–940.

[27] Hohn, K. L.; Lin, Y. Catalytic Partial Oxidation of Methanol and Ethanol for Hydrogen Generation. *ChemSusChem* **2009**, *2*, 927–940.

[28] Agrell, J.; Boutonnet, M.; Fierro, J. L. . Production of hydrogen from methanol over binary Cu/ZnO catalysts: Part II. Catalytic activity and reaction pathways. *Applied Catalysis A: General* **2003**, *253*, 213–223.

[29] Rennard, D. C.; Kruger, J. S.; Schmidt, L. D. Autothermal Catalytic Partial Oxidation of Glycerol to Syngas and to Non-Equilibrium Products. *ChemSusChem* **2009**, *2*, 89–98.

[30] Lin, Y.-C.; Hohn, K. L.; Stagg-Williams, S. M. Hydrogen generation from methanol oxidation on supported Cu and Pt catalysts: Effects of active phases and supports. *Applied Catalysis A: General* **2007**, *327*, 164–172.

[31] Velu, S.; Suzuki, K.; Okazaki, M.; Kapoor, M. P.; Osaki, T.; Ohashi, F. Oxidative Steam Reforming of Methanol over CuZnAl(Zr)-Oxide Catalysts for the Selective Production of Hydrogen for Fuel Cells: Catalyst Characterization and Performance Evaluation. *Journal of Catalysis* **2000**, *194*, 373–384.

[32] Papavasiliou, J.; Avgouropoulos, G.; Ioannides, T. Combined steam reforming of methanol over Cu–Mn spinel oxide catalysts. *Journal of Catalysis* **2007**, *251*, 7–20.

[33] Navarro, R. M.; Peña, M. A.; Fierro, J. L. G. Production of Hydrogen by Partial Oxidation of Methanol over a $Cu/ZnO/Al_2O_3$ Catalyst: Influence of the Initial State of the Catalyst on the Start-Up Behaviour of the Reformer. *Journal of Catalysis* **2002**, *212*, 112–118.

[34] Choi, Y.; Stenger, H. G. Fuel cell grade hydrogen from methanol on a commercial $Cu/ZnO/Al_2O_3$ catalyst. *Applied Catalysis B: Environmental* **2002**, *38*, 259–269.

[35] Kudo, A.; Miseki, Y. Heterogeneous photocatalyst materials for water splitting. *Chem. Soc. Rev.* **2008**, *38*, 253–278.

[36] Maeda, K.; Domen, K. Photocatalytic Water Splitting: Recent Progress and Future Challenges. *J. Phys. Chem. Lett.* **2010**, *1*, 2655–2661.

[37] Kato, H.; Asakura, K.; Kudo, A. Highly Efficient Water Splitting into H_2 and O_2 over Lanthanum-Doped $NaTaO_3$ Photocatalysts with High Crystallinity and Surface Nanostructure. *J. Am. Chem. Soc.* **2003**, *125*, 3082–3089.

[38] Kurihara, T.; Okutomi, H.; Miseki, Y.; Kato, H.; Kudo, A. Highly Efficient Water Splitting over $K_3Ta_3B_2O_{12}$ Photocatalyst without Loading Cocatalyst. *Chemistry Letters* **2006**, *35*, 274–275.

[39] Maeda, K.; Teramura, K.; Domen, K. Effect of post-calcination on photocatalytic activity of $(Ga_{1-x}Zn_x)(N_{1-x}O_x)$ solid solution for overall water splitting under visible light. *Journal of Catalysis* **2008**, *254*, 198–204.

[40] Artero, V.; Chavarot-Kerlidou, M.; Fontecave, M. Splitting Water with Cobalt. *Angewandte Chemie International Edition* **2011**, *50*, 7238–7266.

[41] *"Novel Alloy Could Produce Hydrogen Fuel from Sunlight"*, Sience Daily, **2011**, LLC 2011-08-30.

[42] Sheetz, R. M.; Richter, E.; Andriotis, A. N.; Lisenkov, S.; Pendyala, C.; Sunkara, M. K.; Menon, M. Visible-light absorption and large band-gap bowing of $GaN_{\{1-x\}}Sb_{\{x\}}$ from first principles. *Phys. Rev. B* **2011**, *84*, 075304.

[43] Abanades, S.; Charvin, P.; Flamant, G.; Neveu, P. Screening of water-splitting thermochemical cycles potentially attractive for hydrogen production by concentrated solar energy. *Energy* **2006**, *31*, 2805–2822.

[44] Tarquini P., *Grande Progetto Solare Termodinamico, Produzione di idrogeno con cicli termochimici alimentati da energia solare concentrata*. **2004**, Solterm-Svil ENEA Casaccia

[45] J.M. Norbeck, J.W. Heffel, T.D. Durbin, B. Tabbara, J.M. Bowden, M.C. Montani, *Hydrogen Fuel for Surface Transportation, Society of Automotive Engineers Inc.*, Warrendale, PA, **1996**, p. 548.

[46] SattlerC. Thermochemical cycles. In Stolten D., *Hydrogen and Fuel cells: fundamentals, technologies and applications*. Wiley-VCH, **2010**, ISBN 978-3-527-32711-9.

[47] James, E. F. Thermochemical hydrogen production: past and present. *International Journal of Hydrogen Energy* **2001**, *26*, 185–190.

[48] Naterer, G.; Suppiah, S.; Lewis, M.; Gabriel, K.; Dincer, I.; Rosen, M. A.; Fowler, M.; Rizvi, G.; Easton, E. B.; Ikeda, B. M.; Kaye, M. H.; Lu, L.; Pioro, I.; Spekkens, P.; Tremaine, P.; Mostaghimi, J.; Avsec, J.; Jiang, J. Recent Canadian advances in nuclear-based hydrogen production and the thermochemical Cu–Cl cycle. *International Journal of Hydrogen Energy* **2009**, *34*, 2901–2917.

[49] Petri M.C.; Yildiz B.; Klickman A.E. US work on technical and economic aspects of electrolytic, thermochemical, and hybrid processes for hydrogen production at temperatures below 550°C. *International Journal of Nuclear Hydrogen Production and Applications*, **2006**,*1* (1), 79 - 91

[50] Nakamura T. Hydrogen production from water utilizing solar heat at high temperatures. *Solar Energy* **1977**, *19*, 467–475.

[51] Kodama, T.; Gokon, N. Thermochemical Cycles for High-Temperature Solar Hydrogen Production. *Chem. Rev.* **2007**, *107*, 4048–4077.

[52] Fresno, F.; Fernández-Saavedra, R.; Belén Gómez-Mancebo, M.; Vidal, A.; Sánchez, M.; Isabel Rucandio, M.; Quejido, A. J.; Romero, M. Solar hydrogen production by two-step thermochemical cycles: Evaluation of the activity of commercial

ferrites. *International Journal of Hydrogen Energy* **2009**, *34*, 2918–2924.

[53] Han, S. B.; Kang, T. B.; Joo, O. S.; Jung, K. D. Water splitting for hydrogen production with ferrites. *Solar Energy* **2007**, *81*, 623–628.

[54] Fresno, F.; Yoshida, T.; Gokon, N.; Fernández-Saavedra, R.; Kodama, T. Comparative study of the activity of nickel ferrites for solar hydrogen production by two-step thermochemical cycles. *International Journal of Hydrogen Energy* **2010**, *35*, 8503–8510.

[55] Fresno, F.; Yoshida, T.; Gokon, N.; Fernández-Saavedra, R.; Kodama, T. Comparative study of the activity of nickel ferrites for solar hydrogen production by two-step thermochemical cycles. *International Journal of Hydrogen Energy* **2010**, *35*, 8503–8510.

[56] Fresno, F.; Yoshida, T.; Gokon, N.; Fernández-Saavedra, R.; Kodama, T. Comparative study of the activity of nickel ferrites for solar hydrogen production by two-step thermochemical cycles. *International Journal of Hydrogen Energy* **2010**, *35*, 8503–8510.

[57] Kodama, T.; Kondoh, Y.; Yamamoto, R.; Andou, H.; Satou, N. Thermochemical hydrogen production by a redox system of ZrO_2-supported Co(II)-ferrite. *Solar Energy* **2005**, *78*, 623–631.

[58] Tamaura, Y.; Kaneko, H. Oxygen-releasing step of $ZnFe_2O_4/(ZnO + Fe_3O_4)$-system in air using concentrated solar energy for solar hydrogen production. *Solar Energy* **2005**, *78*, 616–622.

[59] Hiroshi Kaneko, Nobuyuki Gokon, Noriko Hasegawa, Yutaka Tamaura, Energy 30, 2005, pp.2171–2178

[60] Padella, F.; Alvani, C.; Barbera, A. L.; Ennas, G.; Liberatore, R.; Varsano, F. Mechanosynthesis and process characterization of nanostructured manganese ferrite. *Materials Chemistry and Physics* **2005**, *90*, 172–177.

[61] Varsano, F.; Padella, F.; La Barbera, A.; Alvani, C. The carbonatation reaction of layered Na(Mn1/3Fe2/3)O2: A high temperature study. *Solid State Ionics* **2011**, *187*, 19–26.

[62] Seralessandri, L.; Bellusci, M.; Alvani, C.; La Barbera, A.; Padella, F.; Varsano, F. Chemical equilibria involved in the oxygen-releasing step of manganese ferrite water-splitting thermochemical cycle. *Journal of Solid State Chemistry* **2008**, *181*, 1992–1997.

[63] Bhosale, R. R.; Shende, R. V.; Puszynski, J. A. Thermochemical water-splitting for H2 generation using sol-gel derived Mn-ferrite in a packed bed reactor. *International Journal of Hydrogen Energy* **2012**, *37*, 2924–2934.

[64] Pickles, C.A. Thermodynamic modelling of the formation of zinc–manganese ferrite spinel in electric arc furnace dust. *Journal of Hazardous Materials* **2010**, *179*, 309–317.

[65] Inoue, M.; Hasegawa, N.; Uehara, R.; Gokon, N.; Kaneko, H.; Tamaura, Y. Solar hydrogen generation with $H_2O/ZnO/MnFe_2O_4$ system. *Solar Energy* **2004**, *76*, 309–315.

[66] Richter, H.J. and Knoche, K.F. Reversibility of combustion processes, in Efficiency and Costing – Second law analysis of processes. *ACS symposium series*, **1983**, pp.71–85.

[67] Ishida, M.; Jin, H. CO_2 recovery in a power plant with chemical looping combustion. *Energy Conversion and Management* **1997**, *38, Supplement*, S187–S192.

[68] Naqvi, R.; Bolland, O.; Brandvoll, Ø.; Helle, K. Chemical looping combustion-analysis of natural gas fired power cycles with inherent CO_2 capture *Proceedings of the ASME Turbo Expo* **2004,** *7*, pp. 301-309.

[69] Hossain, M. M.; de Lasa, H. I. Chemical-looping combustion (CLC) for inherent separations—a review. *Chemical Engineering Science* **2008**, *63*, 4433–4451.

[70] Wang, Q., Cheng, Y., Wu, C., Jin, Y. A Novel Energy Conservation Process for Zero Emission of Carbon Dioxide : Chemical Looping Combustion. *Progress in Chemistry*, **2008**, *20* (10) , 1612-1620

[71] He Fang, Li Haibin, and Zhao Zengli. Advancements in Development of Chemical-Looping Combustion: A Review. *International Journal of Chemical Engineering*, **2009**

[72] Rydén, M.; Lyngfelt, A.; Mattisson, T. Synthesis gas generation by chemical-looping reforming in a continuously operating laboratory reactor. *Fuel* **2006**, *85*, 1631–1641.

[73] Kodama, T.; Ohtake, H.; Matsumoto, S.; Aoki, A.; Shimizu, T.; Kitayama, Y. Thermochemical methane reforming using a reactive WO_3/W redox system. *Energy* **2000**, *25*, 411–425.

[74] Gupta, P.; Velazquez-Vargas, L. G.; Fan, L.-S. Syngas Redox (SGR) Process to Produce Hydrogen from Coal Derived Syngas. *Energy Fuels* **2007**, *21*, 2900–2908.

[75] Steinfeld, A.; Frei, A.; Kuhn, P.; Wuillemin, D. Solar thermal production of zinc and syngas via combined ZnO-reduction and CH_4-reforming processes. *International Journal of Hydrogen Energy* **1995**, *20*, 793–804.

[76] Martin, F. Theoretical investigation of the system SnO_x/Sn for the thermochemical storage of solar energy. *Energy* **2004**, *29*, 789–799.

[77] Richard C. Breitkopf, Yardlynne Smalley, Zhong-Lin Wang, Robert Snyder, Michael Haluska, and Andrew T. Hunt, *Mater. Res. Soc. Symp. Proc.,* **2006**, Vol.885E

[78] Evdou, A.; Zaspalis, V.; Nalbandian, L. $La_{(1-x)}Sr_xMnO_{3-\delta}$ perovskites as redox materials for the production of high purity hydrogen. *International Journal of Hydrogen Energy* **2008**, *33*, 5554–5562.

[79] Evdou, A.; Nalbandian, L.; Zaspalis, V. T. Perovskite membrane reactor for continuous and isothermal redox hydrogen production from the dissociation of water. *Journal of Membrane Science* **2008**, *325*, 704–711.

[80] Howard Lane. The Lane Hydrogen Producer. **1909**, available online at http://www.flightglobal.com/pdfarchive/view/1909/1909%20-%200522.html

[81] Hurst, S. Production of hydrogen by the steam-iron method. *Oil & Soap*, **1939**, 16 (2)

[82] Dicke Hugo, Reducing and oxidizing apparatus for generating hydrogen from iron ore and steam. *Berlin anhaltische maschb aktien ges*, us1129559, **1913**

[83] AA.VV., Improvements in or relating to Reducing and Oxidising Apparatus for Generating Hydrogen from Iron Ore and Steam, *Berlin Anhaltische Maschb Akti*, Gb191328390, **1912**

[84] *Patent n° US3684447 (A), US3726966 (A)*

[85] *Patent n° US3442619 (A), US3442620 (A)*

[86] Tarman PB, Punwani DV. *Proc-Intersoc Energy Convers Eng Cont*, **1976**, 11(1), pp.286–93.

[87] Tarman PB, Biljetina R., *Coal Process Technol.,* **1979**, 5(1), pp.114–6.

[88] Mignard, D.; Pritchard, C. A review of the sponge iron process for the storage and transmission of remotely generated marine energy. *International Journal of Hydrogen Energy* **2007**, *32*, 5039–5049.

[89] Lorente, E.; Cai, Q.; Peña, J. A.; Herguido, J.; Brandon, N. P. Conceptual design and modelling of the Steam-Iron process and

fuel cell integrated system. *International Journal of Hydrogen Energy* **2009**, *34*, 5554–5562.

[90] Lorente, E.; Herguido, J.; Peña, J. A. Steam-iron process: Influence of steam on the kinetics of iron oxide reduction. *International Journal of Hydrogen Energy* **2011**, *36*, 13425–13434.

[91] Otsuka, K.; Yamada, C.; Kaburagi, T.; Takenaka, S. Hydrogen storage and production by redox of iron oxide for polymer electrolyte fuel cell vehicles. *International Journal of Hydrogen Energy* **2003**, *28*, 335–342.

[92] Imanishi, H.; Maeda, A.; Maegawa, T.; Matsuno, S.; Aida, T. Effects of reduction conditions on the cycling performance of hydrogen storage by iron oxides: Storage stage. *Chemical Engineering Science* **2008**, *63*, 4974–4980.

[93] Peña, J. A.; Lorente, E.; Romero, E.; Herguido, J. Kinetic study of the redox process for storing hydrogen: Reduction stage. *Catalysis Today* **2006**, *116*, 439–444.

[94] Otsuka, K.; Mito, A.; Takenaka, S.; Yamanaka, I. Production of hydrogen from methane without CO_2-emission mediated by indium oxide and iron oxide. *International Journal of Hydrogen Energy* **2001**, *26*, 191–194.

[95] Sanfilippo et al, **2001**, *Patent n° EP1134187A9*

[96] Cornaro and Sanfilippo, **2004**, *Patent n° US2004152790A1*

[97] Sanfilippo et al., **2005**, *Patent n° US6875411B2*

[98] Chiesa, P.; Lozza, G.; Malandrino, A.; Romano, M.; Piccolo, V. Three-reactors chemical looping process for hydrogen production. *International Journal of Hydrogen Energy* **2008**, *33*, 2233–2245.

[99] Takenaka, S.; Dinh Son, V. T.; Otsuka, K. Storage and Supply of Pure Hydrogen from Methane Mediated by Modified Iron Oxides. *Energy Fuels* **2004**, *18*, 820–829.

[100] Takenaka, S.; Hanaizumi, N.; Son, V. T. D.; Otsuka, K. Production of pure hydrogen from methane mediated by the redox of Ni- and Cr-added iron oxides. *Journal of Catalysis* **2004**, *228*, 405–416.

[101] Yamaguchi, D.; Tang, L.; Wong, L.; Burke, N.; Trimm, D.; Nguyen, K.; Chiang, K. Hydrogen production through methane–steam cyclic redox processes with iron-based metal oxides. *International Journal of Hydrogen Energy* **2011**, *36*, 6646–6656.

[102] Kang, K.-S.; Kim, C.-H.; Cho, W.-C.; Bae, K.-K.; Woo, S.-W.; Park, C.-S. Reduction characteristics of $CuFe_2O_4$ and Fe_3O_4 by methane; $CuFe_2O_4$ as an oxidant for two-step thermochemical methane reforming. *International Journal of Hydrogen Energy* **2008**, *33*, 4560–4568.

[103] Cha, K.-S.; Kim, H.-S.; Yoo, B.-K.; Lee, Y.-S.; Kang, K.-S.; Park, C.-S.; Kim, Y.-H. Reaction characteristics of two-step methane reforming over a Cu-ferrite/Ce–ZrO_2 medium. *International Journal of Hydrogen Energy* **2009**, *34*, 1801–1808.

[104] 1. Kang, K.-S.; Kim, C.-H.; Bae, K.-K.; Cho, W.-C.; Kim, W.-J.; Kim, Y.-H.; Kim, S.-H.; Park, C.-S. Redox cycling of $CuFe_2O_4$

supported on ZrO_2 and CeO_2 for two-step methane reforming/water splitting. *International Journal of Hydrogen Energy* **2010**, *35*, 568–576.

[105] Kodama, T.; Shimizu, T.; Satoh, T.; Nakata, M.; Shimizu, K.-I. Stepwise production of CO-rich syngas and hydrogen via solar methane reforming by using a Ni(II)–ferrite redox system. *Solar Energy* **2002**, *73*, 363–374.

[106] Hacker V. A novel process for stationary hydrogen production: the reformer sponge iron cycle (RESC). *Journal of Power Sources* **2003**, *118*, 311–314.

[107] Li, F.; Kim, H. R.; Sridhar, D.; Wang, F.; Zeng, L.; Chen, J.; Fan, L.-S. Syngas Chemical Looping Gasification Process: Oxygen Carrier Particle Selection and Performance. *Energy Fuels* **2009**, *23*, 4182–4189.

[108] Heidebrecht, P.; Sundmacher, K. Thermodynamic analysis of a cyclic water gas-shift reactor (CWGSR) for hydrogen production. *Chemical Engineering Science* **2009**, *64*, 5057–5065.

[109] Gupta, P.; Velazquez-Vargas, L. G.; Fan, L.-S. Syngas Redox (SGR) Process to Produce Hydrogen from Coal Derived Syngas. *Energy Fuels* **2007**, *21*, 2900–2908.

[110] Zhou, Y.; Jia, C.; Zhang, Y.; Liu, C.; Huang, D.; Sun, Y.; Zhou, L. Experimental study on a new process of producing hydrogen in consumption of water and coal. *AIChE Journal* **2008**, *54*, 1388–1395.

[111] Yang, J.; Cai, N.; Li, Z. Hydrogen Production from the Steam−Iron Process with Direct Reduction of Iron Oxide by Chemical Looping Combustion of Coal Char. *Energy Fuels* **2008**, *22*, 2570–2579.

[112] Bleeker, M. F.; Kersten, S. R. A.; Veringa, H. J. Pure hydrogen from pyrolysis oil using the steam-iron process. *Catalysis Today* **2007**, *127*, 278–290.

[113] Bleeker, M.; Gorter, S.; Kersten, S.; van der Ham, L.; van den Berg, H.; Veringa, H. Hydrogen production from pyrolysis oil using the steam-iron process: a process design study. *Clean Technologies and Environmental Policy* **2010**, *12*, 125–135.

[114] Hacker, V.; Fankhauser, R.; Faleschini, G.; Fuchs, H.; Friedrich, K.; Muhr, M.; Kordesch, K. Hydrogen production by steam–iron process. *Journal of Power Sources* **2000**, *86*, 531–535.

[115] Hacker, V.; Faleschini, G.; Fuchs, H.; Fankhauser, R.; Simader, G.; Ghaemi, M.; Spreitz, B.; Friedrich, K. Usage of biomass gas for fuel cells by the SIR process. *Journal of Power Sources* **1998**, *71*, 226–230.

[116] Sime, R.; Kuehni, J.; D'Souza, L.; Elizondo, E.; Biollaz, S. The redox process for producing hydrogen from woody biomass. *International Journal of Hydrogen Energy* **2003**, *28*, 491–498.

[117] Calin-Cristian, C. Evaluation of iron based chemical looping for hydrogen and electricity co-production by gasification process with carbon capture and storage. *International Journal of Hydrogen Energy* **2010**, *35*, 2278–2289.

[118] Calin-Cristian, C. Hydrogen production from fossil fuels with carbon capture and storage based on chemical looping systems. *International Journal of Hydrogen Energy* **2011**, *36*, 5960–5971.

[119] Otsuka, K.; Kaburagi, T.; Yamada, C.; Takenaka, S. Chemical storage of hydrogen by modified iron oxides. *Journal of Power Sources* **2003**, *122*, 111–121.

[120] Lorente, E.; Peña, J. A.; Herguido, J. Cycle behaviour of iron ores in the steam-iron process. *International Journal of Hydrogen Energy* **2011**, *36*, 7043–7050.

[121] Lorente, E.; Peña, J. A.; Herguido, J. Separation and storage of hydrogen by steam-iron process: Effect of added metals upon hydrogen release and solid stability. *Journal of Power Sources* **2009**, *192*, 224–229.

[122] Takenaka, S.; Kaburagi, T.; Yamada, C.; Nomura, K.; Otsuka, K. Storage and supply of hydrogen by means of the redox of the iron oxides modified with Mo and Rh species. *Journal of Catalysis* **2004**, *228*, 66–74.

[123] Takenaka, S.; Nomura, K.; Hanaizumi, N.; Otsuka, K. Storage and formation of pure hydrogen mediated by the redox of modified iron oxides. *Applied Catalysis A: General* **2005**, *282*, 333–341.

[124] Ryu, JC; Lee, DH; Kang, KS; Park, CS; Kim, JW; Kim, YH et al. *Eng Chem.* **2008**, *14*, 252-60.

[125] Lee, D. H.; Cha, K. S.; Lee, Y. S.; Kang, K. S.; Park, C. S.; Kim, Y. H. Effects of CeO2 additive on redox characteristics of Fe-based mixed oxide mediums for storage and production of hydrogen. *International Journal of Hydrogen Energy* **2009**, *34*, 1417–1422.

[126] Ballarini, N.; Cavani, F.; Passeri, S.; Pesaresi, L.; Lee, A. F.; Wilson, K. Phenol methylation over nanoparticulate $CoFe_2O_4$ inverse spinel catalysts: The effect of morphology on catalytic performance. *Applied Catalysis A: General* **2009**, *366*, 184–192.

[127] Meng, Y.; Chen, D.; Jiao, X. Synthesis and Characterization of $CoFe_2O_4$ Hollow Spheres. *European Journal of Inorganic Chemistry* **2008**, *2008*, 4019–4023.

[128] Waldron, R. D. Infrared Spectra of Ferrites. *Phys. Rev.* **1955**, *99*, 1727–1735.

[129] Gillot, B.; Jemmali, F.; Rousset, A. Infrared studies on the behavior in oxygen of cobalt-substituted magnetites: Comparison with zinc-substituted magnetites. *Journal of Solid State Chemistry* **1983**, *50*, 138–145.

[130] Kumar, V.; Rana, A.; Kumar, N.; Pant, R. P. Investigations on Controlled-Size-Precipitated Cobalt Ferrite Nanoparticles. *International Journal of Applied Ceramic Technology* **2011**, *8*, 120–126.

[131] Guido, B. Infrared studies of the reactive adsorption of organic molecules over metal oxides and of the mechanisms of their

heterogeneously-catalyzed oxidation. *Catalysis Today* **1996**, *27*, 457–496.

[132] Desautels, R. D.; Lierop, J. van; Cadogan, J. M. Disproportionation of cobalt ferrite nanoparticles upon annealing. *Journal of Physics: Conference Series* **2010**, *217*, 012105.

[133] Li, X.; Kutal, C. Synthesis and characterization of superparamagnetic $Co_xFe_{3-x}O_4$ nanoparticles. *Journal of Alloys and Compounds* **2003**, *349*, 264–268.

[134] Lee, S. W.; Kim, C. S. Mössbauer studies on the superparamagnetic behavior of $CoFe_2O_4$ with a few nanometers. *Journal of Magnetism and Magnetic Materials* **2006**, *303*, e315–e317.

[135] Sawatzky, G. A.; Van Der Woude, F.; Morrish, A. H. Mössbauer Study of Several Ferrimagnetic Spinels. *Phys. Rev.* **1969**, *187*, 747–757.

[136] Sawatzky, G. A.; VAN DER Woude, F.; Morrish, A. H. Cation Distributions in Octahedral and Tetrahedral Sites of the Ferrimagnetic Spinel $CoFe_2O_4$. *Journal of Applied Physics* **1968**, *39*, 1204–1205.

[137] Chandramohan, P.; Srinivasan, M. P.; Velmurugan, S.; Narasimhan, S. V. Cation distribution and particle size effect on Raman spectrum of $CoFe_2O_4$. *Journal of Solid State Chemistry* **2011**, *184*, 89–96.

[138] Ferreira, T. A. S.; Waerenborgh, J. C.; Mendonça, M. H. R. M.; Nunes, M. R.; Costa, F. M. Structural and morphological characterization of $FeCo_2O_4$ and $CoFe_2O_4$ spinels prepared by a coprecipitation method. *Solid State Sciences* **2003**, *5*, 383–392.

[139] Johnson, C. E.; Ridout, M. S.; Cranshaw, T. E. The M ssbauer Effect in Iron Alloys. *Proceedings of the Physical Society* **1963**, *81*, 1079–1090.

[140] Sawatzky, G. A.; Coey, J. M. D.; Morrish, A. H. Mössbauer Study of Electron Hopping in the Octahedral Sites of Fe_3O_4. *Journal of Applied Physics* **1969**, *40*, 1402–1403.

[141] Kniep, B.; Constantinescu, A.; Niemeier, D.; Becker, K. D. An in-situ Mössbauer Study of the Formation of Cementite, Fe_3C. *Zeitschrift für anorganische und allgemeine Chemie* **2003**, *629*, 1795–1804.

[142] Herreyre, S.; Gadelle, P.; Moral, P.; Millet, J. M. M. Study by mössbauer spectroscopy and magnetization measurement of the evolution of iron catalysts used in the disproportionation of CO. *Journal of Physics and Chemistry of Solids* **1997**, *58*, 1539–1545.

[143] Zhang, J.; Schneider, A.; Inden, G. Characterisation of the coke formed during metal dusting of iron in $CO–H_2–H_2O$ gas mixtures. *Corrosion Science* **2003**, *45*, 1329–1341.

[144] Mondal, K.; Lorethova, H.; Hippo, E.; Wiltowski, T.; Lalvani, S. B. Reduction of iron oxide in carbon monoxide atmosphere—reaction controlled kinetics. *Fuel Processing Technology* **2004**, *86*, 33–47.

[145] Park, E.; Ostrovski, O.; Zhang, J.; Thomson, S.; Howe, R. Characterization of phases formed in the iron carbide process by X-ray diffraction, mossbauer, X-ray photoelectron spectroscopy, and raman spectroscopy analyses. *Metallurgical and Materials Transactions B* **2001**, *32*, 839–845.

[146] Schneeweiss, O.; Zbořil, R.; David, B.; Heřmánek, M.; Mashlan, M. Solid-state synthesis of α-Fe and iron carbide nanoparticles by thermal treatment of amorphous Fe_2O_3. *Hyperfine Interactions* **2009**, *189*, 167–173.

[147] Niemantsverdriet, J. W.; Van der Kraan, A. M.; Van Dijk, W. L.; Van der Baan, H. S. Behavior of metallic iron catalysts during Fischer-Tropsch synthesis studied with Moessbauer spectroscopy, x-ray diffraction, carbon content determination, and reaction kinetic measurements. *J. Phys. Chem.* **1980**, *84*, 3363–3370.

[148] Persoons, R. M.; De Grave, E.; de Bakker, P. M. A.; Vandenberghe, R. E. Mössbauer study of the high-temperature phase of Co-substituted magnetites, Co_{x}Fe_{3-x}O_{4}. II. x≥0.1. *Phys. Rev. B* **1993**, *47*, 5894–5905.